A COMPARISON OF QUANTUM MECHANICAL AND QUASICLASSICAL REACTION DYNAMICS FOR AN ASYMMETRIC A + BC EXCHANGE REACTION

By

GLEN EDWARD KELLERHALS

Bachelor of Science

Upper Iowa College

Fayette, Iowa

1967

Submitted to the Faculty of the Graduate College
of the Oklahoma State University
in partial fulfillment of the requirements
for the Degree of
DOCTOR OF PHILOSOPHY
July, 1974

A COMPARISON OF QUANTUM MECHANICAL AND

QUASICLASSICAL REACTION DYNAMICS

FOR AN ASYMMETRIC A + BC

EXCHANGE REACTION

Thesis Approved:

Lionel M. Raff
Thesis Adviser

J. Paul Devlin

Paul Westhaus

Jim Wilson

D. D. Dunlap
Dean of the Graduate College

ACKNOWLEDGEMENTS

The author would like to express his sincere gratitude to Dr. Lionel M. Raff, Research Adviser, for his patience and guidance throughout this investigation and in particular thank him for initially suggesting the research problem.

Thanks are extended to Drs. J. Paul Devlin, Paul Westhaus, and T. M. Wilson for serving as my advisory committee.

Financial assistance consisting of a National Aeronautics and Space Administration Traineeship, various teaching assistantships in the Department of Chemistry, and support from a National Science Foundation research grant, NSF-GP-35869X, is acknowledged. Without monetary support the pursuit of an advanced degree would not have been possible.

I am indebted to the very capable University Computer Center staff for their computing assistance and thank the Research Foundation for making available generous amounts of computer time for calculational purposes.

Special thanks go to Dr. Ron Oines of the Research Foundation for providing the perspective plotting subroutine and for assisting me in its use.

I am especially grateful for Shirley's loving care and patient endurance during the latter part of my graduate tenure and also recognize the camaraderie of fellow graduate students during my graduate years.

TABLE OF CONTENTS

LIST OF TABLES

LIST OF FIGURES

LIST OF FIGURES (continued)

LIST OF FIGURES (continued)

CHAPTER I

INTRODUCTION

Historical and Background Material

One of the first attempts to mathematically describe chemical exchange reactions of the type

$$A + BC \rightarrow AB + C, \qquad [1]$$

where A represents an atom and BC represents a diatomic molecule, was by Eyring (1). He used the idea of London (2) that the possible course of a chemical reaction is that of an adiabatic interaction in which the energy of the system varies as a continuous function of the interatomic distances.

Since this early calculation theoretical, chemical kinetics has undergone revolutionary progress. Probably more than any other single innovation, the electronic computer has revolutionized the number and varieties of calculations that can be performed. Within this realm of theoretical computations are elastic, inelastic, and reactive scattering calculations.

In many cases the complete detailed description of the molecular dynamics of exchange reactions such as [1] would enable one to calculate the rates of laboratory reactions as well as to determine the energy partitioning, scattering behavior, and reaction mechanism. Experimental techniques are now refined to such a degree that chemical reactions are

accessible to direct examination on the molecular level. Studies of infrared chemiluminescence and of reactions in crossed molecular beams provide detailed information about the way in which reactive collisions occur and about the way in which the energy released in reaction is distributed among the products. A complete three-dimensional, ab initio calculation has not been published for the Schrödinger (3) wave equation describing the simplest exchange reaction.

An approach to this computationally difficult problem is to simplify the problem and/or simplify the computation. In practice both simplifications are made, and models in chemistry and physics are thus formed to approximate and mimic the actual state of affairs. However, not all is lost by any means, as the solution of the simplified problem may provide valuable insights into the nature of the exact description of the complete problem. The insights may suggest approximate schemes to be utilized to reduce the computational labor of the complete problem.

At the molecular level the symbolic equation [1] cannot be regarded as a chemical process involving two single entities, atom A and molecule BC. Rather, atom A can only be understood in terms of the nucleus and electrons of which it is comprised. Analogously molecule BC cannot be treated as atom B and C, that is, the molecular properties of BC are vastly different from the properties of the individual atoms. Molecules themselves are properly considered as quantum mechanical systems and normally exist in a variety of rotational, vibrational, and electronic states. In this sense, a transition in the vibration or electronic state of a molecule is the simplest type of chemical reaction. Furthermore, it is expected that the reactivity of atoms and molecules in different internal energy states will be different and therefore it is

necessary to treat each possible state individually, if such a procedure is computationally tractable. Accordingly, the treatment of Elaison and Hirschfelder (4) treats molecules in different internal quantum states as though they were distinct species and takes into account transitions between these internal states.

Even one of the simplest atom-molecule chemical reactions, $H + H_2 \rightarrow H_2 + H$, consisting of three nuclei and three electrons, cannot be completely treated dynamically (5). Radical simplifications are therefore needed to reduce even the most elementary chemical reaction problems to levels suitable for computation. One such simplification is the Born-Oppenheimer (6) approximation.

The Born-Oppenheimer Approximation: Potential Energy Surfaces

In general the motion of the electrons of the colliding atom and molecule may be considered very fast in comparison with the motion of the nuclei. A Born-Oppenheimer separation of the nuclear and electronic wavefunctions may therefore be made, and the Schrödinger equation for the electronic motion in the field of a clamped or fixed nuclear configuration may be considered. The solutions of the time independent wave equation form an infinite set of electronic states which may be labeled by a set of quantum numbers. The lowest state of the set is referred to as the ground electronic state. Solutions of the electronic Schrödinger equation may, in principle, be obtained for every possible fixed nuclear configuration. The energy associated with a particular electronic state will vary as the relative nuclear separations are changed. Stated another way, the Born-Oppenheimer approximation consists

of first determining the electronic wavefunction for various values of the fixed nuclear coordinates and then using this electronic energy (usually just the ground state electronic energy is used) as a potential-energy function in describing the motion of the nuclei (7). If the reaction takes place on more than one electronic surface, the process is said to be "nonadiabatic" and the theoretical investigation of the dynamics becomes considerably more difficult.

Provided that the Born-Oppenheimer approximation holds and provided also that the electrons remain in one state (the adiabatic assumption), a single potential-energy surface or hypersurface for more than two independent variables may be constructed to give the potential energy for all fixed nuclear configurations for an assembly of atoms. As Levine (8) points out, transitions of atom A in the internal (electronic) state i to the internal state j, cannot take place in the adiabatic approximation. Mortensen (9) has stated that for energies less than one electron volt, the Born-Oppenheimer approximation is applicable and the nuclear and electronic motions can be separated. He does not substantiate his claim. One should remember that the very existence of an electronic energy depends on the Born-Oppenheimer separation, an approximation which may or may not be valid in certain cases. At high enough energies the separation will surely fall. The mathematical development leading to the Born-Oppenheimer approximation for a diatomic molecule can be found in several standard textbooks (10).

The calculation of the electronic energy poses a formidable problem in stationary-state quantum mechanics. The computations are extremely expensive for the large number of nuclear configurations required for the calculation of a reaction potential-energy surface. One of the most

severe mathematical difficulties in the computations is the evaluation of the integrals which arise. Accordingly, in semiempirical calculations the integral evaluations are performed by systematically approximating the integrals with experimental information about the atoms or molecules involved. In addition, calculations on many-electron atoms and molecules frequently restrict consideration to valence electrons. Models which take into account only a few valence electrons for complex systems are discussed by Hopper (11).

The approximate schemes for obtaining the potential energy are grouped by Laidler (12) as: a) purely quantum mechanical, which includes treatments based on the work by London (2) and variational calculations, b) semiempirical treatments, and c) empirical procedures. He presents a good discussion of each category and gives extensive references. Computational approaches to chemical kinetics can be divided into two classes (12): (I) theories not related to potential-energy surfaces and (II) theories based on passage over potential-energy surfaces. Category (I) includes nonequilibrium statistical mechanics, hard-sphere collision theory, and stochastic (13) theories; theories based on the principles of probability. Classification (II) contains a) activated-complex theory (14) or transition-state theory, in which activated complexes are assumed to be in equilibrium with reactants and b) classical and quantum mechanical treatments with no equilibrium assumption. In summary, calculations can proceed in one of several directions; a choice must be made as to the direction to be taken.

Mechanics and Dynamics

The subject of molecular dynamics (15) is concerned with theories

of the movement of systems over potential-energy surfaces. The nuclear-dynamics problem may be stated as follows: Among all possible motions of the chemical system we seek to accurately determine which motion will actually take place in any given case, that is, under the action of given forces. Physics supplies two systems of mechanics which are available for the description of the nuclear motion, classical mechanics and quantum mechanics.

Rigorously, classical mechanics is not applicable on the microscopic scale, that is, the atomic or subatomic domain where the unit of length is the angstrom. Nevertheless, several criteria indicate that classical mechanics may be able to give a worthwhile account of the nuclear dynamics of a reacting system (16). The criteria, however, do not provide a good quantitative estimate of the error that will be incurred, if classical mechanics is employed. Two main sources of error are inherent in a purely classical mechanical calculation. The first of these is energy quantization; the second is quantum mechanical tunneling. The importance of these quantal phenomena in a dynamical calculation should be a measure of the extent of the success (or failure) of classical mechanics.

The first classical calculations of the motion over a potential energy surface were performed by Eyring and Polanyi (1) for the $H + H_2$ system. Further investigations were carried out by Hirschfelder, Eyring, and Topley (17) and later by Hirschfelder and Wigner (18). In these pioneering calculations point-by-point computations had to be made by hand for the successive coordinates of the system. The results of these calculations are discussed in reference (19). The earliest studies on any reaction more complex than the $H_2 + H$ exchange were the calculations

on the hydrogen-halogen reactions by Eyring and Polanyi (1), Eyring (20), and Wheeler, Topley, and Eyring (21). These calculations employing transition-state theory showed that the combination of hydrogen and iodine would not involve the atoms since this would require an activation energy (22) greater than if the reaction involved only molecules. Wall, Hiller, and Mazur (23) performed the first computer calculations of reaction dynamics. Since this work several such classical calculations (classical trajectory calculations) have been carried out on a variety of reactions using many different kinds of potential-energy surfaces (24-78). The majority of these calculations is quasiclassical (the vibrational energy of the reactant molecule is quantized) rather than classical. Summaries of the techniques and methods employed in these calculations and assessments of the results may be found in several sources (79). At present, the absolute accuracy of these calculations is not known. Two major difficulties arise when direct comparisons with experiment are attempted: 1) agreement or disagreement with experiment may result due to unknown errors in the potential surface used in the calculation, and 2) the experimentally observed properties involve averaging over molecular properties and hence the observed properties may be quite insensitive to the fine details of the molecular dynamics. The most fruitful comparisons would seem to be between classical and quantal calculations using the same potential surface. A few comparison studies utilizing several different computational approaches have been made (9) (39) (63) (80) (81) (82) (83).

The fundamental theory of reactive collision processes is well understood quantum mechanically (and classically) but many approximations, simplifications, and models have been utilized in order to obtain

results (84). The procedures used vary greatly and no single approach has been outstandingly successful. The quantum mechanical approaches can be divided into three general sections. (The division could also consist of two categories, time-independent and time-dependent quantum mechanics.) These are briefly described below.

Calculations of reaction systems on highly simplified potential-energy surfaces using formal theories: Perturbation theory may be applied to the reactive scattering problem, if an approximate wavefunction for the reactant state is available. If the approximate wavefunction consists of the product of the distorted initial translational wave and a wavefunction describing the initial internal state, the approximation is called the distorted wave Born approximation. Calculations performed using the distortion of waves method have been done by Micha (85), Karplus and Tang (86)(87), and Walker and Wyatt (88). The latter calculation was performed on a realistic semiempirical potential surface. Analytic solutions to the wave equation may be found for collinear systems if a simple model potential is used. The partial wave formalism (89) of time-independent quantum mechanics provides the exact solution to the atom-atom scattering problem (90). The same approach can be applied to inelastic scattering without rearrangements (91). In 1943 Hulbert and Hirschfelder (92) and later Tang, Kleinman, and Karplus (93)(94) performed calculations using a square channel potential for three atoms on a line.

Detailed numerical calculations on more realistic potential energy surfaces: In many of these calculations it is only the dimensionality of the problem which precludes a direct comparison between the results and experimental findings. The numerical methods for the solution of

the Schrödinger equation for three atoms constrained to the collinear case can be classed into two categories. The first method consists of writing the Schrödinger equation as a set of finite difference equations on a two dimensional (each dimension is related to the relative distance between two atoms) grid of points. These equations are then solved by some numerical technique subject to the appropriate asymptotic boundary conditions. Secondly, the wavefunction may be expanded in terms of a complete basis set for one of the variables. The resulting coupled differential equations may then be solved by a numerical technique. Mortensen and Pitzer (95) first used numerical techniques to solve the time-independent Schrödinger equation. They applied a finite difference method to the collinear reactive $H + H_2$ system. More recently other calculations employing finite difference methods have been performed (96-104).

In the second approach the problem of the different basis sets for reactants and products has been resolved to a large degree by Marcus (105)(106) who introduced reaction coordinates in a mathematical fashion. He used the reaction path (107) to define a new coordinate system. Using this method Light and co-workers (108-110) have found it advantageous to define the reaction coordinates independently of the reaction path and have used this procedure on the $H + Cl_2$ system. In this calculation it was found that the vibrational excitation of the products was increased by a combination of moving the col (111) toward the reactant side and by making the reaction path sharply curved. Duff and Truhlar (78) have recently noted the same effect in a quasiclassical calculation. Recently, Diestler (112), studying a different reaction having a very different potential surface, drew similar conclusions. The method

was also applied by Wyatt (113) who studied the effects of several approximations.

One alternative approach is the variational technique used by Mortensen and Gucwa (98) and Crawford (114) on the $H + H_2$ collinear system. As in many other methods, the problems encountered when application to higher dimension is attempted seem formidable. Another approach is the formulation of the problem in terms of an equivalent (or optical) component in the potential. The effective component represents the disappearance of amplitude from the elastic scattering channel into inelastic channels not directly considered.

Miller and co-workers (47) (50) (51) (115) have shown how exact classical mechanics (i.e. numerically computed classical trajectories) for a collision system can be used semiclassically to construct the classical limit of the quantum mechanical S matrix. A very intriguing aspect of this classical S matrix theory is the possibility of using classical trajectories to obtain transition probabilities for classically forbidden processes. One example of a classically forbidden process that may be extremely important is reactive tunneling.

In spite of the idea that a chemical reaction suggests a time-dependent phenomenon, time-dependent quantum mechanics has been almost neglected in reaction dynamics calculations. The approach possesses some unique assets as demonstrated by a few investigators. The results of Goldberg, et al. (116) on the penetration of one-dimensional potential barriers by wavepackets were displayed graphically in the form of a movie. Wilson and co-workers (102) have performed calculations on the time evolution of anharmonic oscillators.

McCullough and Wyatt (80) solved the time-dependent Schrödinger

equation and followed the motion in time and space of an initial wave packet. The Hamiltonian operator was approximated by a finite difference expression and the method applied to the H + H_2 collinear reaction using the potential-energy surface developed by Porter and Karplus (117). Very recently Truhlar and Kuppermann (82) presented numerical quantum mechanical scattering calculations for the collinear H + H_2 system. Extensive comparisons with other methods of treating the problem are made and 76 references are cited.

Selected Studies of Chemical Dynamics

Several quasiclassical trajectory studies have been made by Raff, Porter, et al. (40) (41) (60) (118) on the hydrogen-halogen exchange reactions using semiempirical potential-energy surfaces. Their results for the hydrogen molecule-iodine atom exchange reaction (40) indicate that virtually all of the reaction product is produced from vibrationally excited hydrogen molecules. The requirement of vibrational excitation for reaction is in accord with the experimental measurements of Sullivan (119). In the case of H_2 + X (X = Br or I) exchange reactions in which H_2 has initial vibrational energy corresponding to the ground state, calculated reaction probabilities exhibit translational threshold energies in considerable excess of the potential-energy barrier (40) (41) (118). The authors attribute the excess as resulting from the imposed dynamic constraints (41) (120) and varies from a maximum of 35 kcal/mole for H_2 + I down to a few kilocalories per mole for H_2 + Br. In contrast, dynamic constraints appear to play a relatively minor role in determining the reaction mechanism in the H_2 + Cl reaction. The results indicate that dynamic effects increase as the saddle point

shifts toward the exit or retreat valley.

One dynamical property playing an important role in the A + BC exchange reaction is linear momentum. The two (B and C) atoms can be accelerated during interaction with an attacking A atom but their response may be relatively slow. Thus, as the velocity of the A atom increases (momentum increases), the B and C atoms have less time to respond, and the A atom tends to move into and out of the interaction region before the B-C distance can be increased enough to "turn the corner" into the product region. Noyes (121) in his discussion of the H_2-I_2 reaction has suggested the important role played by momentum in the dynamics of certain reactions. The significance of momentum may be expressed qualitatively by realizing that a) any chemical reaction requires momentum transfer between the colliding species, b) the time required for momentum transfer is finite, and c) a momentum transfer time less than or equal to the collision time is required for successful passage from reactants to products. In summary, for those cases where the collision time is much larger than the time required for momentum transfer, dynamic effects will not be particularly crucial. On the other hand when the collision time becomes less than the time for momentum transfer or when these two characteristic times become more nearly equal, then momentum is a significant variable and its importance is evident in a lower reaction probability.

A few investigators (24) (34) (37) (122-126) have explicitly studied the effects of variations of the potential-energy surface on attributes of exchange reactions using classical mechanics. Variations include total energy, translational energy, vibrational energy, barrier position, barrier height, masses of the reacting atoms, curvature of the

reaction path, and rotational energy in the reactants. Interests are centered on reaction probability, threshold for reaction, and the distribution of internal energies for both reactants and products. Polanyi (122) examined the effects on the dynamics of a shift in the energy barrier from the entrance valley of the potential energy surface to the exit valley. The most apparent effect of the change was to replace relative translation of the reagent as the form of energy required for barrier crossing by vibration in the molecule under attack.

The position of the energy barrier and its height have been correlated by Mok and Polanyi (123). They found that for substantially exothermic reactions the barrier is in the entrance valley and for substantially endothermic reactions the barrier is in the exit valley. In addition, with increasing barrier height for exothermic reactions the barrier shifts to a later position along the reaction coordinate. In exact analogy there is also a shift in the barrier to a later position along the reaction coordinate with increasing barrier height for endothermic reactions.

An attempt has been made to present a somewhat general but yet concise survey of the rapidly expanding field of theoretical chemical kinetics. The reference list is certainly not complete but hopefully many of the most active workers in the field have been mentioned.

The Present Investigation

A comparison of the results of a three-dimensional quasiclassical calculation with corresponding three-dimensional quantum mechanical ones is very desirable to establish the importance of quantum effects. Such a comparison supplies an assessment of the usefulness of classical

mechanics to treat the dynamics of a chemical reactive scattering system. The present investigation is limited to a study of the collinear A + BC reaction [1]. The assumption that reaction [1] proceeds on a single potential energy surface which is defined in terms of the Born-Oppenheimer approximation is made. The nuclear dynamics of the reaction on this surface are examined using time-dependent quantum mechanics. Accordingly the study consists of a hypothetical chemical reaction which occurs in one dimensional space. The formulation and details are reserved for the following chapters.

Not surprisingly, the most extensively studied exchange reaction is the $H + H_2$ reaction and isotopically related reactions. The potential-energy surface for this thermoneutral reaction is obviously symmetrical. As stated earlier, quasiclassical three-dimensional trajectory calculations carried out on unsymmetrical surfaces, whose barriers lie in the exit channel, characteristically exhibit dynamic effects. A quantum calculation on such an unsymmetrical surface should be fruitful and provide valuable insights into the quantum and classical dynamics of exchange reactions.

Potential surfaces which retain thermoneutrality but which are non-symmetric with respect to energy barrier location have been constructed by Polanyi, et al. (34) (122). The thermoneutrality of the exchange process should be an especially desirable characteristic when comparisons of this investigation are made with previous work on the thermoneutral $H + H_2$ reaction. The present study investigates the particular case of equation [1] in which the masses of the atoms m_a, m_b, and m_c are all equal to the mass of hydrogen but a purely hypothetical potential-energy surface is used.

In particular, the impetus for such a study dictates the investigation be undertaken to clarify and promote explanation of: a) discrepancies, if any, between classical reaction probabilities and the corresponding quantum probabilities, which seem to be dependent on the asymmetry of the potential-energy surface (63), b) differences between the dependence of the classical and quantum reaction probabilities on the translational energy of the reactants, c) evidence, if any, for the formation of long-lived intermediates, and d) the overall effects of the position of the energy barrier on the classical and quantum dynamics.

The quantum calculation by McCullough and Wyatt (80) was carried out on a semiempirical, symmetric potential-energy surface corresponding to the thermoneutral $H + H_2$ reaction. The study reveals classical mechanics to give a fairly good account of the reaction dynamics. Kuppermann and co-workers (63) (82) have performed quantum mechanical calculations on the collinear $F + H_2$ and $H + H_2$ systems. The potential-energy surface employed to study the exothermic $F + H_2$ reaction was a nonsymmetric, semiempirical one published by Muckerman (44). At low energy, reaction probabilities calculated in the case of $F + H_2$ utilizing quasiclassical mechanics are 2.5 times greater than for the quantum calculation.

In recapitulation, a very high degree of understanding of the exact computationally intractable problem is not yet available. A massive effort is currently being directed toward remedying this situation. The present investigation is intended to provide a small contribution to that campaign.

CHAPTER II

FORMULATION OF THE PROBLEM

The Equations of Motion

In the reactive collinear atom-diatomic collision, Equation [1] in which the atoms are represented by spinless point masses, let the atoms lie on the axis with x_a, x_b, and x_c denoting their respective positions. Furthermore define r_1 as equal to the difference, $x_a - x_b$ and let r_2 equal $x_b - x_c$. This is indicated schematically in the upper half of Figure 1. If m_a, m_b, and m_c denote the masses of atoms A, B, and C respectively, then the classical kinetic energy, T, of the three atom system is

$$2T = m_a\dot{x}_a^2 + m_b\dot{x}_b^2 + m_c\dot{x}_c^2 \qquad [2]$$

where the dots represent time derivatives. The kinetic energy terms of the three particle system are not separable when expressed in terms of the interparticle coordinates, r_1, r_2 (127). A coordinate transformation is applied to explicitly show the center of mass dependence and simultaneously make the kinetic energy diagonal. That is, the kinetic energy, when expressed in terms of the transformed coordinates, is the sum of two square terms with no cross terms. The coordinate transformation is given by

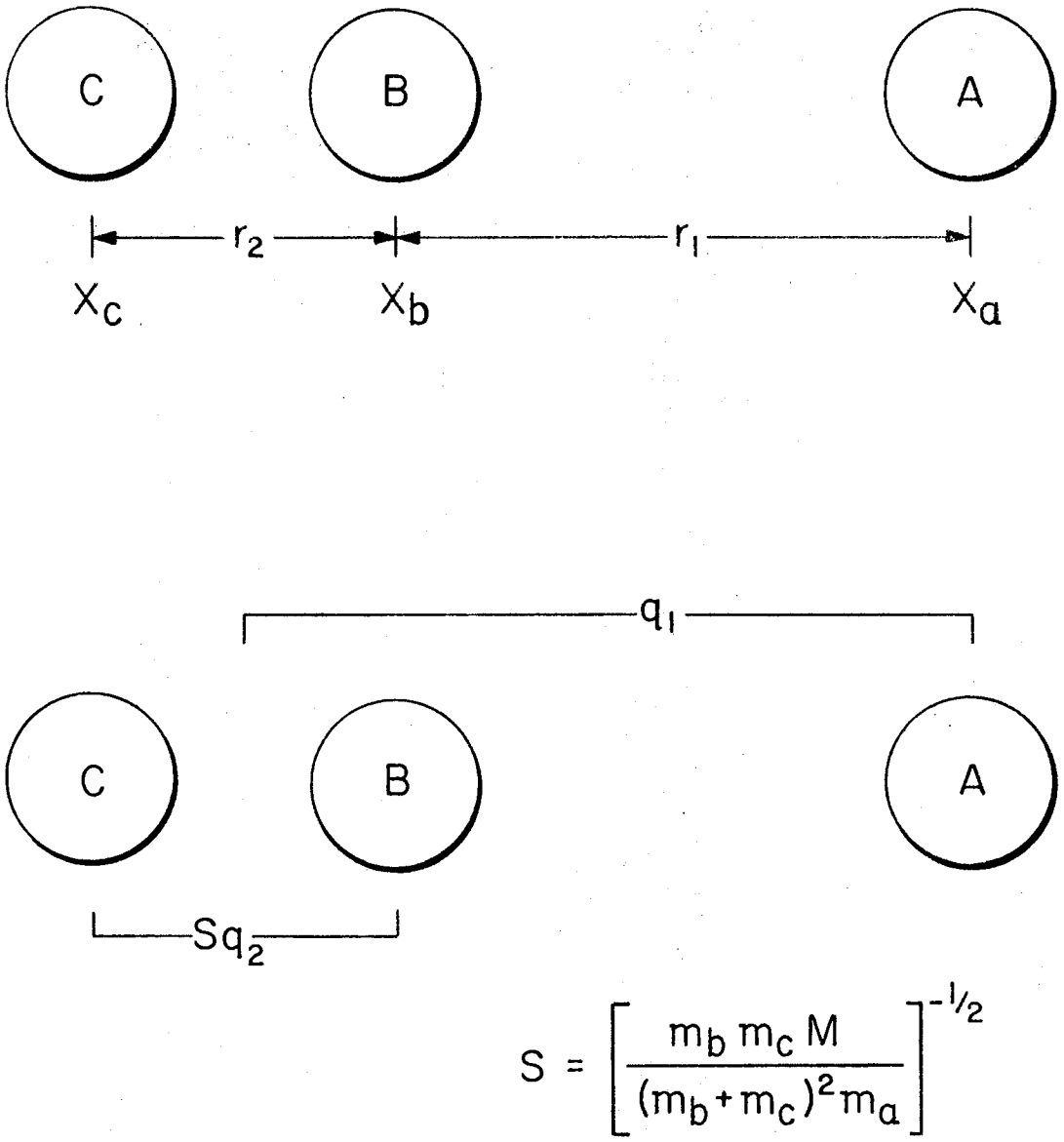

Figure 1. Linear Model, A + BC

$$X = (m_a x_a + m_b x_b + m_c x_c)/M$$

$$q_1 = x_a - (m_b x_b + m_c x_c)/(m_b + m_c) \qquad [3]$$

$$q_2 = (x_b - x_c)[m_b m_c M/(m_b + m_c)^2 m_a]^{\frac{1}{2}}$$

where M is the total mass of the system $(m_a + m_b + m_c)$. The lower half of Figure 1 illustrates these coordinates. X is the position of the center of mass of the system; q_1 locates atom A relative to the center of mass of the molecule BC; and q_2 is simply a mass-scaled internuclear BC distance. The task now is to invert the equations, that is express $\dot{x}_a$, $\dot{x}_b$, and $\dot{x}_c$ each as a function of $\dot{x}$, $\dot{q}_1$, $\dot{q}_2$ and the masses of the system. These expressions are then substituted into equation [2] to yield,

$$2T = M\dot{X}^2 + \mu(\dot{q}_1^2 + \dot{q}_2^2) \qquad [4]$$

where μ is the reduced mass, $m_a(m_b + m_c)/M$. With the following usual definitions,

$$L = T - V, \quad p_i = \partial L/\partial \dot{q}_i, \quad H = \sum_i p_i \dot{q}_i - L \qquad [5]$$

we have,

$$H = (M/2)\dot{X}^2 + \mu/2(\dot{q}_1^2 + \dot{q}_2^2) + V(q_1, q_2). \qquad [6]$$

The center of mass dependence can be dropped from [6] in both quantum and classical mechanics since the potential energy of the system does not depend on the location of the center of mass of the system. The classical Hamiltonian function for the internal motion of the system becomes,

$$H = \mu/2(\dot{q}_1^2 + \dot{q}_2^2) + V(q_1, q_2). \qquad [7]$$

In terms of the conjugate momenta defined by Equation [5], we can write,

$$H = (p_1^2 + p_2^2)/2\mu + V(q_1, q_2). \qquad [8]$$

Since the coordinates q are cartesian coordinates, the correspondence operation (128) can be carried out and the quantum mechanical Hamiltonian operator constructed with the form,

$$\underline{H} = \frac{-\hbar^2}{2\mu}\left(\frac{\partial^2}{\partial q_1^2} + \frac{\partial^2}{\partial q_2^2}\right) + \underline{V}(q_1, q_2) \qquad [9]$$

where $\underline{V}(q_1, q_2)$ is the potential energy operator within the framework of the Born-Oppenheimer approximation. Attention is now directed toward the specification of the potential-energy surface, $V(q_1, q_2)$.

The Potential-Energy Surface

Our present inability to compute accurate <u>a priori</u> multi-electron potential-energy surfaces with a reasonable amount of computer time precludes the use of such surfaces for dynamic studies. Recourse must be made to empirical or semiempirical methods. Unsymmetrical potential-energy surfaces which display dynamic effects and correspond to known chemical reactions have been published. An attempt to carry out a quantal study on a surface descriptive of one such chemical system ($I + H_2$) proved unsuccessful. This study will be discussed in more detail later.

In 1929, using the simplest valence-bond treatment, London (2) demonstrated that the potential energy of a system of three H atoms, A, B, and C could be expressed as

$$V(r_1,r_2,r_3) = Q_1 + Q_2 + Q_3 - (J_1^2 + J_2^2 + J_3^2 - J_{12} - J_{23} - J_{13})^{\frac{1}{2}} \qquad [10]$$

where r_1, r_2, and r_3 are the internuclear separations for AB, BC, and

AC respectively. Q_1, Q_2, and Q_3 are the coulomb integrals, J_1, J_2, and J_3 are the exchange integrals. Neglecting overlap the required coulomb and exchange integrals can be obtained in terms of the singlet and triplet state energies of the diatomic systems by use of the Heitler-London energy expression:

$$^1E_i = (Q_i + J_i)/S_i \quad \text{and} \quad ^3E_i = (Q_i - J_i)/S_i \qquad [11]$$

where ^1E_i and ^3E_i are the binding energies of the ground electronic state (singlet) and the first repulsive state (triplet) for the i-th diatomic pair. The overlap for the i-th diatomic pair is represented by S_i. The three sets of two equations like [11] can be solved for each Q_i and J_i for the three two-body interactions in terms of their ^1E_i and ^3E_i only if the singlet and triplet energies are known. A method of evaluating the London equation using spectroscopic information was proposed by Eyring and Polanyi (1) who used the Morse equation (129) to obtain singlet state energies. In order to have an analytic expression for $^3E(r)$, Sato (130) modified the Morse equation by changing the sign between the two exponential terms from minus to plus, and divided by two since he found that for H_2 this gave fairly good agreement with the shape of the triplet curve. His proposed form has been called the "anti-Morse" function. The singlet and triplet energy expressions are

$$^1E(r_1) = D[\exp\{-2\alpha(r_1-R_e)\} - 2\exp\{-\alpha(r_1-R_e)\}] \qquad [12]$$

and

$$^3E(r_1) = \tfrac{1}{2}D[\exp\{-2\alpha(r_1-R_e)\} + 2\exp\{-\alpha(r_1-R_e)\}] \qquad [13]$$

where D is the dissociation energy plus zero-point energy of AB, R_e the equilibrium separation between A and B, and α is a constant derived from

spectroscopic data, $\alpha = \pi\nu_o(2\mu/D)^{\frac{1}{2}}$. The experimental value of the fundamental vibration frequency is ν_o.

Sato (130) introduced an adjustable constant, which bears a formal resemblance to the square of the overlap integral, into the original London equation [10] and used the form,

$$V(r_1,r_2,r_3) = \frac{1}{1+S^2}\left[Q_1+Q_2+Q_3-(J_1^2+J_2^2+J_3^2-J_{12}-J_{23}-J_{13})^{\frac{1}{2}}\right] . \qquad [14]$$

The author prefers to write K instead of S^2 and simply regard K as a single adjustable parameter and make no resemblance to an overlap integral. It appears that there is no theoretical basis for equation [14] containing the S^2 term. The LEPS (London-Eyring-Polanyi-Sato) formulation must therefore be justified empirically. The LEPS potential and an empirical extension of the LEPS formulation are used in the present work. The extended LEPS surface is described by Polanyi (34). Three constants which provide flexibility in the shape of the energy surface are introduced. The S^2 term in the Sato modification is replaced by an S^2 for each atomic pair, symbolized a, b, and c:

$$V(r_1,r_2,r_3) = \frac{Q_1}{(1+a)} + \frac{Q_2}{(1+b)} + \frac{Q_3}{(1+c)} - \left[\frac{J_1^2}{(1+a)^2} + \frac{J_2^2}{(1+b)^2} + \frac{J_3^2}{(1+c)^2} - \frac{J_1 J_2}{(1+a)(1+b)} - \frac{J_2 J_3}{(1+b)(1+c)} - \frac{J_1 J_3}{(1+a)(1+c)}\right]^{\frac{1}{2}} \qquad [15]$$

The extended LEPS equation with the three extra empirical parameters is semitheoretically justified for triatomic systems composed of three hydrogen atoms (56). But systems containing more valence electrons require more configurations in their treatment by the valence-bond method. Hence, the secular equation is not solved analytically for a

simple energy expression. For systems with more than three valence electrons and with valence p electrons the LEPS and extended LEPS equations can more readily be interpreted as analytical interpolation devices rather than as semiempirical valence-bond calculations. It should be noted that in using this extended LEPS equation the expressions for the coulomb integrals and the exchange integrals are

$$\frac{Q_1}{(1+a)} = \tfrac{1}{2}\left[{}^1E(r_1) + \left(\frac{1-a}{1+a}\right){}^3E(r_1)\right] \qquad [16]$$

and

$$\frac{J_1}{(1+a)} = \tfrac{1}{2}\left[{}^1E(r_1) - \left(\frac{1-a}{1+a}\right){}^3E(r_1)\right] \qquad [17]$$

with similar expressions for Q_2 (Q_3) and J_2 (J_3) where a is replaced by b (or c) and r_1 by r_2 (or r_3).

The constants, a, b, and c for this investigation were chosen so as to obtain an asymmetric location for the crest of the energy barrier. It has been found (122) that for $b = c < a$ the barrier lies in the exit valley. The parameters used in constructing the surface are listed in Table I. The parameter AA, represents the a, b, and c values for AB, BC, and AC respectively. In this work the equilibrium internuclear distance for the ground electronic state R_e, the Morse constant α, for each pair of atoms, and the bond dissociation energies for AB and BC are the constants for H_2. The parameters correspond to those used by Polanyi and co-workers (122) to construct what they refer to as "surface II." In Figure 2 a contour map of the potential surface is shown. The contour values are in kilocalories per mole relative to molecule AB and atom C separated at infinity taken as zero. The classical barrier height (discounting zero point energy) was determined to be 7.05 ± 0.03 kcal/mole.

TABLE I

PARAMETERS USED IN CONSTRUCTING
THE EXTENDED LEPS SURFACE

Parameter	AB	BC	AC
D	4.7466 eV	4.7466 eV	3.4447 eV
α	1.027 a.u.$^{-1}$	1.027 a.u.$^{-1}$	1.027 a.u.$^{-1}$
R_e	1.402 a.u.	1.402 a.u.	1.402 a.u.
AA	0.30	0.05	0.05

A contour map of the potential surface in q-space (q_1, q_2 used as coordinates) is displayed in Figure 3.

The potential-energy surface employed in this study displays characteristics of the H + H_2 reaction since it is thermoneutral, the diatomic limits yield the correct H_2 fundamental vibration frequency and the barrier height is close to the experimental value of 8-10 kcal/mole (131) for the H + H_2 system. However, as Figures 2 and 3 show, the surface is asymmetric in contrast to the normal situation for the H + H_2 exchange. The representation is therefore ideally suited to determine the effects of surface asymmetry upon the adequacy of approximate scattering theories. The surface has an analytic representation in terms of elementary functions which allows the surface and its derivatives to be evaluated rather easily and quickly by a computer.

Quantum Dynamics

According to the Schrödinger postulate, the wavefunction of our

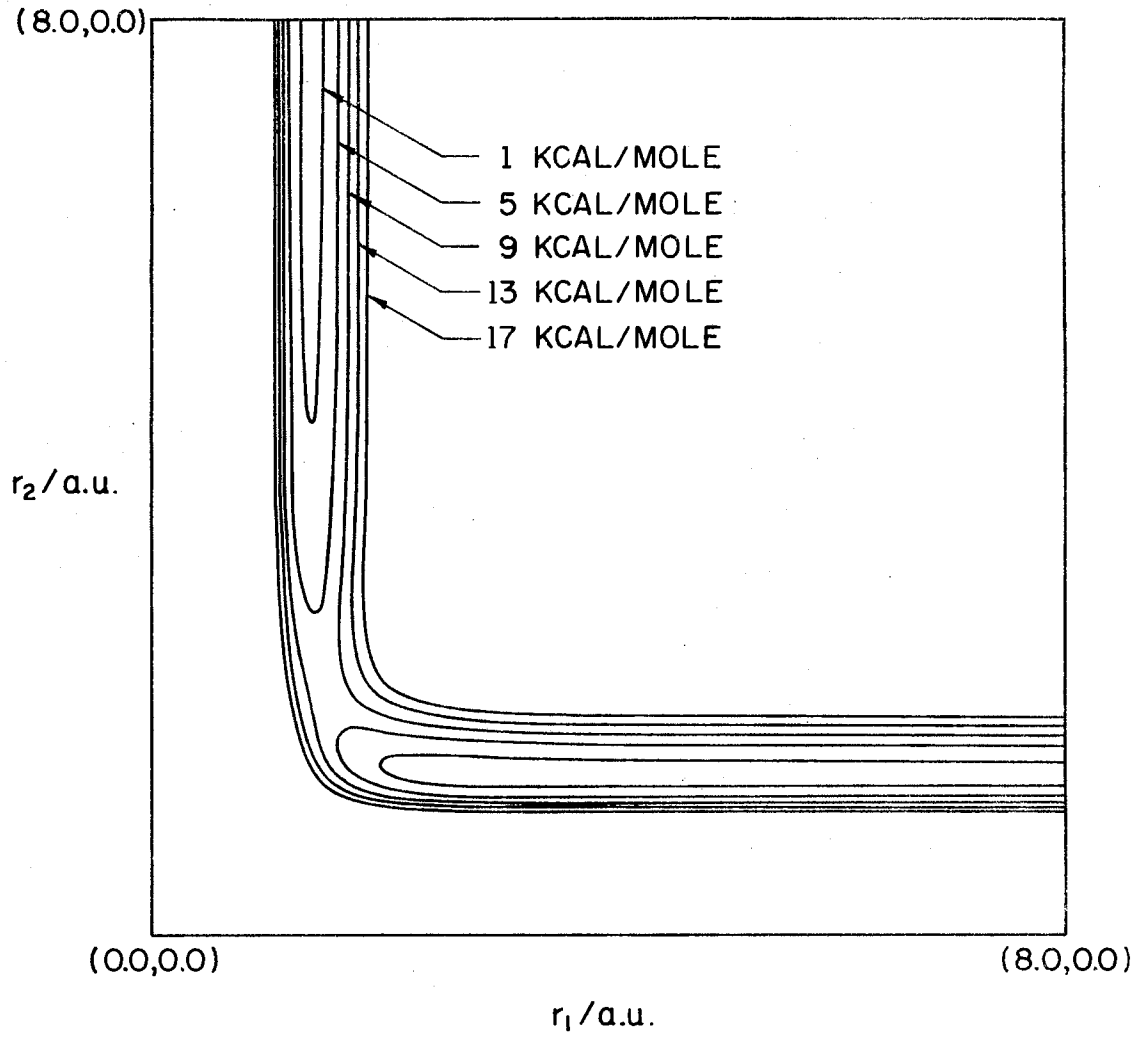

Figure 2. Contour Map of Potential Energy Surface in (r_1, r_2) Coordinate Space

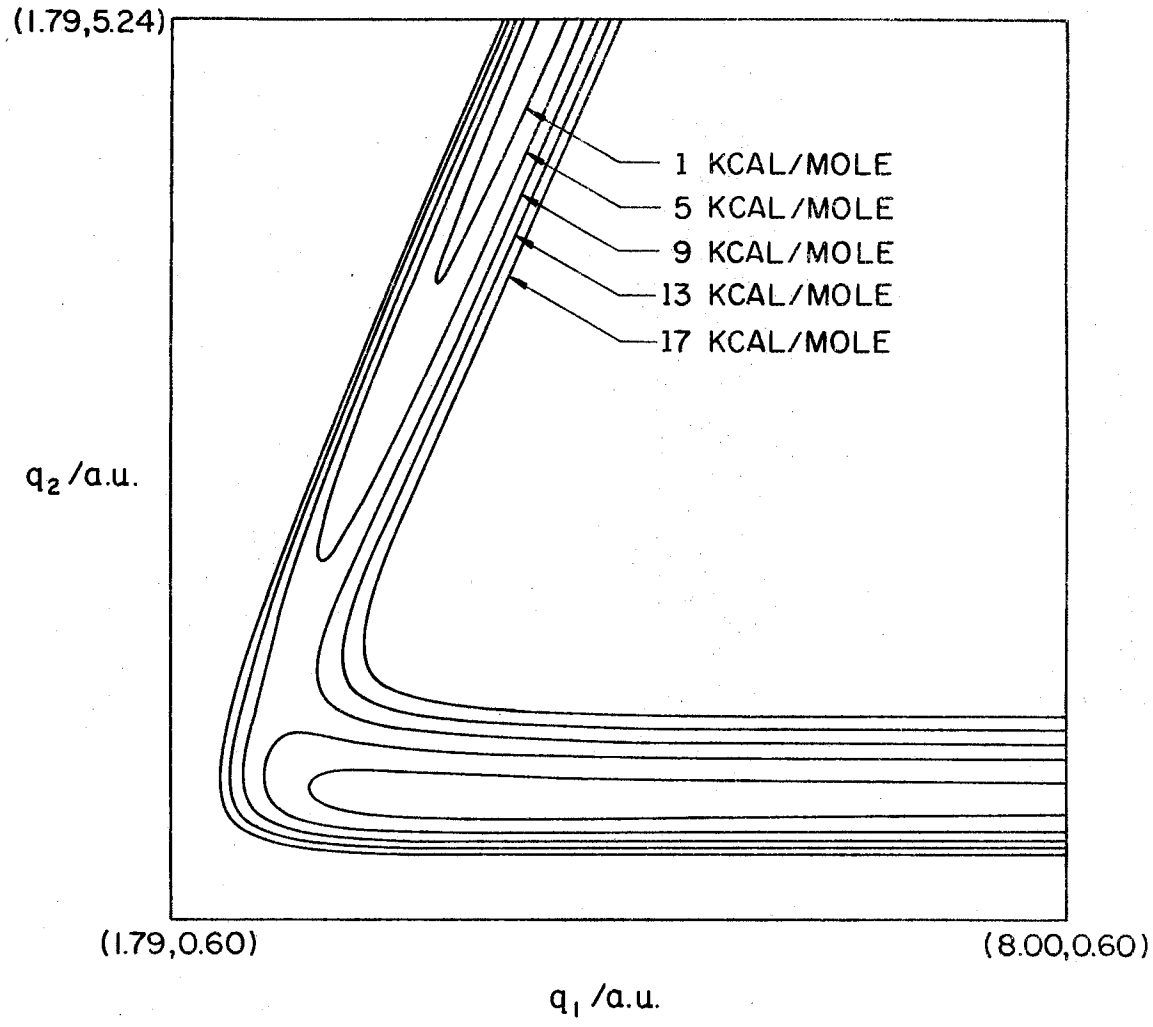

Figure 3. Contour Map of Potential Energy Surface in (q_1,q_2) Coordinate Space

model system is parameterized by time (t is not a dynamical observable) and develops in time according to the time-dependent Schrödinger equation

$$\underline{H}\Psi(q_1,q_2,t) = i\hbar \frac{\partial \Psi}{\partial t}(q_1,q_2,t) \qquad [18]$$

where $\underline{H}$ is the Schrödinger Hamiltonian operator equation [9], and $\Psi(q_1,q_2,t)$ is the system wavefunction in coordinate space. At $t = t_o$ the initial condition for [18] may be represented as

$$\Psi(q_1,q_2,t_o) = \Psi_o(q_1,q_2) \ . \qquad [19]$$

Henceworth the explicit dependence of Ψ on (q_1,q_2) will be surpressed in the notation to place emphasis on the time dependence of the wavefunction. However, it should be remembered that Ψ does depend on the variables q_1 and q_2 describing the positions of the nuclei of our system.

Recalling the definition of a derivative, it is apparent that for small Δt, $\Psi(t+\Delta t)$ is obtained from $\Psi(t)$ by means of a linear operator (132). For a finite time interval $t-t_o$, successive application on Ψ_o by an infinite number of infinitestimal time translational operators yields $\Psi(t)$ (132). Formally we write

$$\Psi(t) = \underline{U}(t,t_o)\Psi_o \qquad [20]$$

where $\underline{U}(t,t_o)$ is called the evolution operator and describes the time dependence of the system completely. Equation [20] shows that Ψ_o changes (or evolves) as time passes in a well defined way. From the definition [20] follows the relation

$$\underline{U}(t_3,t_o) = \underline{U}(t_3,t_2)\ \underline{U}(t_2,t_1)\ \underline{U}(t_1,t_o) \qquad [21]$$

where $t_o \leq t_1 \leq t_2 \leq t_3$. Furthermore, at $t=t_o$ the initial condition is

$$\underline{U}(t_o, t_o) = \underline{1}. \qquad [22]$$

Since the Hamiltonian operator is hermitian, the evolution operator can be shown to be a Unitary operator (133). Substitution of the relation $\Psi(t) = \underline{U}(t,t_o)\Psi_o$ into [18] gives

$$\begin{aligned} i\hbar\frac{\partial}{\partial t}(\underline{U}\Psi_o) &= \underline{H}(\underline{U}\Psi_o) \\ i\hbar\frac{\partial}{\partial t}\underline{U}(t,t_o) &= \underline{H}\,\underline{U}(t,t_o)\,. \end{aligned} \qquad [23]$$

To obtain the explicit form for the evolution operator, the solution to the partial differential equation [23] with the initial condition given by [22] is required. Three different cases may be considered in the solution to [23] (134). For this particular study, only one example is investigated, that being the case where the Hamiltonian does not contain the time explicitly. Under this restriction one can immediately solve [23] and represent the evolution operator in the form

$$\underline{U}(t,t_o) = \exp\left[-\frac{i}{\hbar}\underline{H}(t-t_o)\right] \qquad [24]$$

where the exponential of the operator $\underline{H}$ is defined by series expansion of the exponential function. The solution of [20] may then be written as

$$\Psi(t) = \exp\left(\frac{-i\underline{H}(t-t_o)}{\hbar}\right)\Psi_o \qquad [25]$$

In this case the evolution operator is translationally invariant (134) with respect to the time axis, that is,

$$\underline{U}(t+\delta t, t_o+\delta t) = \underline{U}(t,t_o)\,. \qquad [26]$$

This is in contrast to the general case in which the evolution operator $\underline{U}(t,t_o)$ is parameterized by time and at each instant, a different $\underline{U}(t,t_o)$ is required to transform the wavefunction. In this study $\underline{U}(\Delta t)$ is time invariant since H is independent of time. If the total time span $t-t_o$ is divided into n intervals of equal size, we may write

$$\begin{aligned}
\Psi(t_o + \Delta t) &= \underline{U}(\Delta t)\Psi_o \\
\Psi(t_o + 2\Delta t) &= \underline{U}(\Delta t)\Psi(t_o + \Delta t) = \underline{U}(\Delta t)\ \underline{U}(\Delta t)\Psi_o \\
\Psi(t_o + 3\Delta t) &= \underline{U}(\Delta t)\Psi(t_o + 2\Delta t) = \underline{U}(\Delta t)\ \underline{U}(\Delta t)\ \underline{U}(\Delta t)\Psi_o \\
&\ \ \vdots \\
(t_o + n\Delta t) &= [\underline{U}(\Delta t)]^n \Psi_o \ .
\end{aligned} \qquad [27]$$

When the Hamiltonian does not contain the time explicitly, the result of operating on Ψ_o with $\underline{U}(t,t_o)$ can be found quite easily. The normalized eigenfunctions of $\underline{H}$ satisfying the relation

$$\underline{H}\phi_k = E_k\phi_k \qquad [28]$$

may be introduced as a basis, and since the basis forms a complete set $\{\phi_k\}$, the expansion of Ψ_o in terms of this set can be made

$$\Psi_o = \sum_k c_k\phi_k \qquad [29]$$

$$\begin{aligned}
\Psi_o &= \underline{U}(\textstyle\sum_k c_k\phi_k) \\
&= \textstyle\sum_k c_k \underline{U}\phi_k \\
&= \textstyle\sum_k c_k [\exp(\frac{-i\Delta t}{\hbar}\underline{H})]\phi_k \\
&= \textstyle\sum_k c_k \left(\underline{1} - \frac{i\Delta t}{\hbar 1!}\underline{H} + (\frac{i\Delta t}{\hbar})^2 \frac{HH}{2!} - (\frac{i\Delta t}{\hbar})^3 \frac{HHH}{3!} + \ldots\right)\phi_k
\end{aligned}$$

$$= \sum_k c_k \left(1 - \frac{i\Delta t}{\hbar}\epsilon_k + \left(\frac{i\Delta t}{\hbar}\right)^2 \frac{\epsilon_k^2}{2!} - \left(\frac{i\Delta t}{\hbar}\right)^3 \frac{\epsilon_k^3}{3!} + \ldots\right)\phi_k$$

$$= \sum_k c_k \exp[-i\Delta t/\hbar\epsilon_k]\phi_k \qquad [30]$$

The result is simply the expansion of the solution into stationary states with the time dependence contained within the phase terms $\exp[-i\Delta t\epsilon_k/\hbar]$.

In the case of a free particle in which all values of the momentum are allowed, the summation index in the expansion [29] may assume continuous values. In carrying out the above expansion progress toward the solution of the scattering problem, has been nil. Indeed the task has simply been amended to one of finding the eigenfunctions and the expansion coefficients. Wilson, et al. (135) have used the expansion method to calculate the time evolution of anharmonic oscillators. Since the time and effort involved in finding the eigenfunctions and expansion coefficients would be large, the present problem is studied by an alternate procedure.

The effect of operating by the evolution operator directly on Ψ_o is sought. An approximate $\underline{U}'(\Delta t)$ to the time evolution operator is required since the infinite series expansion [24] of $\underline{U}$ is not computationally suitable. Once $\underline{U}'(\Delta t)$ is chosen the calculation proceeds in the manner suggested by [27]; the evolution of Ψ_o in finite time steps is carried out by repeated application of $\underline{U}'(\Delta t)$. Successive application of $\underline{U}'(\Delta t)$ n times on the initial wavefunction advances the wavefunction through n time steps.

Selection of Numerical Method and Derivation of Numerical Equations

Equation [18] belongs to the class of partial differential equations referred to as parabolic partial differential equations. Varga (136) has shown that the solution of parabolic partial differential equations can be reduced to one of approximating an "exponential" matrix of the form exp(-S) where S represents a matrix. In analogy, solution of equation [18] requires an approximation to the exponential expansion representing the time evolution operator,

$$\underline{U}'(\Delta t) = \exp[-i\underline{H}\Delta t/\hbar] \ . \qquad [31]$$

Possible approximations to the exponential expansion are discussed by Varga (136) and McCullough (5) and include a) the first-order and b) second-order forward difference methods, c) the first-order backward difference method, and d) the Crank-Nicholson (137) method. These are listed below in the aforementioned order.

$$\underline{U}(\Delta t) \simeq \underline{I} - (i\Delta t/\hbar)\underline{H} \qquad [32]$$

$$\underline{U}(\Delta t) \simeq \underline{I} - (i\Delta t/\hbar)\underline{H} - \tfrac{1}{2}(\Delta t/\hbar)^2 \underline{H}^2 \qquad [33]$$

$$\underline{U}(\Delta t) \simeq [\underline{I} + (i\Delta t/\hbar)\underline{H}]^{-1} \qquad [34]$$

$$\underline{U}(\Delta t) \simeq [\underline{I} + (i\Delta t/2\hbar)\underline{H}]^{-1} [\underline{I} - (i\Delta t/2\hbar)\underline{H}] \qquad [35]$$

Since $\underline{H}$ is Hermitian, the exact evolution operator is unitary. The unitarity of the evolution operator implies that probability is conserved and therefore the approximate method used for $\underline{U}(\Delta t)$ should also be unitary. The approximation used should be computationally stable. That is, errors (roundoff, for instance) introduced during the

calculation do not become so large that they overwhelm the true solution. A third and very important requirement of the approximate operator is that it should be as accurate an approximation as possible to the exact evolution operator. The highest order term in the series expansion for the exact operator that is correctly reproduced by the approximate operator may be taken as the order of accuracy. Since the Crank-Nicholson method is unitary, accurate to second order, stable (136) (138) and relatively easy to use, we follow the procedure used by McCullough and Wyatt (80) in selecting form [35] as the basic approximate method for our numerical scheme. More complete descriptions of the above approximate methods are available (5) (136) and in general all of the methods may be generated or described in terms of Padé matrix approximations (136).

Substituting [35] into [27] yields

$$[\underline{I} + (i\Delta t/2\hbar)\underline{H}]\Psi(t_o + \Delta t) = [\underline{I} - (i\Delta t/2\hbar)\underline{H}]\Psi_o \ . \qquad [36]$$

The time development of Ψ_o is carried out by solving for $\Psi(t_o + \Delta t)$, substituting this result back into the right hand side of [36] generating $\Psi(t_o + 2\Delta t)$, and continuing this process to develop the wavefunction in time. Equation [36] does not represent an applicable numerical shceme since the Hamiltonian operator contains the second partial derivatives of the wavefunction with respect to the spatial variables q_1 and q_2. Discretizing the spatial variables requires the values of Ψ be calculated at a set of points in the q_1,q_2-plane given by $q_1 = (j-1)\Delta q_1 + q_1^0$, $q_2 = (i-1)\Delta q_2 + q_2^0$ where $j = 1,2,\ldots J$, and $i = 1,2,\ldots I$, called a grid (or net or mesh) and q_1^0 and q_2^0 are convenient starting values for q_1 and q_2 respectively. Δq_1 and Δq_2 are small increments and determine

the mesh size. Since Ψ is defined throughout (q_1,q_2) configuration space, the exact grid is of infinite area (I and J are infinite). The calculation is made feasible by reducing the grid size to finite dimension and imposing the boundary condition that the wavefunction is zero in all space not encompassed by the mesh. Chemically, the most interesting region of q-space is that region displayed by the contour map (Figure 3). Accordingly, we choose to superimpose an L-shaped grid on this region. (See Figure 4).

The replacement of derivatives and partial derivatives by finite difference quotients can be found in most standard numerical analysis texts (138). Second partial derivatives of functions of several variables can be expressed by a difference formula simply by holding all but one of the variables constant. Ralston (139) derives the necessary equations required to make the standard replacement for a partial derivative (138). Referring to Figure 4 the second partial derivative of some function $u(q_1,q_2)$ with respect to q_1 is sought at the point $q_1 = x$, $q_2 = y$. Application of the standard finite difference formula gives

$$\left.\frac{\partial^2 u}{\partial q_1^2}\right|_{\substack{q_1=x \\ q_2=y}} \approx [u(x_o,y) - 2u(x,y) + u(x_1,y)] / (\Delta x)^2 \qquad [37]$$

$$\left.\frac{\partial^2 u}{\partial q_2^2}\right|_{\substack{q_1=x \\ q_2=y}} \approx [u(x,y_o) - 2u(x,y) + u(x,y_1)] / (\Delta y)^2 \qquad [38]$$

where Δx and Δy are the grid spacings in the x and y directions. In this investigation equal horizontal and vertical grid spacings are used,

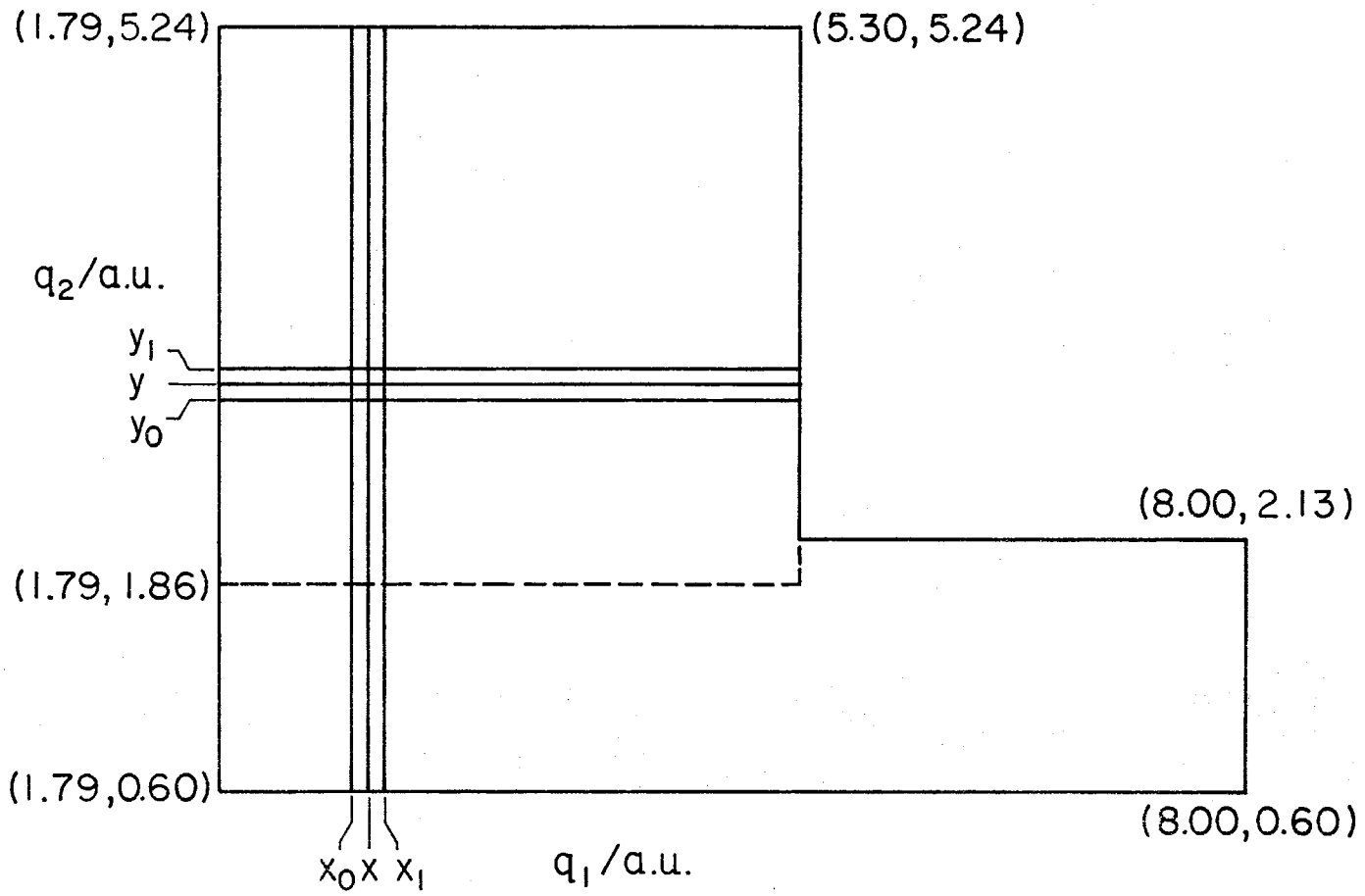

Figure 4. Region in Which Solution of [36] Is Desired

that is, $\Delta x = \Delta y = \Delta q_1 = \Delta q_2 = \Delta q$. Substituting Ψ for u and inserting q_1 and q_2 into [37] and [38] yields

$$\frac{\partial^2\Psi}{\partial q_1^2} + \frac{\partial^2\Psi}{\partial q_2^2} \approx \frac{[\Psi(q_1 - \Delta q, q_2) - 2\Psi(q_1,q_2) + \Psi(q_1 + \Delta q, q_2) + \Psi(q_1, q_2 - \Delta q) - 2\Psi(q_1,q_2) + \Psi(q_1, q_2 + \Delta q)]}{(\Delta q)^2} \quad [39]$$

Recalling that $q_1 = (j-1)\Delta q_1 + q_1^0$ and $q_2 = (i-1)\Delta q_2 + q_2^0$ Equation [39] can be rewritten as

$$\frac{\partial^2\Psi}{\partial q_1^2} + \frac{\partial^2\Psi}{\partial q_2^2} \approx [\Psi_{i,j-1} - 2\Psi_{i,j} + \Psi_{i,j+1} + \Psi_{i-1,j} - 2\Psi_{i,j} + \Psi_{i+1,j}]/(\Delta q)^2 \quad [40]$$

Application of [40] transforms [18] into a useable numerical procedure in the form of a matrix equation. The region of q-space of Figure 4 is covered by a grid or mesh produced by the intersection points of m vertical and n horizontal lines. Any convenient numbering scheme can be used to assign a number or set of numbers to each point in the region. If the address consists of one number then the values of a function at the grid points of the region can be represented by a vector, each component referring to a function value at a given point of the grid. On the other hand if each point is addressed by a set of two numbers, the first referring to a particular horizontal line and the second to a specific vertical line, then function values at grid points in the region can be conveniently stored in a two dimensional matrix. The right hand side of our matrix equation contains the matrix (or vector) $\underline{\Psi}_o$ which contains values of the wavefunction at all points on the grid at time t_o; the unknowns consist of values of the wavefunction at all points on the grid at time, $t_o + \Delta t$, represented by the matrix (vector) $\underline{\Psi}\ (t_o + \Delta t)$.

Substitution of [40] into [36] yields

$$\Psi_{i,j} + (i\Delta t/2\hbar)\left[\frac{-\hbar^2}{2\mu}(\Psi_{i,j-1} - 4\Psi_{i,j} + \Psi_{i,j+1} + \Psi_{i-1,j} + \Psi_{i+1,j})/(\Delta q)^2 + V_{i,j}\Psi_{i,j}\right] =$$

$$\Psi^0_{i,j} - (i\Delta t/2\hbar)\left[\frac{-\hbar^2}{2\mu}(\Psi^0_{i,j-1} - 4\Psi^0_{i,j} + \Psi^0_{i,j+1} + \Psi^0_{i-1,j} + \Psi^0_{i+1,j})/(\Delta q)^2 + V_{i,j}\Psi^0_{i,j}\right] \quad [41]$$

where $V_{i,j}$ is the potential energy at the point (q_1,q_2) with q_1 and q_2 expressed in terms of i and j as above. All Ψ values on the left hand side (LHS) are at time $t_o + \Delta t$, and all Ψ^0 values on the right hand side (RHS) are for time t_o. Introduction of the definitions,

$$r = \hbar\Delta t/2\mu(\Delta q)^2 \quad \text{and} \quad U_{i,j} = [2\mu(\Delta q)^2/\hbar^2]V_{i,j} \quad [42]$$

allows [41] to be written as

$$\Psi_{i,j} + ir/2\left[4\Psi_{i,j} - \Psi_{i+1,j} - \Psi_{i-1,j} - \Psi_{i,j+1} - \Psi_{i,j-1} + U_{i,j}\Psi_{i,j}\right] = K_{i,j} \quad [43]$$

where $K_{i,j}$ represents the RHS of [41]. The requirement that Ψ vanish at all times outside the L-shaped region dictates the boundary conditions,

$$\Psi_{i,0} = \Psi_{i,m+1} + \Psi_{0,j} = \Psi_{n+1,j} = 0 \quad [44]$$

Equation [43] may be multiplied by $-2i/r$ to give

$$(4 + U_{i,j} - 2i/r)\,\Psi_{i,j} - \Psi_{i+1,j} - \Psi_{i-1,j} - \Psi_{i,j+1} - \Psi_{i,j-1} = B_{i,j} \quad [45]$$

where $B_{i,j} = -2iK_{i,j}/r$. Assuming for the moment that the RHS of [45] is known, then the values of $\Psi_{i,j}(t_o + \Delta t)$ on the LHS for all i and j are sought.

Two general matrix methods are available for the solution of [45], the point iterative method and the line iterative method. In applying

the point method to [45], an initial Ψ matrix is obtained (perhaps by guess) and then [45] is solved for each $\Psi_{i,j}(t_o + \Delta t)$ by using the assumed values of the other elements of $\underline{\Psi}$ that are needed. The solution of [45] for all i and j gives a new estimate of $\underline{\Psi}$. The process is repeated to refine $\underline{\Psi}$ and when successive estimates of $\underline{\Psi}$ differ by less than some allowed tolerance, the resulting matrix is the desired solution of [36] and gives the values of $\Psi_{i,j}(t_o + \Delta t)$ at each point on the grid.

The point iterative methods often converge slowly (5) to the desired solution and hence the line Gauss-Seidel method (140) is used in this work. This line-iterative method attempts to speed up the convergence by solving for all $\Psi_{i,j}$ on a row or line (fixed i) simultaneously. For the i-th row of $\underline{\Psi}$ the following definitions are made,

$$\underline{D}_i = \begin{bmatrix} a_{i1} & -1 & 0 & \cdots & 0 \\ -1 & a_{i2} & -1 & \cdots & 0 \\ \cdot & \cdot & & & \cdot \\ \cdot & \cdot & & & \cdot \\ \cdot & \cdot & & & \cdot \\ 0 & 0 & \cdots & -1 & a_{im} \end{bmatrix} \qquad \underline{\Psi}_i = \begin{bmatrix} \Psi_{i1} \\ \Psi_{i2} \\ \cdot \\ \cdot \\ \cdot \\ \Psi_{im} \end{bmatrix} \qquad [46]$$

$$\underline{B}_i = \begin{bmatrix} B_{i1} \\ B_{i2} \\ \cdot \\ \cdot \\ \cdot \\ B_{im} \end{bmatrix}$$

where $a_{i,j} = [4 + U_{i,j} - 2i/r]$, and the line method converts [45] to

$$\underline{D}_i \underline{\Psi}_i - \underline{\Psi}_{i+1} - \underline{\Psi}_{i-1} = \underline{B}_i \quad . \qquad [47]$$

The solution of [45] is obtained by assuming a value for each element of $\underline{\Psi}$, and then solving [47] for each row of $\underline{\Psi}$. The solution of [47] for each row gives the values of the wavefunction at each point on the grid for time $t_o + \Delta t$. The Line Gauss-Seidel method utilizes each new row or line of points in the iteration procedure just as soon as it is available. The solution of the points on the i-th row, for instance, is obtained by using the values of the points just calculated for the (i-1) row. Accordingly, the Line Gauss-Seidel method presents a distinct advantage over other line methods which do not use the new values for a row at such an early stage. Rearranging [47] the Line Gauss-Seidel method may be explicitely expressed as

$$\underline{D}_i \underline{\Psi}_i^{(k+1)} = \underline{B}_i + \underline{\Psi}_{i-1}^{(k+1)} + \underline{\Psi}_{i+1}^{(k)} \qquad [48]$$

where the superscript represents the iteration cycle. For the first iteration cycle it is necessary to have a guess or approximation for $\underline{\Psi}$. The Line Gauss-Seidel method will converge for any starting $\underline{\Psi}$ if the $V_{i,j}$ (or equivalently $U_{i,j}$) are all non-negative (5). In practice, however, since one attempts to minimize the computation time (or computing bill) a good choice for the initial $\underline{\Psi}$ is needed. Given the values for $\Psi_{i,j}$ for the entire grid at time t_o, an initial guess for $\Psi_{i,j}$ at time $t_o + \Delta t$, is obtained by applying approximation [33]. The iterative computation becomes much more efficient since the starting $\underline{\Psi}$ is a reasonable approximation to the correct answer. An unreasonable initial guess for $\underline{\Psi}$ can cause the number of operations to become depressingly large. Applying the initial guess procedure outlined above, the rate of convergence was found to depend on the time step size

Δt used. If the time step size is halved, the number of iterations required for convergence is reduced almost exactly to one-half of its previous amount. The solution of [48] for each line or row of the Ψ matrix yields the results for the $(k+1)$ iteration. When successive cycles give values of $\Psi_{i,j}$ which differ by less than a small amount, ε, the desired solution to [36] has been obtained. It was found that the real and imaginary parts of the wavefunction converged simultaneously and hence the following convergence criteria was sufficient.

$$\left| \text{Real } (\Psi_{i,j}^{(k+1)} - \Psi_{i,j}^{(k)}) \right| < \varepsilon \qquad [49]$$

where the vertical bars represent the absolute value. The desired solution was assumed when the above condition was satisfied for all grid points (all i and j). The value of ε used was 1.0×10^{-5}. The solution to [48] was obtained directly by using a well known algorithm (141) applicable to matrix equations like [48] where the $\underline{D}_i$ are tridiagonal matrices.

In practice $\Psi_{i,j}$ values for each point of the L-shaped grid were stored in two matrices, one matrix contained values for all $\Psi_{i,j}$ on the lower part of the L, another matrix was used to store values for all $\Psi_{i,j}$ on the upper portion of the L. The dimensions of the "lower" matrix were 35 rows and 139 columns; for the "upper" matrix, 69 rows and 79 columns. Therefore the grid contained (consisted of) $35 \times 139 + 69 \times 79 = 10,316$ points. The grid spacing used in each direction was $\Delta q = 0.045$ a.u., which is slightly smaller than the value of 1/22 used in case c of Mazur and Rubin's paper (101).

Numerical values for distance, time, mass, and energy used in this work are in so called "molecular units" described in reference 118 and

are defined in Table II

TABLE II

MOLECULAR UNITS

Quantity		
Mass	1 atomic mass unit = 1 a.m.u.	$= 1.6604345 \times 10^{-24}$ g
Distance	1 atomic unit = 1 a.u.	$= 0.529167 \times 10^{-8}$ cm
Energy	1 Electron Volt = 1 eV	$= 1.60210 \times 10^{-12}$ erg
Time	1 time unit = 1 t.u.	$= 0.53871469 \times 10^{-14}$ sec

Initial Conditions

Formal time-dependent quantum mechanics does not directly give the exact initial wavefunction for a complex system but rather describes the evolution of some chosen Ψ_o. For the chemical reaction being studied, an initial wavefunction Ψ_o is sought to describe a free (or unbound) A atom far removed from the bound BC molecule. Evolution of Ψ_o should result in the approach of A toward BC and eventually result in a collision with BC. In choosing Ψ_o one is limited to a large degree by the computing machinery and computing time presently available. For example, all of the possible energy states of the BC molecule cannot be accurately represented in a computationally usable

wavefunction. When A is far from BC the initial wavefunction can be written as a product of two functions; one a function of q_1 only and the other a function of q_2 alone:

$$\Psi_o = \phi(q_1)\,\chi(q_2)\ . \qquad [50]$$

As described earlier the potential-energy surface uses Morse potentials to describe the bound molecules, BC and AB. Accordingly Morse wavefunctions are used for $\chi(q_2)$. In all calculations to be described later except one, the ground state Morse wavefunction is used. In order to assess the importance of vibrational energy in the quantal dynamics of the A + BC system the first excited vibrational Morse wavefunction was also utilized.

The Morse potential given by equation [12] can be substituted into the time-independent Schrödinger equation and the Morse wavefunctions can be obtained in closed form (129) (142). The ground state Morse wavefunction is given by

$$\chi_o(q_2) = N_o \exp\left[\frac{-(b+1)}{2}\exp[-\alpha(q_2-q_o)]\right]\left\{(b+1)\exp[-\alpha(q_2-q_o)]\right\}^{b/2} \qquad [51]$$

where N_o is the normalization constant for the ground vibrational state given below, $b = (8\mu D)^{\frac{1}{2}}/\alpha\hbar - 1$, μ is the reduced mass of BC, D and α are the values defined in Table I for BC, and q_o is the q-space value for the equilibrium internuclear distance, namely $q_o = S^{-1}R_e$ where S is defined in Figure 1 and R_e for BC is given in Table I. The normalization constant for the n-th vibrational state Morse wavefunction is

$$N_n = (TN)_n = (1/M_n)^{\frac{1}{2}} \qquad [52]$$

where TN is simply the normalization constant variable name used in the computer program. Following equation [9] of reference (142) M for the

n-th vibrational function is defined as

$$M_n = \frac{(n!)^2}{\alpha A^{(A-2n-1)}} \sum_{s=0}^{n} \frac{\Gamma(A-2n+s-1)}{s!} \qquad [53]$$

where α is defined as above, A = b+1, and Γ represents the gamma function.

The first vibrational state Morse wavefunction can be expressed as

$$\chi_1(q_2) = N_1 F_1 F_2 F_3 \qquad [54]$$

where $F_1 = \exp(-DF)$; $F_2 = F^{((A-2n-1)/2)}$; $F_3 = z^n - (A-n-1)nz^{(n-1)}$; $z = AF$; $D = A/2$; $F = \exp[-\alpha(q_2-q_o)]$; and N_1 is the normalizing constant for the first vibrational state. As will be apparent later, the first vibrational state wavefunction has one node located at the point $q_2 = q_o$.

A brief digression seems appropriate and hopefully will be fruitful before explicitly stating the functional form of $\phi(q_1)$ used. In accounting for experimental observations our theoretical intuition must guide us in finding $\phi(q_1)$ which describes, at least approximately, the classical motion of a particle which has both reasonably definite momentum and reasonably definite position.

By defining a vector $\vec{k}$ which points in the direction of wave propagation and has magnitude $2\pi/\lambda$, one may write the de Broglie relation as $\vec{p} = \hbar\vec{k}$. A plane wave propagating in the x-direction with wavelength $\lambda = 2\pi/k$ and frequency $E/\hbar$ can be associated with the motion of a free particle moving in the x-direction with momentum $p = \hbar k$. A plane wave propagating toward increasing x may be written as

$$\phi_1(x,t) = A\exp[i(kx-\omega t)] \qquad [55]$$

and a wave propagating toward decreasing x is

$$\phi_2(x,t) = A\exp[-i(kx+\omega t)] \; . \qquad [56]$$

The above plane waves correspond to particle motions with momenta which is precisely defined by $\vec{p} = \hbar\vec{k}$ but have absolute squares of the amplitudes which are constant for all x and t and hence these plane waves leave the position of the particle entirely unspecified. However, a degree of localization can be obtained by superposition of several different plane waves of different wave number.

The formation of localized compact wave packets by the superposition of plane waves of differing wave numbers is possible by Fourier analysis (143). One can choose any number of several example functions, for instance, an approximately symmetric distribution of k_x about some mean value $\bar{k}_x$ and form a function called a wave packet. The function or wave disturbance is obtained by superimposing an infinite number of plane waves. If the example function chosen is a Gaussian distribution of k_x values, then the resulting wavepacket formed is also a Gaussian distribution in coordinate space. The interpretation made is that the particle is most likely to be found at a position where the magnitude of the wavepacket function is appreciable. Thus the description of a particle which is localized within a distance, say Δx, of a convenient origin can be accomplished at the expense of combining waves of wave numbers in a range Δk_x about $\bar{k}_x$. The value of the product $\Delta x \Delta k_x$ is dictated by the Heisenberg Uncertainty Principle which limits the accuracy with which position and momentum can be simultaneously ascribed to the particle.

For the somewhat arbitrary choice of $\phi(q_1)$ the normalized Gaussian wavepacket is chosen.

$$\phi(q_1) = (2\pi\delta^2)^{-\frac{1}{4}} \exp[-(q_1-q_{10})^2/4\delta^2] \exp[-ik_0 q_1] \qquad [57]$$

The packet is centered symmetrically in q-space about the point q_{10} and has a root-mean-square width δ. For a Gaussian curve the amplitude is down to $1/\sqrt{e}$ of its maximum at one standard deviation. In the case of the above Gaussian packet whose shape is determined by δ, the standard deviation σ is given simply by $\delta\sqrt{2}$. The complex exponential term furnishes the wavepacket with an initial velocity in toward the interaction region (region of small q_1) with momentum $p = \hbar k_0$. As is generally the case for wavepackets, the Gaussian wavepacket consists of a product of two terms, one of which is an envelope and the other is a rapidly oscillating term (complex exponential) within the envelope. In addition the Gaussian distribution results in the minimum value for the product $\Delta x \Delta k_x$, allowed by the uncertainty principle. The spread in coordinate space, Δx, is the standard deviation σ_x and the range of k values is σ_k. It can be shown that for a Gaussian distribution at time t=0, $\sigma_x \sigma_x = \frac{1}{2}$ or $\sigma_x \sigma_p = \hbar/2$. The particular Gaussian represented by [57] has $\sigma_x = \delta\sqrt{2}$ and therefore $\sigma_k = (\frac{1}{2})(1/\sigma_x) = 1/(2\delta\sqrt{2})$. In all calculations performed $\delta = 0.25$ a.u. and thus the numerical values of σ_x and σ_k are $\sigma_x = \sqrt{2}/4$ and $\sigma_k = \sqrt{2}$. The above wavepacket is used to represent, describe, or mimic atom A initially localized about the point q_{10}. Another form of $\phi(q_1)$ has been used by other investigators (80) (101).

As time proceeds the width of the wavepacket in configuration space increases and at time t an uncertainty in the position of the particle results over and beyond the initial uncertainty. A simple physical interpretation is that two segments of a wavepacket differing in momentum will differ in distance traveled at time t. When this distance becomes comparable with the width of the initial packet, the packet will

begin to spread.

Calculational Procedure and Parameters

The translational packet possesses an average kinetic energy consisting of two sources. The exponential driving term produces a contribution of $\hbar^2 k_0^2/2\mu$ and the "shape" kinetic energy (80) is $(\hbar^2/2\mu)(1/4\delta^2)$. The average translational energy is therefore

$$E_t = \hbar^2 \ (k_0^2 + 1/4\delta^2)/(2\mu). \qquad [58]$$

Various k_0 values were used in the quantum calculations and are given in Table III. Each calculation has been assigned an arbitrary label A, B, C, D, or E, merely for convenience. This label is used when reference is made to a particular calculation.

The total energy of the atom-molecule system is the sum of the translational energy of the packet given above plus the vibrational energy of molecule BC in the n-th vibrational level. The vibrational energy of a "Morse oscillator" in the n-th vibrational level is given by Morse (129) and relative to the "bottom of the well" is

$$E(n) = h\omega(n+\tfrac{1}{2}) - (h^2\omega^2/4D) \ (n+\tfrac{1}{2})^2 \qquad [59]$$

where $\omega = (\alpha/2\pi)(2D/\mu)^{\frac{1}{2}}$. D and α are defined as before for molecule BC and are given in Table I. The reduced mass of BC is μ. The parameter values used for the quantum calculations are given in Table III. The translational energies E_t, are calculated using equation [58] and the vibrational energies E_v are obtained from [59].

In the earlier stages of a calculation a time step size, $\Delta t = 2.155 \times 10^{-16}$ sec was normally used. As the wavepacket moved closer to and into the interaction region, the time step was reduced, usually by a

TABLE III

INITIAL VALUES FOR QUANTUM CALCULATIONS

Calculation	k_0 ($a.u.^{-1}$)	q_{10} (a.u.)	E_t kcal/mole	eV	n^*	E_v kcal/mole	eV	E_T^{**} kcal/mole
A	3.1086	5.50	3.5000	(0.1518)	0	6.1893	(0.2684)	9.6893
B	5.7500	6.50	9.4937	(0.4117)	0	6.1893	(0.2684)	15.6830
C	7.3864	5.50	15.000	(0.6505)	0	6.1893	(0.2684)	21.1893
D	8.9038	5.50	21.3319	(0.9251)	0	6.1893	(0.2684)	27.5212
E	5.7500	5.50	9.4937	(0.4117)	1	18.0283	(0.7818)	27.5220

*n denotes the vibrational quantum number.

**The total average system energy $E_T = E_t + E_v$.

factor of one-half. The numerical procedures presented in this chapter were implemented with a computer program written in Fortran IV and compiled and executed on the Oklahoma State University IBM 360/65 computer in Fortran H language using optimization level 2. The program was compiled and stored on private on-line disk storage and hence execution was initiated simply by "reading in" a deck consisting of the proper Job Control Language cards and approximately 10-12 data cards. Execution of the program compiled in Fortran H level, optimization 2, reduced computation time approximately 10% compared to Fortran G level. A complete calculation required about 5.4 hours of computer time depending somewhat upon the average translational energy of the wavepacket.

The storage requirement of the program is quite large and is a common problem when the solution of a partial differential equation is sought at various points in configuration space. Execution required approximately 395 K bytes of core storage where 1K bytes = 1024 bytes and one single precision variable in Fortran requires four bytes of storage on the IBM machine. For a single precision complex variable ($a + bi$ where $b \neq 0$) eight bytes of storage are required. Because of the large storage requirement, execution of the program in double precision on the IBM machine with the presently available core storage was not possible. However, a comparison program consisting of only the variables needed to study the reactive system on the lower part of the L-shaped grid was written in double precision and executed. There were no deviations between the values of $\Psi_{i,j}$ computed by the double precision version and the values produced by an identical single precision program.

The essential computational procedure of the program is briefly

summarized below.

1. Read in the initial conditions and other required data such as the grid dimensions, the grid spacing, the minimum q_2 value, the maximum q_1 value, the potential energy surface parameters, the variables necessary to specify the shape and energy of the wavepacket, the time step size, and an integer which is the time step number k, which serves to terminate the particular batch run when the wavefunction has been evolved up to and including k steps.
2. Calculate the potential energy values for all points on the grid.
3. If the time step number is zero, generate the values of $\Psi_{i,j}$ at time step zero for all points on the grid.
4. If the time step number is not zero, read the values of $\Psi_{i,j}$ for time step n (typically k has a numerical value 20 greater than n) from on-line disk storage.
5. Calculate the values $B_{i,j}$ for all points on the grid.
6. Obtain a first guess or first approximation for $\Psi_{i,j}$ $[t_o + (n+1)\Delta t]$ for all points on the grid using approximation [34].
7. Solve for $\Psi_{i,j}[t_o + (n+1)\Delta t]$ using the line Gauss-Seidel method.
8. Check on convergence by applying equation [50]. If $\Psi_{i,j}$ for time step n+1 for all points on the grid have not converged, repeat step 7. If the convergence criteria has been met by all points on the grid, continue to step 9.
9. Compute the value of the integral $\langle\Psi|\Psi\rangle$, integrated (summed) over the entire grid, and calculate the quantum reaction

probability.

10. If the time step number of the present calculation is equal to k, then the values of $\Psi_{i,j}$ at all points on the grid are written onto on-line disk storage, otherwise return to step 5 and use the converged values of $\Psi_{i,j}[t_o + (n+1)\Delta t]$ just computed and carry out steps 5 thru 9 to obtain $\Psi_{i,j}[t_o + (n+2)\Delta t]$. Continue the process until the time step number of the calculation is equal to k.

In step 9 above the numerical quadrature method employed to perform the integration and determine $\langle\Psi|\Psi\rangle$ and the reaction probability was a standard technique employing Simpson's one-third rule (144). The quantum reaction probability will be defined later. The value of the integral should be equal to one and remain constant during an entire calculation. Therefore computation of $\langle\Psi|\Psi\rangle$ at each time step serves somewhat as a check on the accuracy of the calculation. The value of the integral changed only slightly during a calculation and showed the greatest deviation from unity when the main bulk of the wavepacket encountered the interaction region. The accuracy of the integration technique was checked by determining the volume under a surface produced by setting $|\Psi_{i,j}|^2$ equal to a constant for all i and j. The value of the integral (volume) computed by the integration subroutine agreed almost exactly (exact agreement is impossible for this case where the volume is formed by perpendicular planes) with the value calculated by hand.

The numerical error produced by applying the finite difference formula, Equation [37], to a plane wave is given by Hamming (145). The relevant equation indicates that errors ranging from a few tenths of a

percent to a few percent are to be expected for the most probable plane wave components of the initial packets. The values of Δq and Δt used in the calculations were arrived at largely through trial and error. One can evolve the wavefunction back in time from time, $t + n\Delta t$, to time, t, by substituting in $-\Delta t$ for the time increment. The difference between these "back evolved" $\Psi_{i,j}$ values and the values at hand serves as a measure of the accuracy of the calculation. As an example, for Calculation A the values of $\Psi_{i,j}$ at time = 32.5 Δt (see Figure 6) were evolved back 20 time steps with $\Delta t = -1.0775 \times 10^{-16}$ sec. and compared to available values of $\Psi_{i,j}$. Considering all of the grid points, the largest difference between the two calculated values at a grid point for the real part of the wavefunction was 5.7×10^{-3}, the average difference for all of the grid points was 1.3×10^{-5}. The largest difference found for the imaginary part was 6.9×10^{-3} (average difference of 1.3×10^{-5}), and for $\Psi^*_{i,j}\Psi_{i,j}$ the largest difference was 4.0×10^{-4} (average difference of 5.5×10^{-6}). An identical back evolution process from time = 92.5 Δt (see Figure 9) yielded the following values: largest real part difference = 2.6×10^{-4} (average = 4.5×10^{-6}), largest imaginary part difference = 1.8×10^{-4} (average = 4.3×10^{-6}), largest difference for $\Psi^*_{i,j}\Psi_{i,j} = 7.9 \times 10^{-5}$ and average = 3.2×10^{-6}. Most books on numerical methods state that an important factor in integrating partial differential equations is the ratio, $(\Delta q/\Delta t)$ and not Δq or Δt alone. Accordingly, the ratio of Δq and Δt was adjusted and the roughness of the plots and the deviation of the integral $\langle\Psi|\Psi\rangle$ from unity were closely followed. In the final choice, of course, the values chosen for Δq and Δt must be commensurate with the computer time and computer storage available.

CHAPTER III

RESULTS

Quantum Probability Density

The solution of equation [36] at a given time yields a complex number $\Psi_{i,j}$ for each grid point. The quantum probability density, $\rho(q_1,q_2,t)$ is given by

$$\rho(q_1,q_2,t) = \Psi^*(q_1,q_2,t)\Psi(q_1,q_2,t) \ . \qquad [60]$$

Since the numerical solution gives $\Psi(q_1,q_2,t)$ only at the grid points, the probability density consists of tables of real numbers, approximately 10^4 for each time step. A more meaningful and instructive way of presenting ρ is given below.

In order to evaluate ρ at any arbitrary point in (q_1,q_2) configuration space an interpolation procedure was used. Any arbitrary point in q-space can be envisioned as being surrounded by four grid points. The value of ρ was determined by adding the values of ρ at a pair of the surrounding points, taking the average of the two points, and weighting the average value inversely to the distance from the arbitrary point at which ρ is desired. In this weighting procedure two pairs are weighted in the q_1 - direction from the arbitrary point and two pairs in the q_2 - direction.

The time evolution of ρ in (q_1,q_2) configuration space shown in Figure 4 is represented by three-dimensional perspective plots given in

Figures 5-67. The height above the (q_1,q_2) plane represents the value of ρ. The labels A, B, C, D, or E refer to the initial conditions given in Table III.

A plot data set for each perspective plot was created by a computer program written in FORTRAN IV by the author and utilizing a perspective plotting subroutine written by Dr. Ronald K. Oines, Research Foundation, Oklahoma State University. The data sets were plotted by the CALCOMP plotter at the University Computer Center, Oklahoma State University. The generation of a perspective plot data set consumed on the average about 20 seconds of execution time (GO step). Approximately 33 minutes was required for the CALCOMP 565 plotter to physically produce a plot. This very versatile subroutine allows the user to choose the line of sight up or down (equivalently tilt the (q_1,q_2) plane) by an angle and to rotate the line of sight to the left or right by any amount and hence enables one to "look" completely around a figure projecting from the (q_1,q_2) plane. Figures 5-67 display the (q_1,q_2) plane shown in Figure 4 with the line of sight 45 degrees up from the (q_1,q_2) plane (equivalently the plane of Figure 4 is tilted down at an angle of 45 degrees) and rotated 135 degrees counterclockwise (equivalently the plane of Figure 4 is rotated 135 degrees clockwise). The line of sight therefore lies along the diagonal which runs from the point of intersection of the upper and lower parts of the L back to the corner where q_1 and q_2 have their minimum values. A complete description of the subroutine is available at the University Computer Center, Oklahoma State University.

Since the figures serve primarily in a qualitative way and provide a means of observing the qualitative characteristics of the reaction

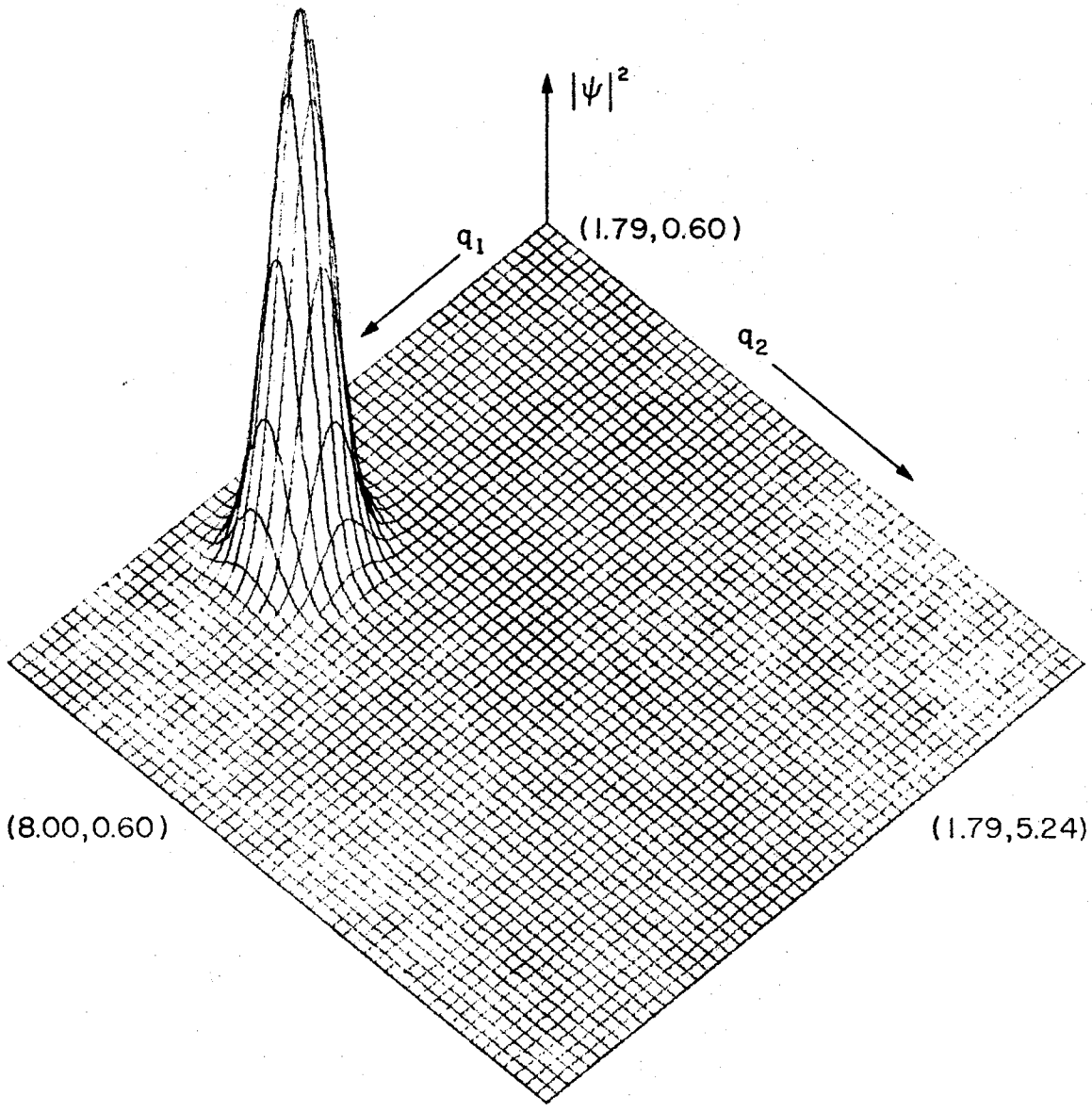

Figure 5. Calculation A, t = 0Δt, FAC = 1.25

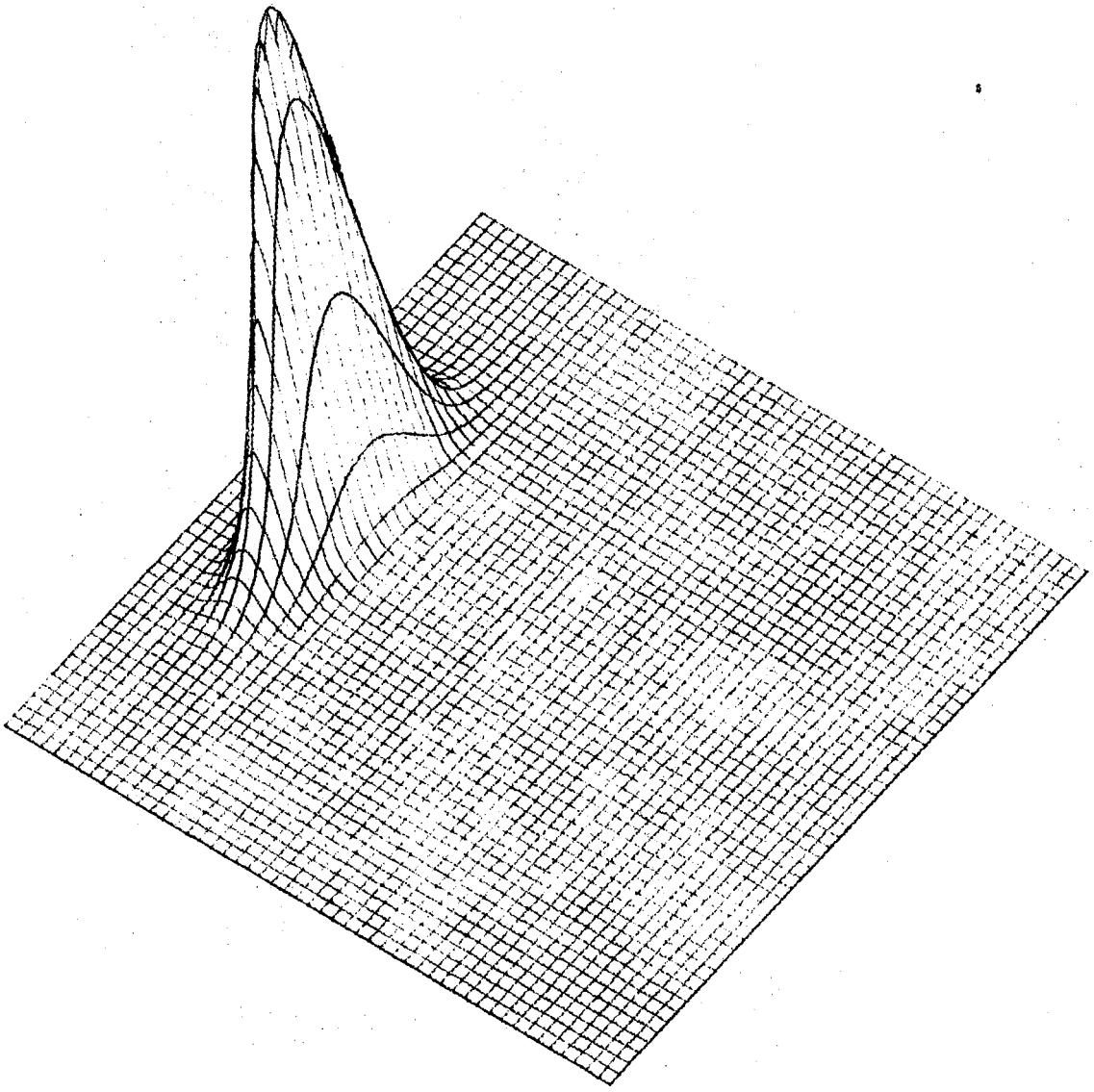

Figure 6. Calculation A, $t = 32.5\ \Delta t$

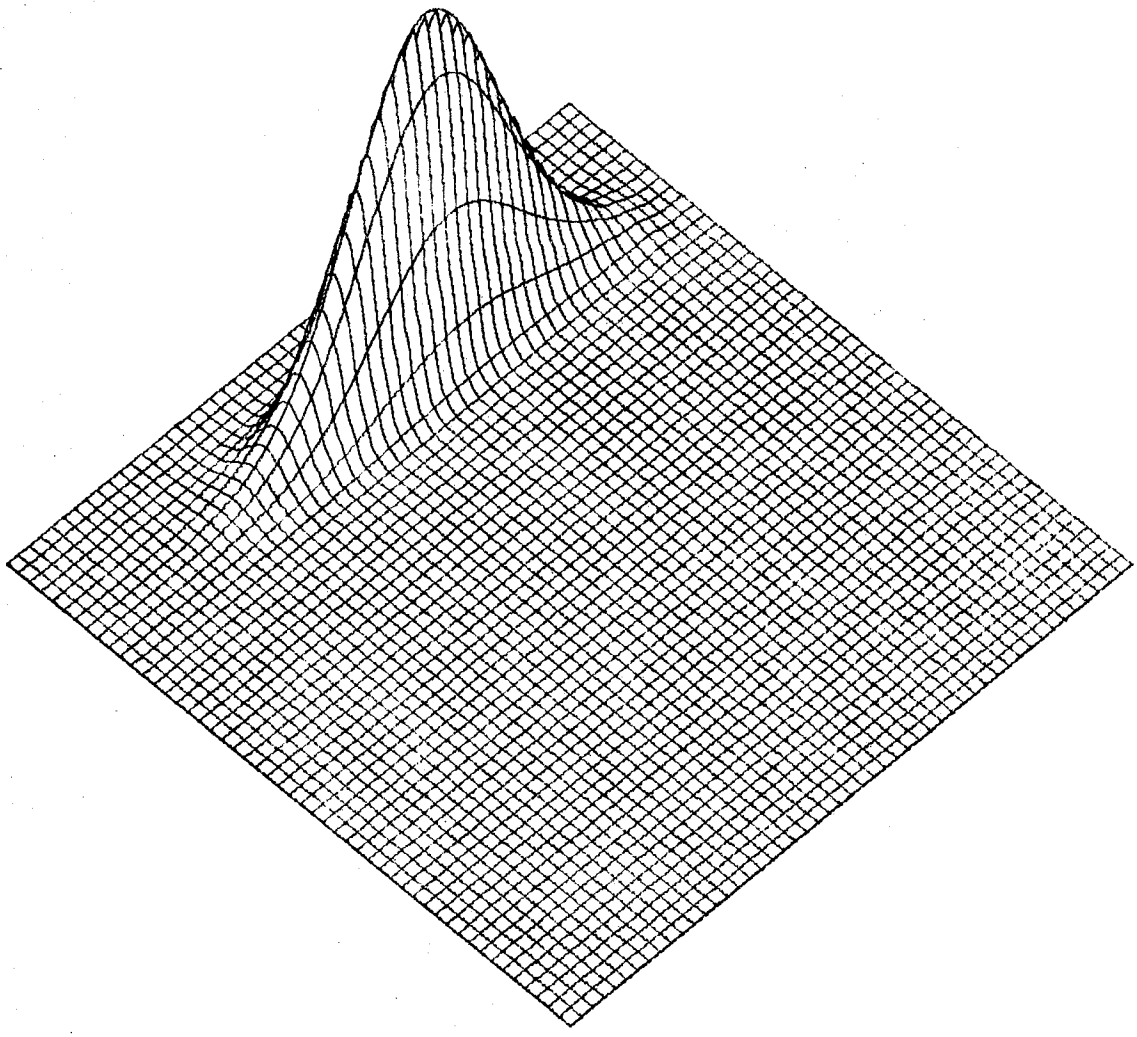

Figure 7. Calculation A, $t = 52.5\,\Delta t$

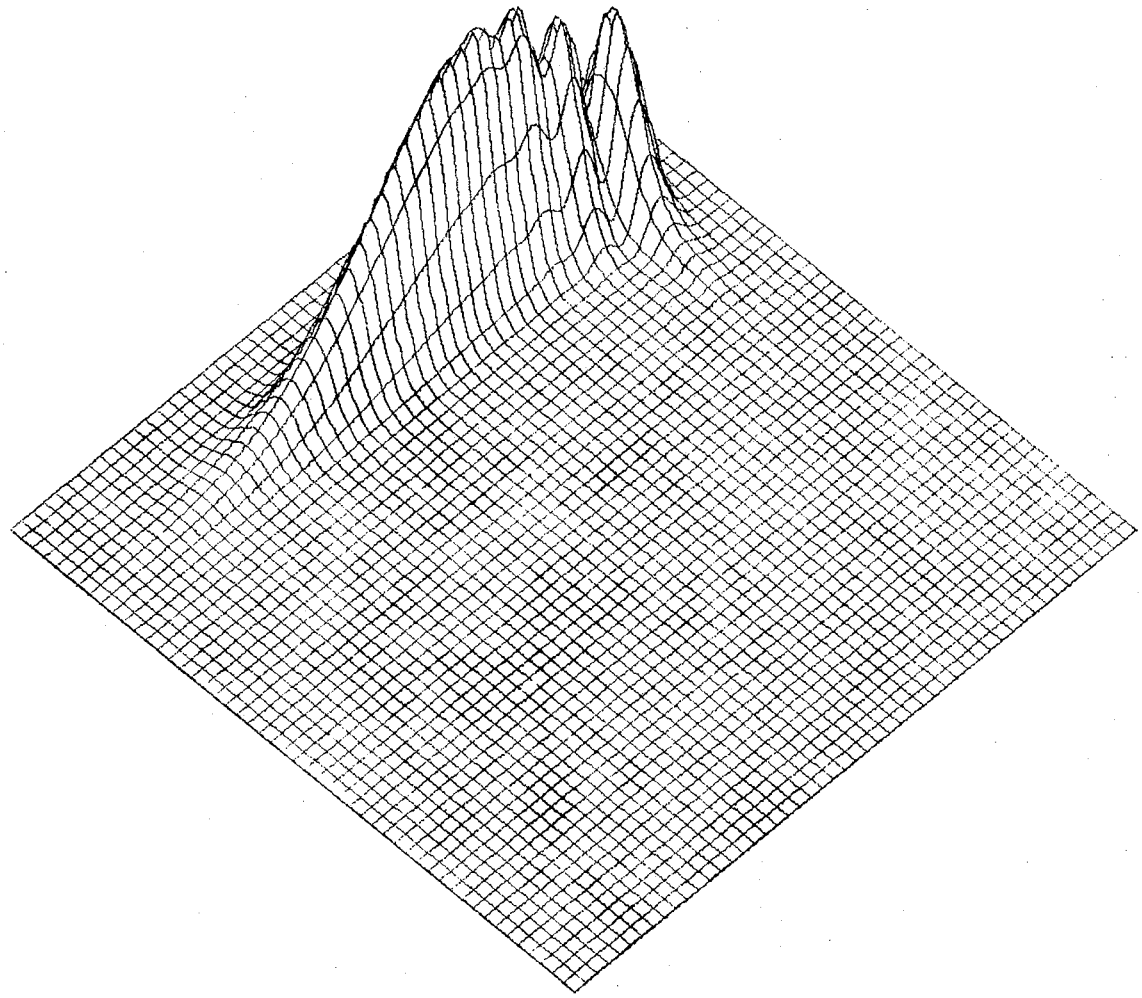

Figure 8. Calculation A, t = 72.5 Δt

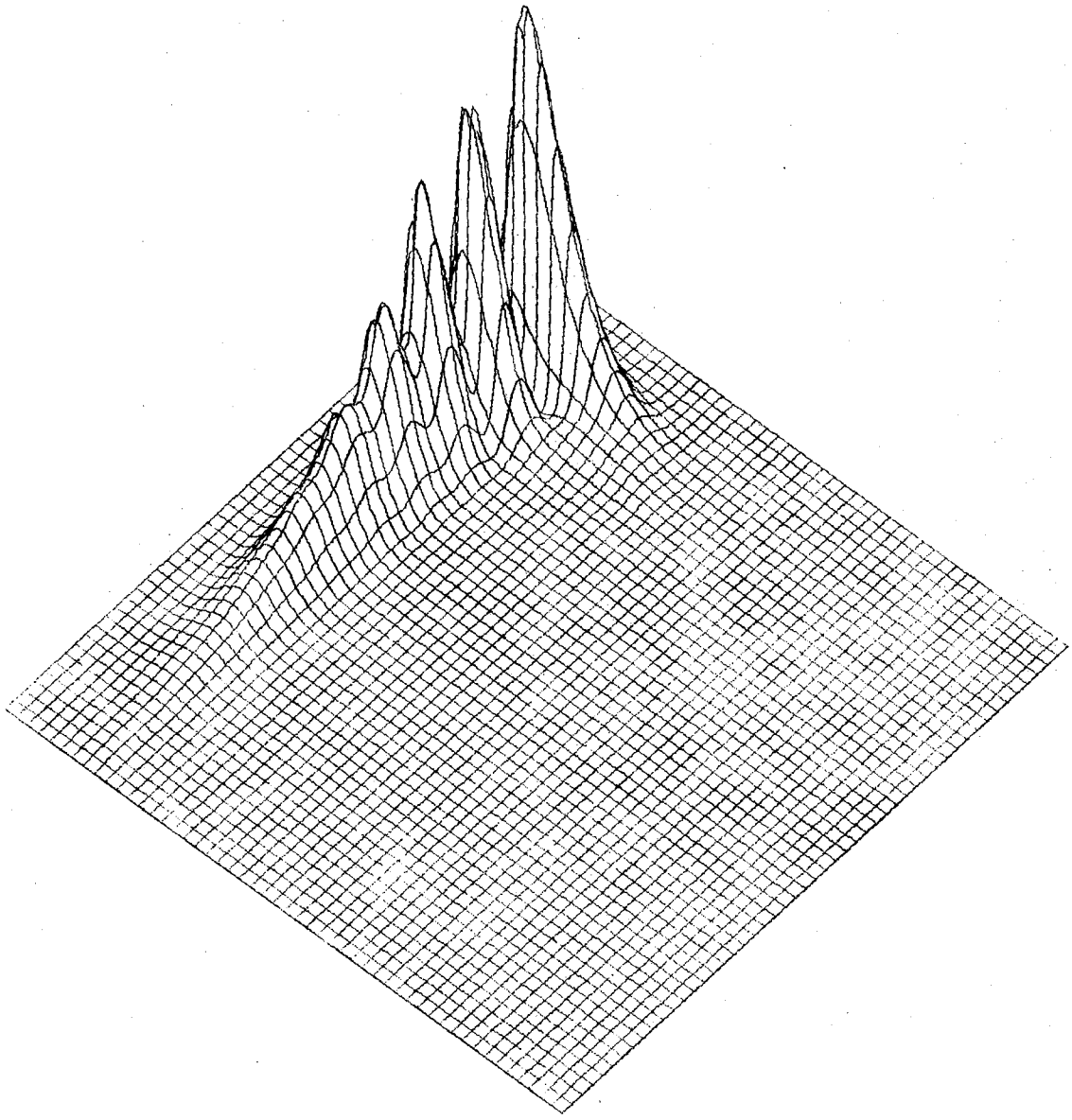

Figure 9. Calculation A, $t = 92.5\,\Delta t$

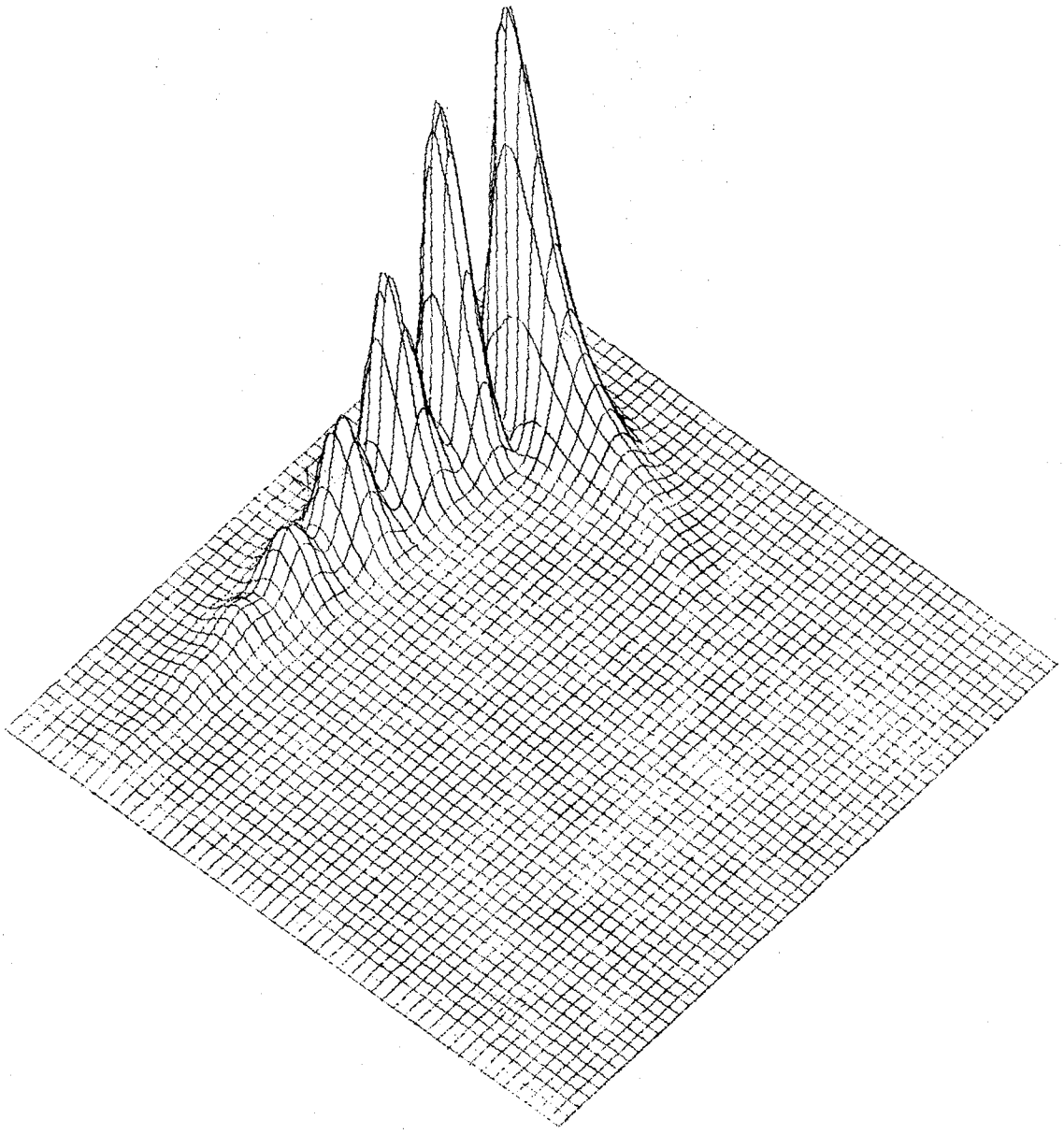

Figure 10. Calculation A, $t = 112.5\,\Delta t$

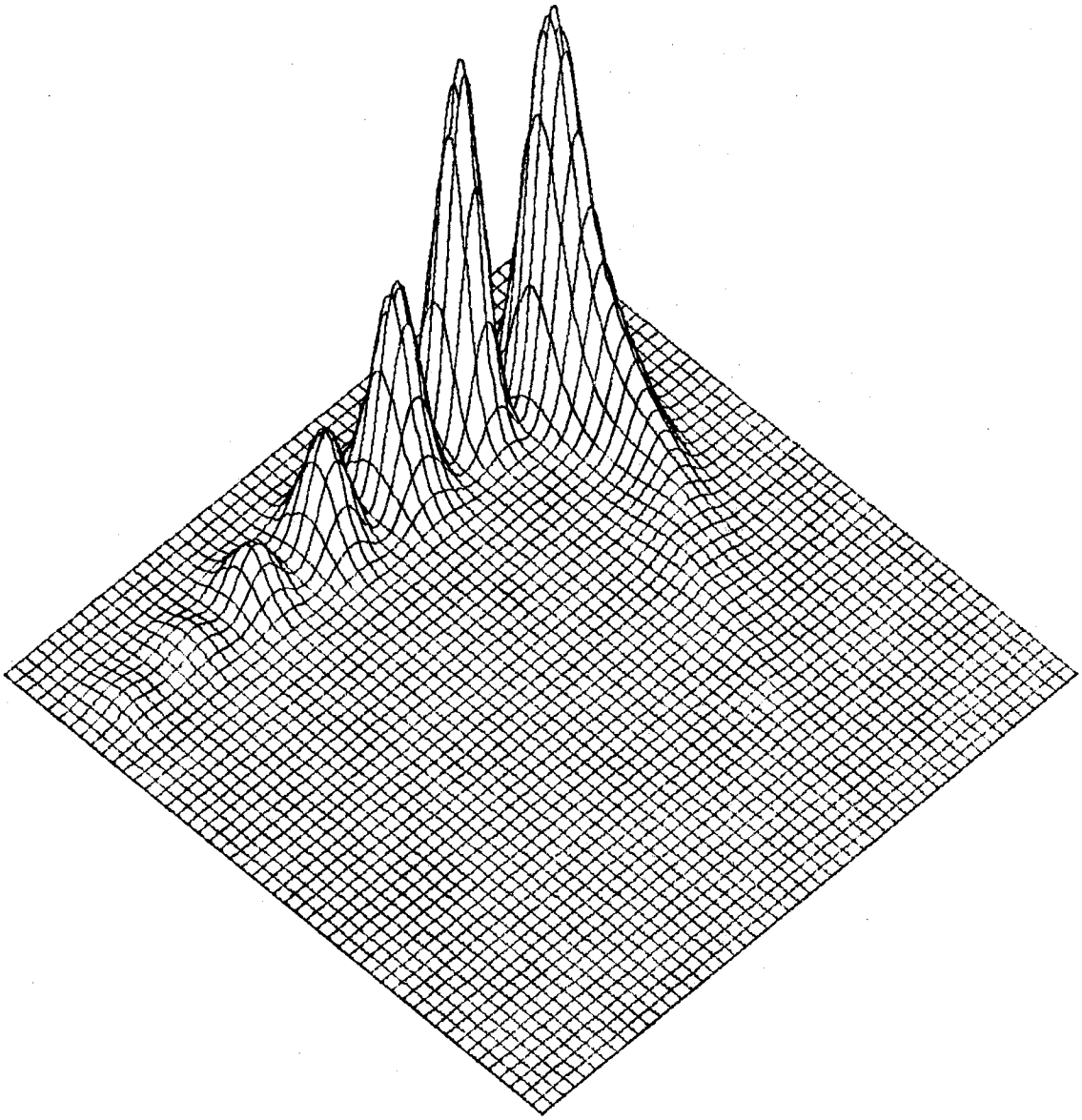

Figure 11. Calculation A, $t = 132.5\,\Delta t$

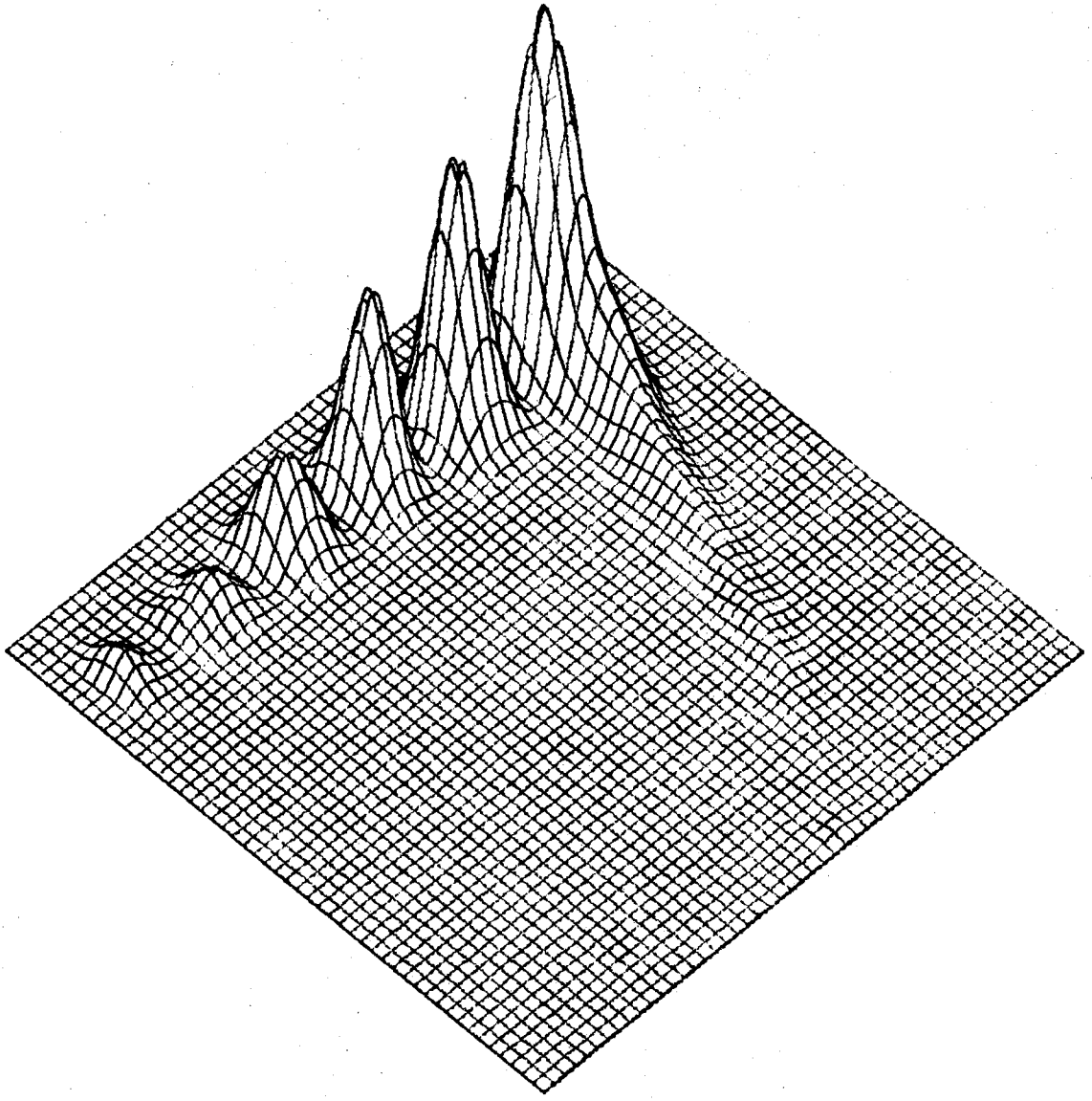

Figure 12. Calculation A, t = 152.5 Δt

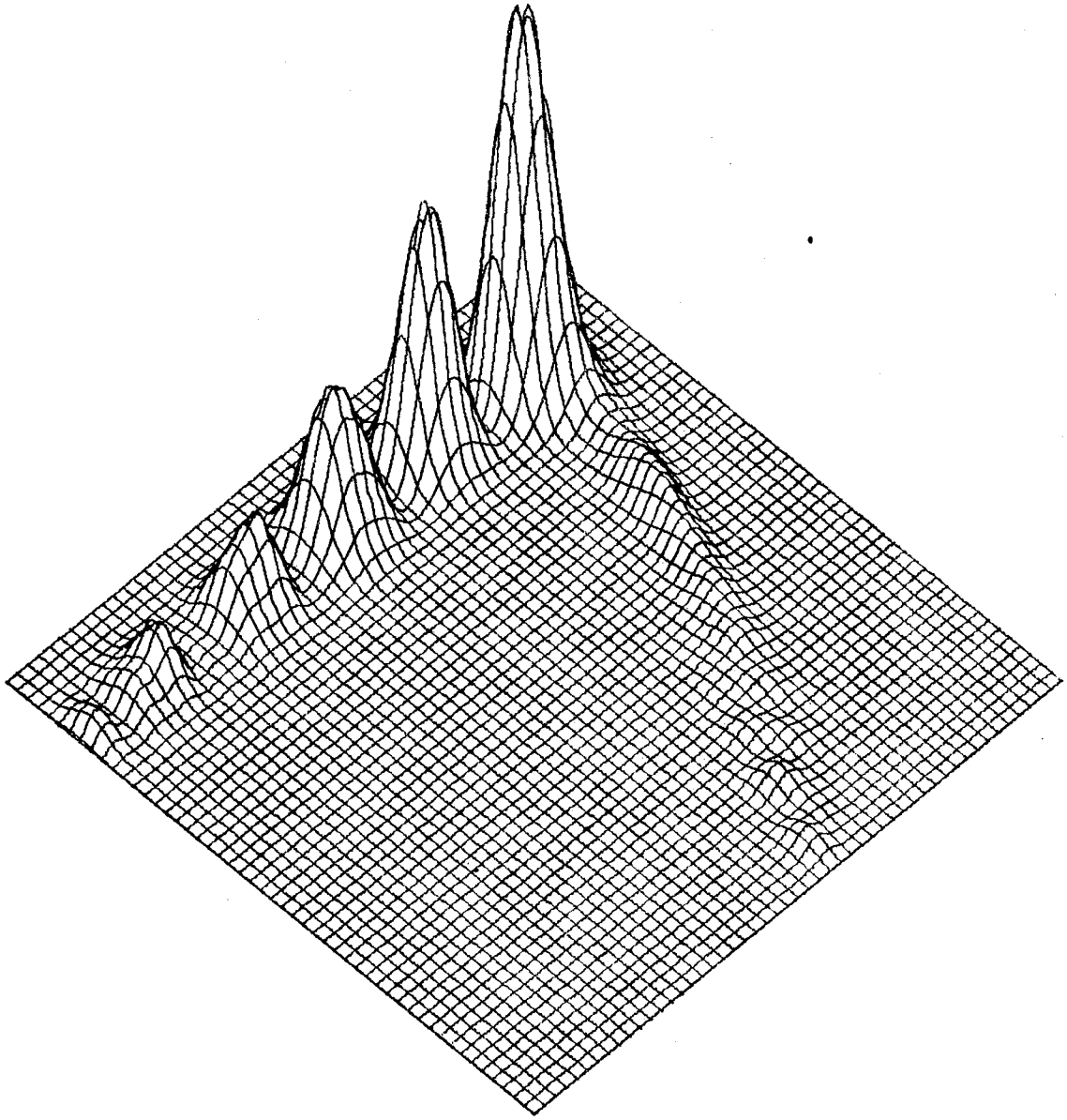

Figure 13. Calculation A, t = 172.5 Δt

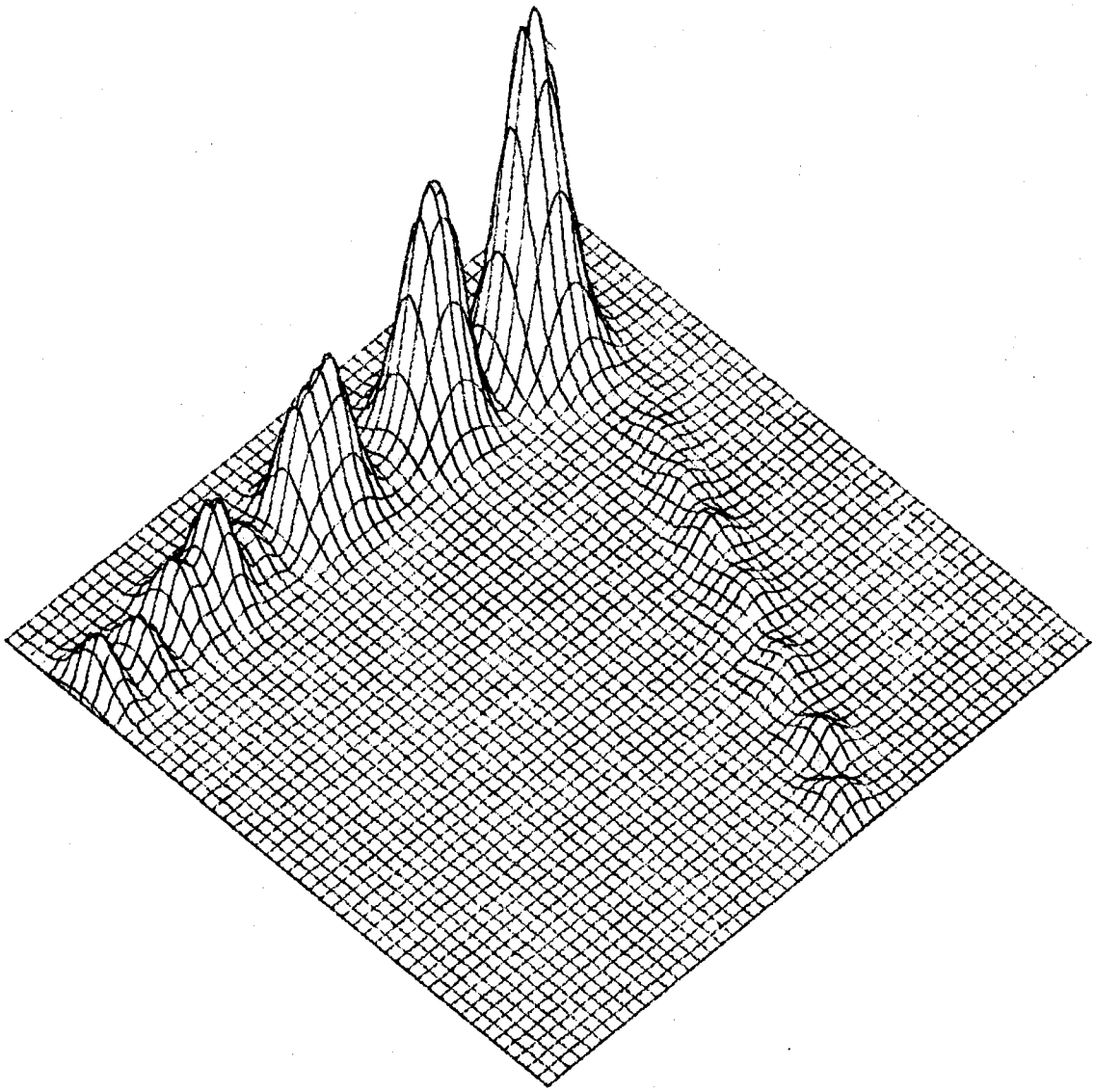

Figure 14. Calculation A, $t = 192.5\,\Delta t$

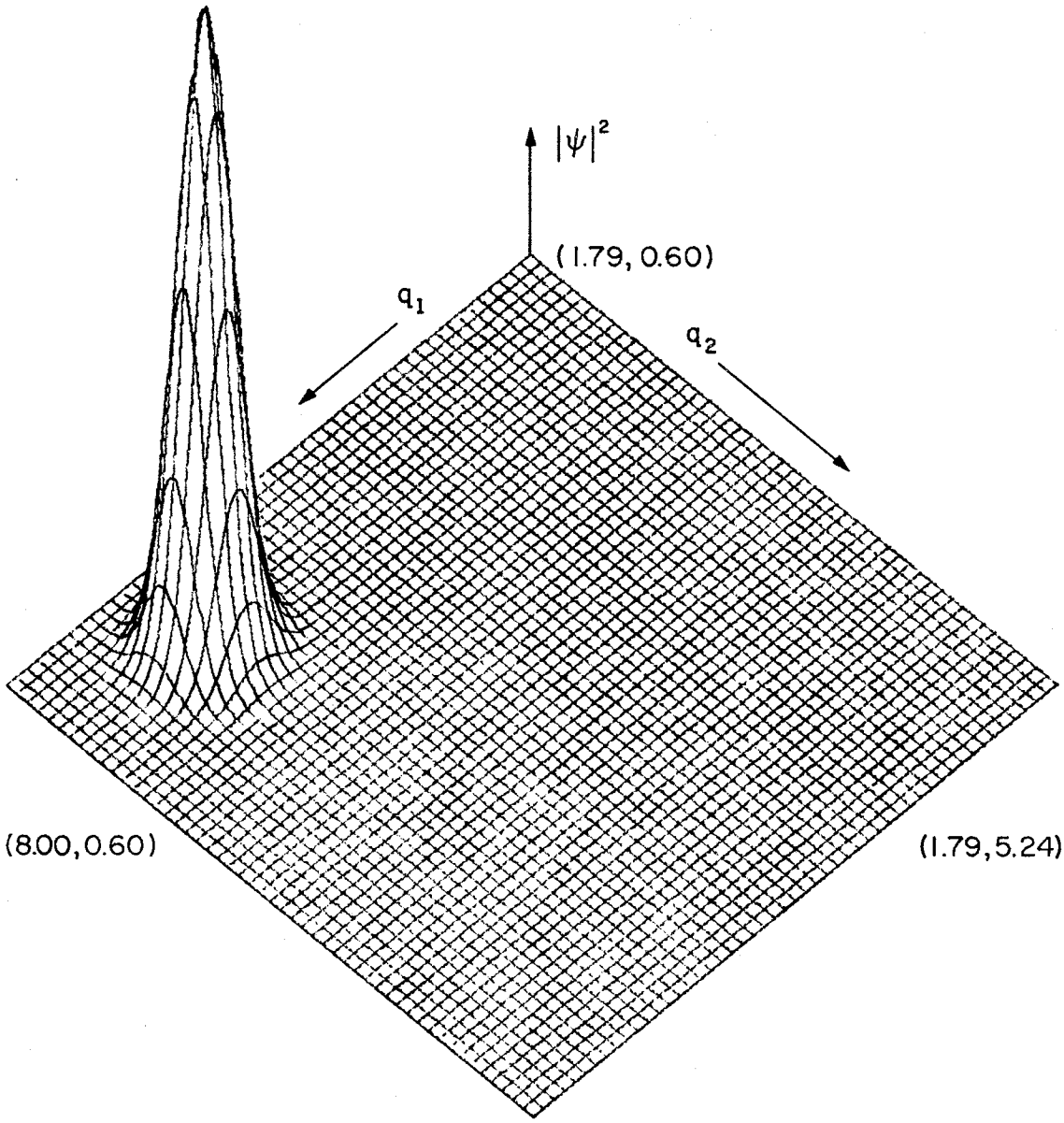

Figure 15. Calculation B, t = 0 Δt

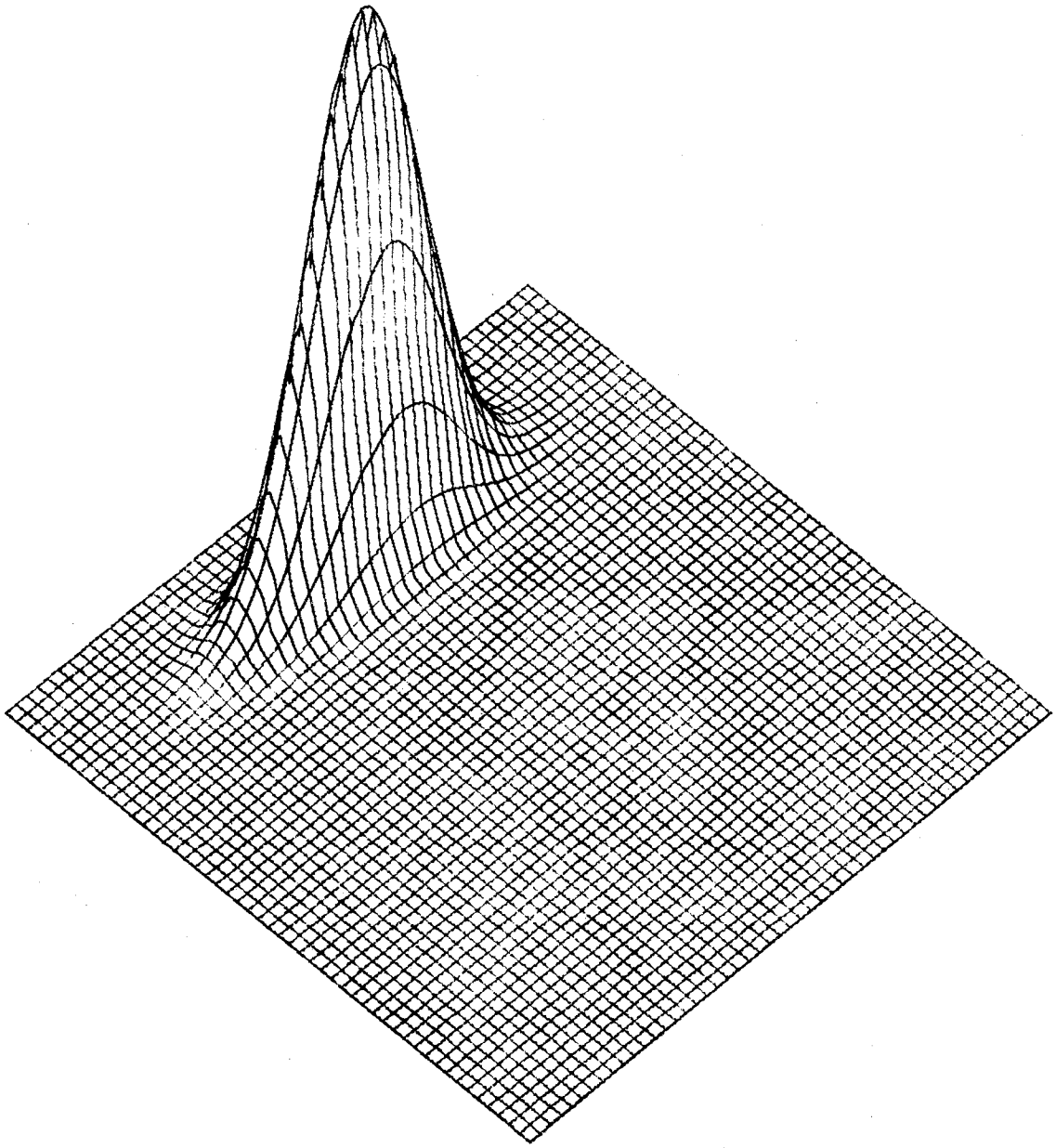

Figure 16. Calculation B, t = 45 Δt, FAC = 3.00

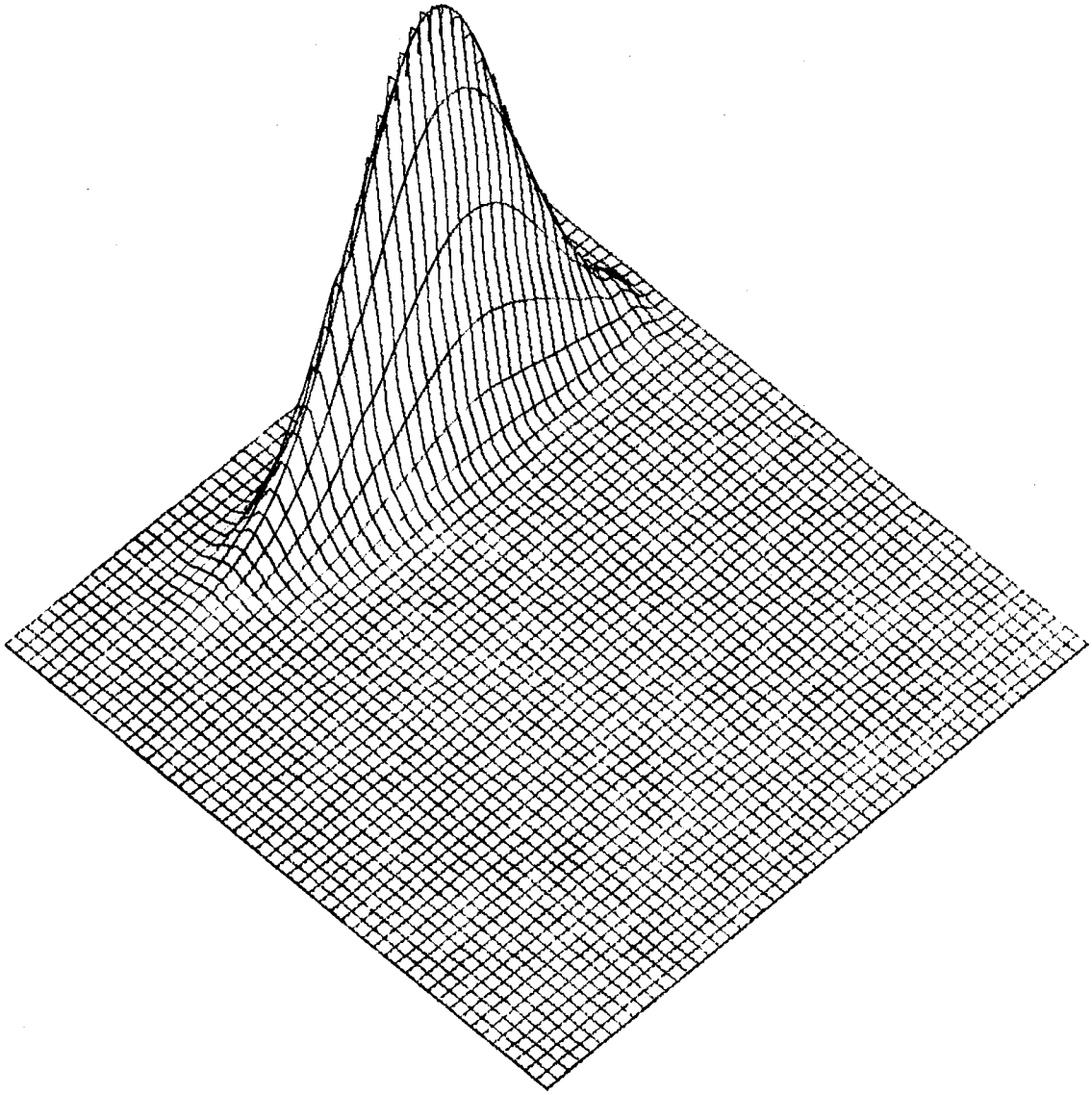

Figure 17. Calculation B, t = 60 Δt, FAC = 3.00

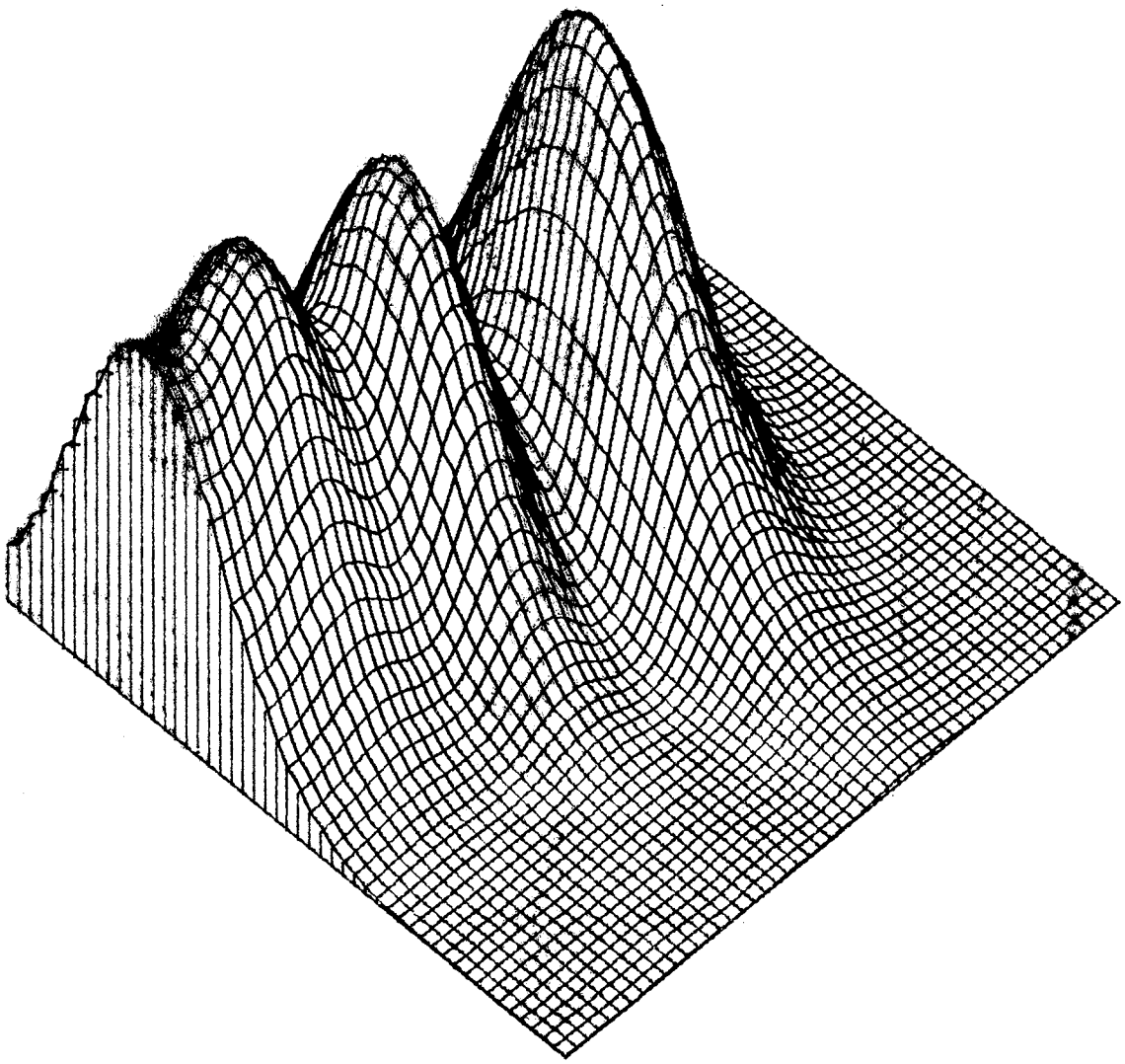

Figure 18. Calculation B, t = 75 Δt, FAC = 0.75

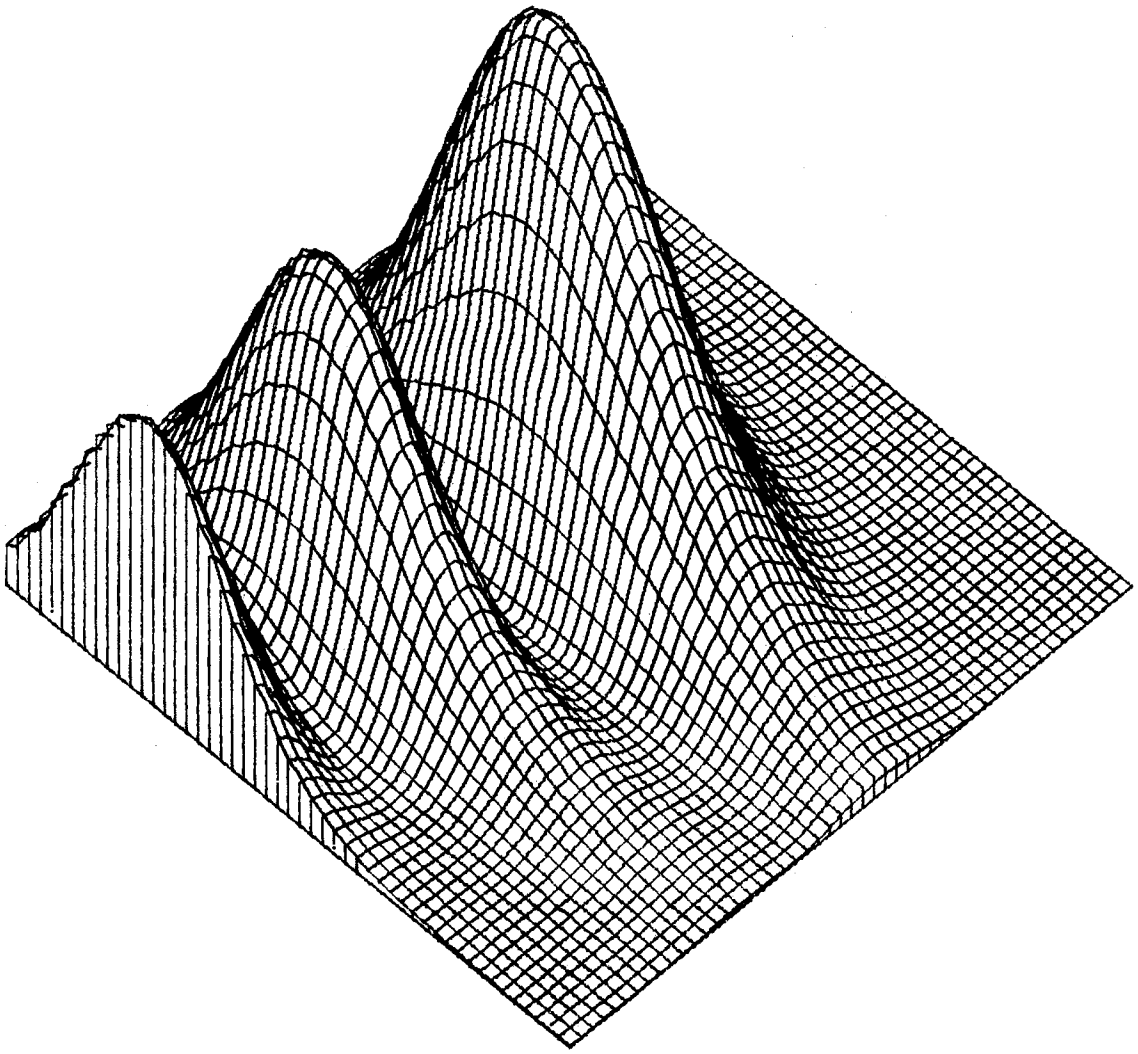

Figure 19. Calculation B, t = 90 Δt, FAC = 0.40

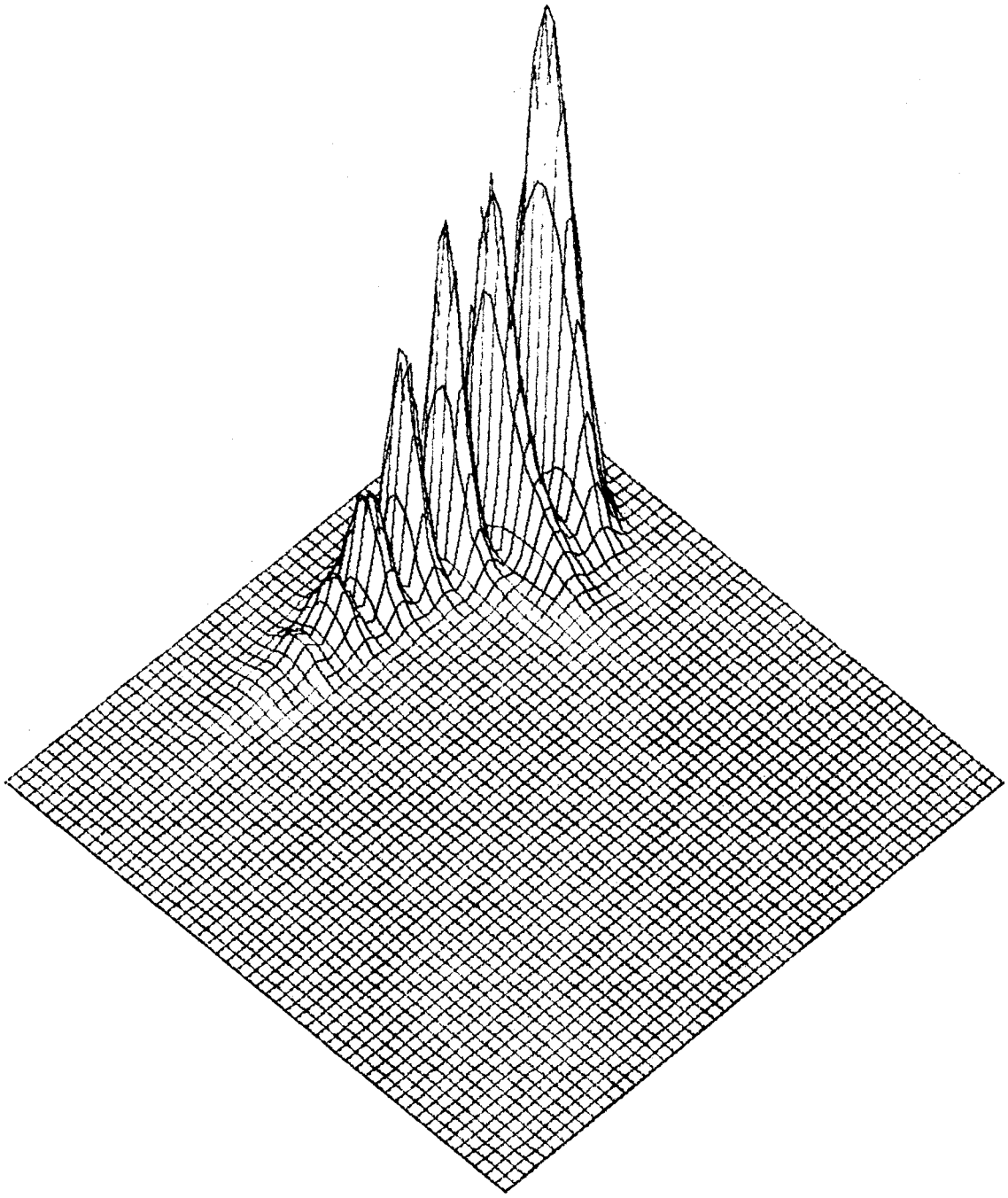

Figure 20. Calculation B, t = 105 Δt

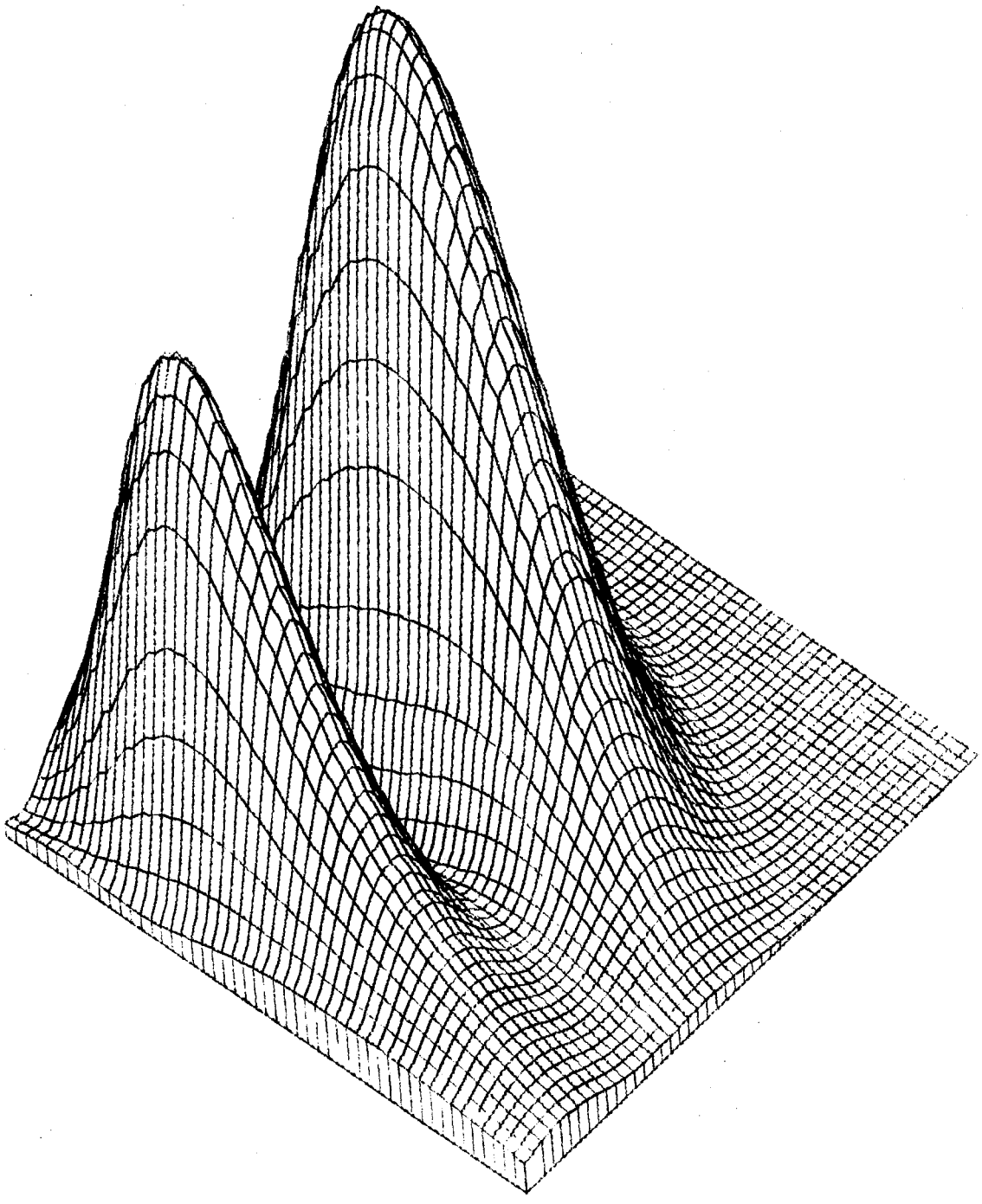

Figure 21. Calculation B, $t = 105\,\Delta t$, FAC = 0.50

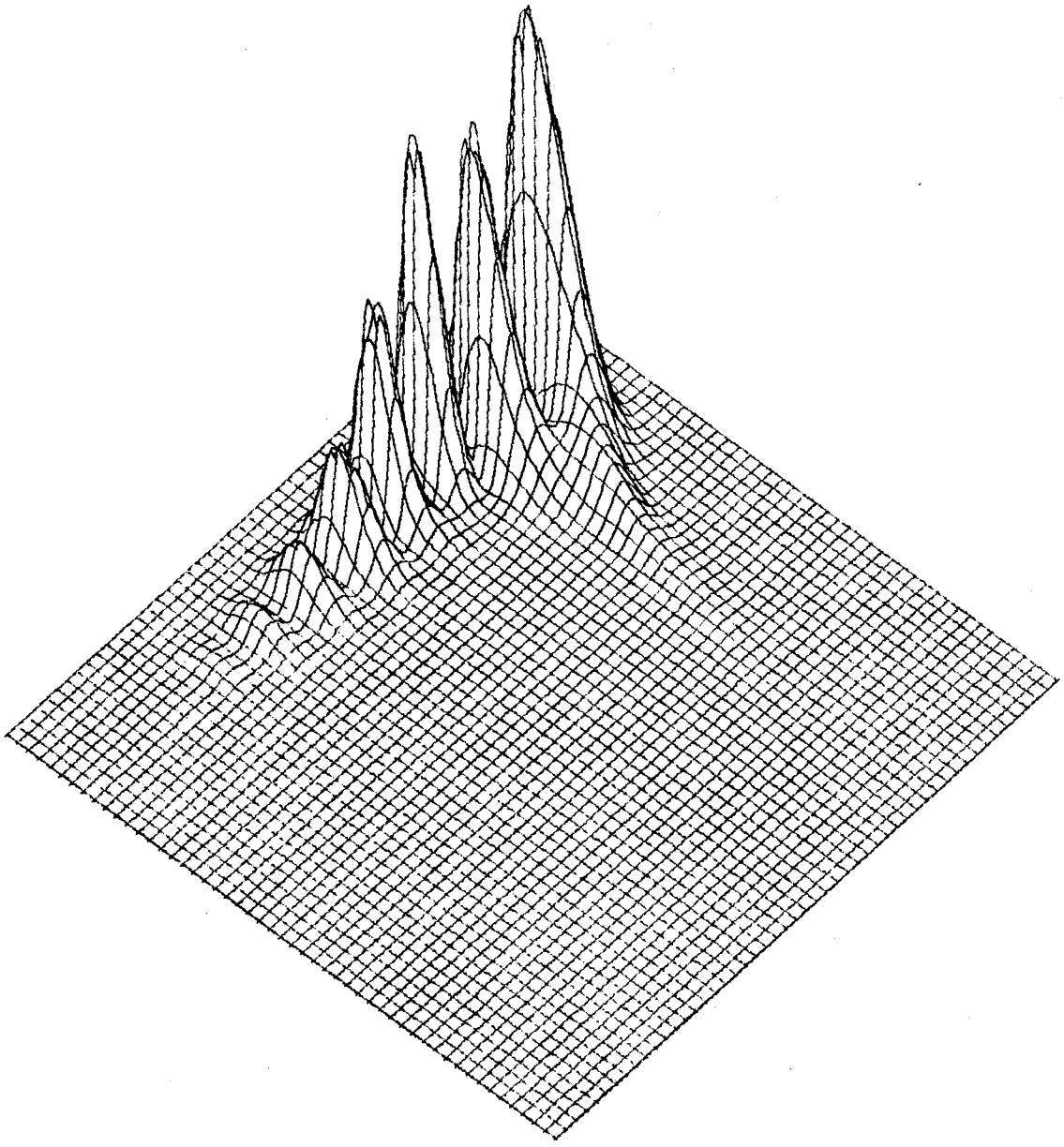

Figure 22. Calculation B, $t = 120\,\Delta t$

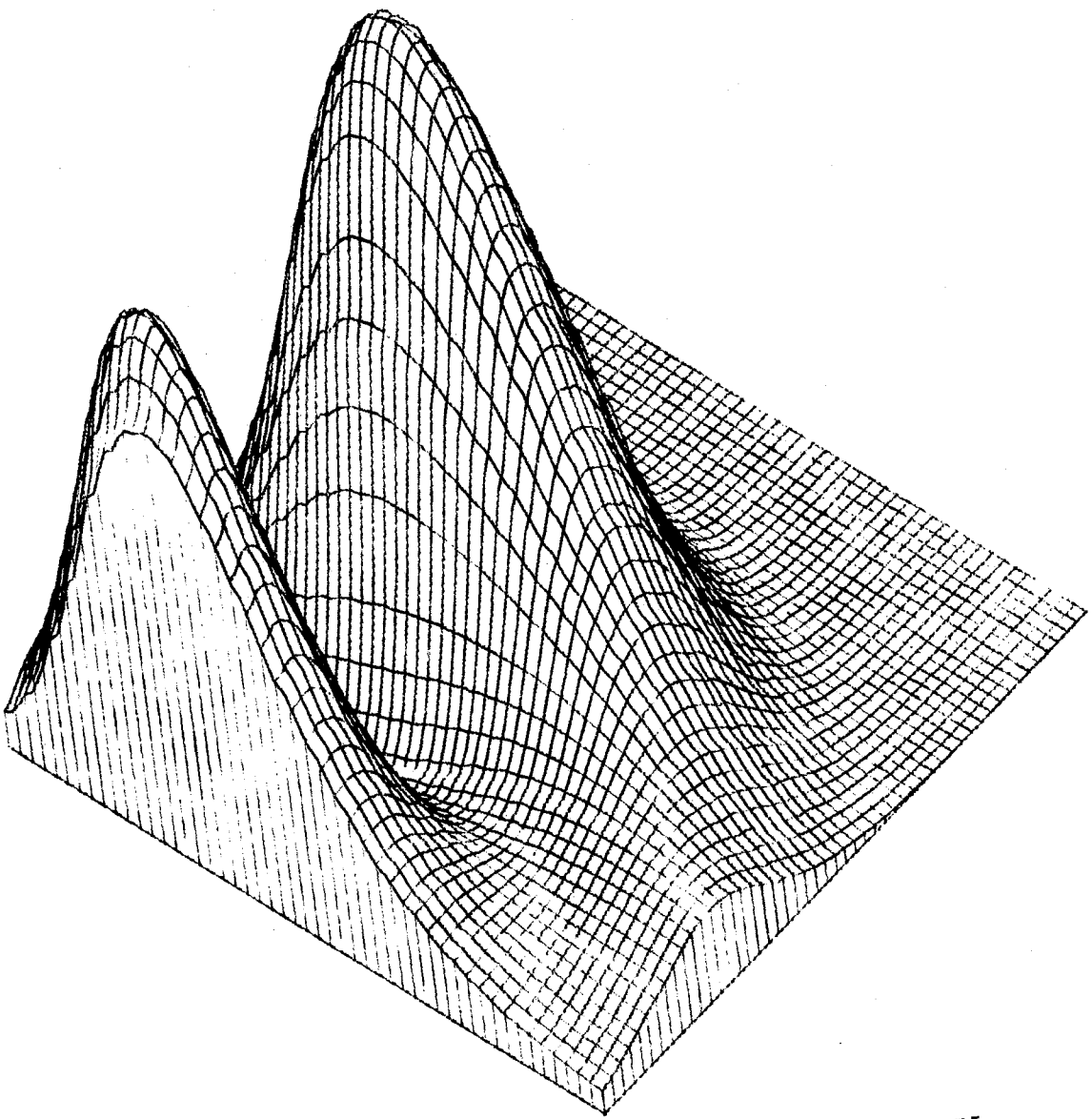

Figure 23. Calculation B, t = 120 Δt, FAC = 0.75

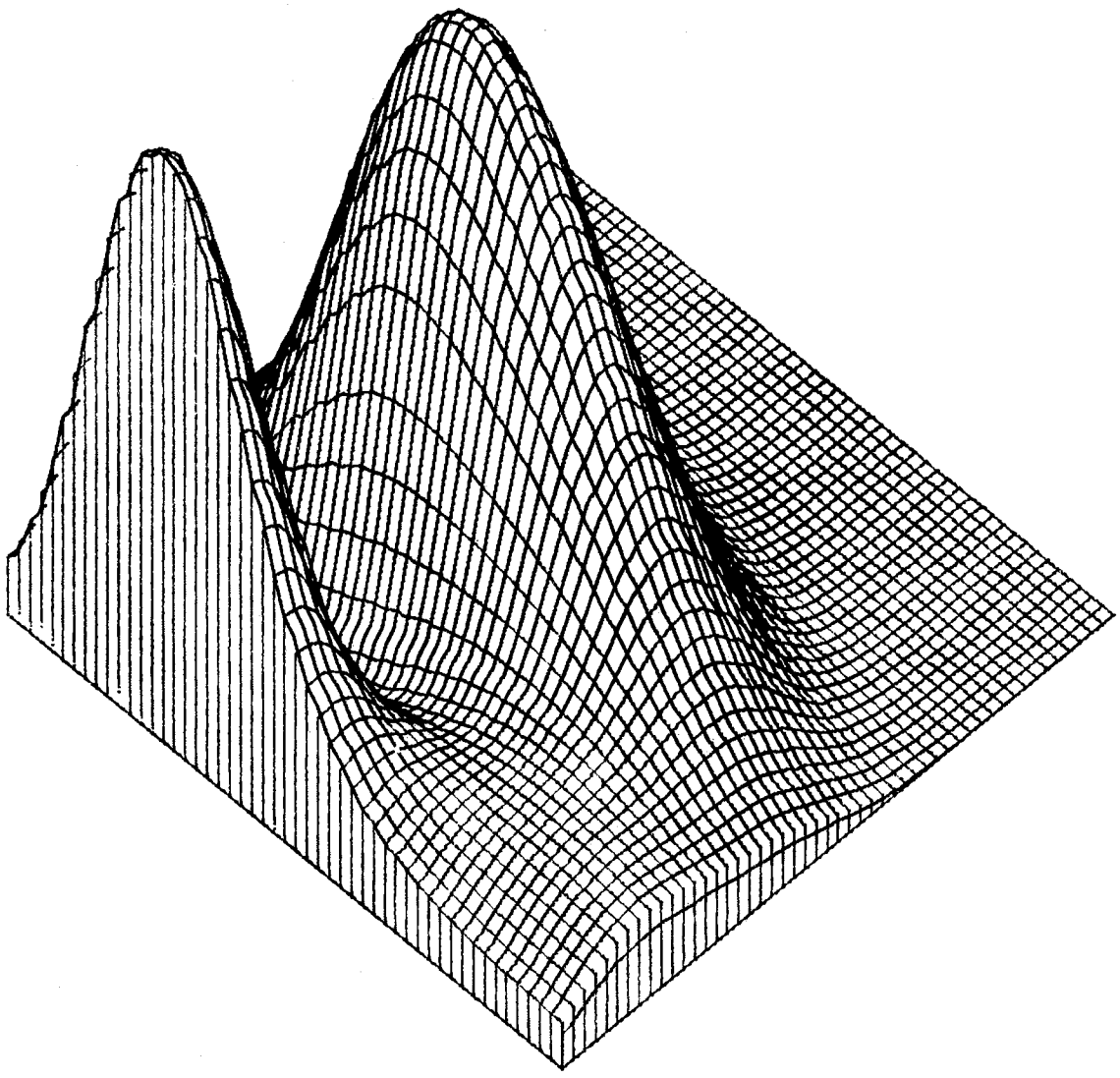

Figure 24. Calculation B, t = 127.5 Δt, FAC = 0.82

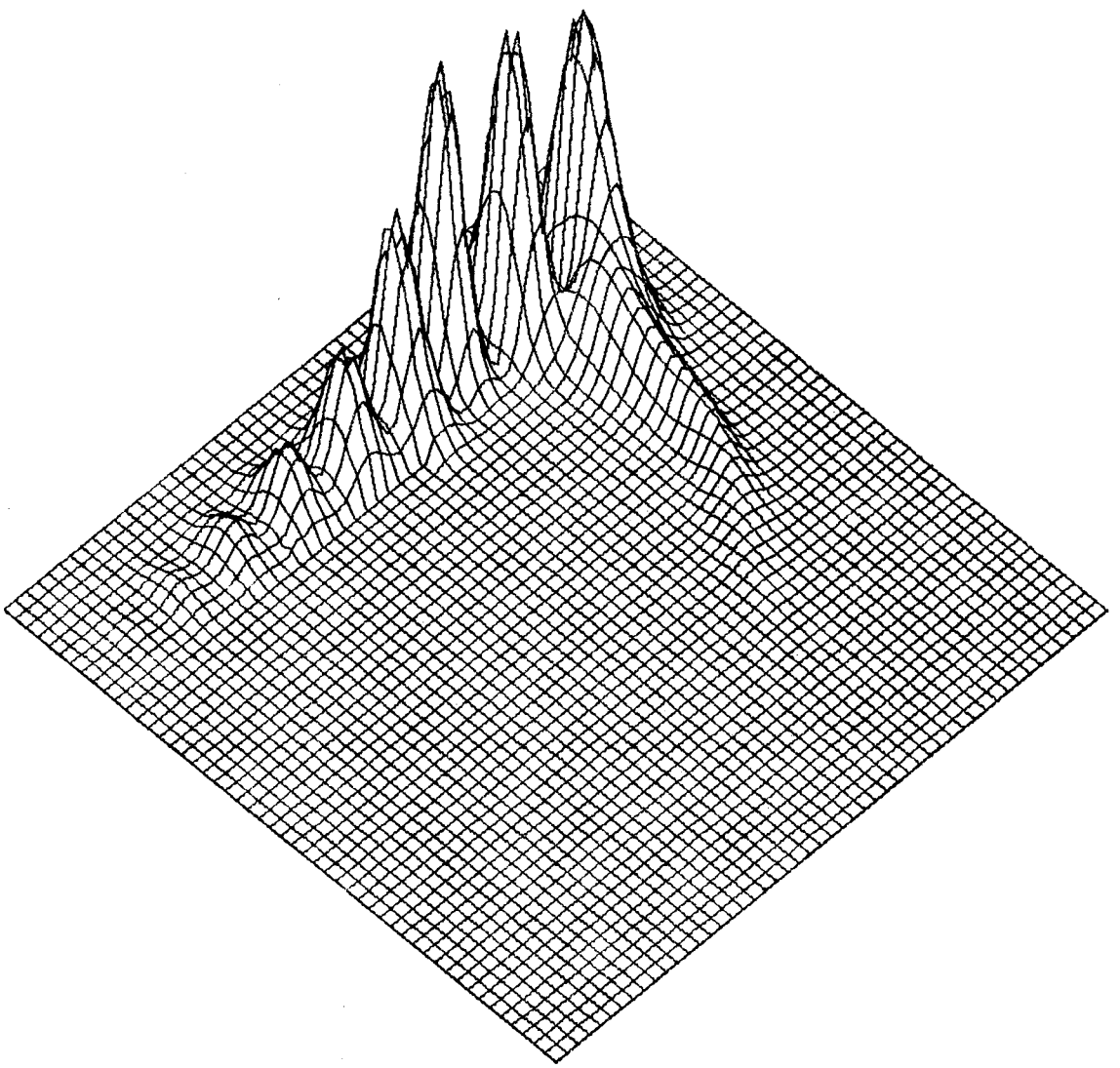

Figure 25. Calculation B, t = 135 Δt

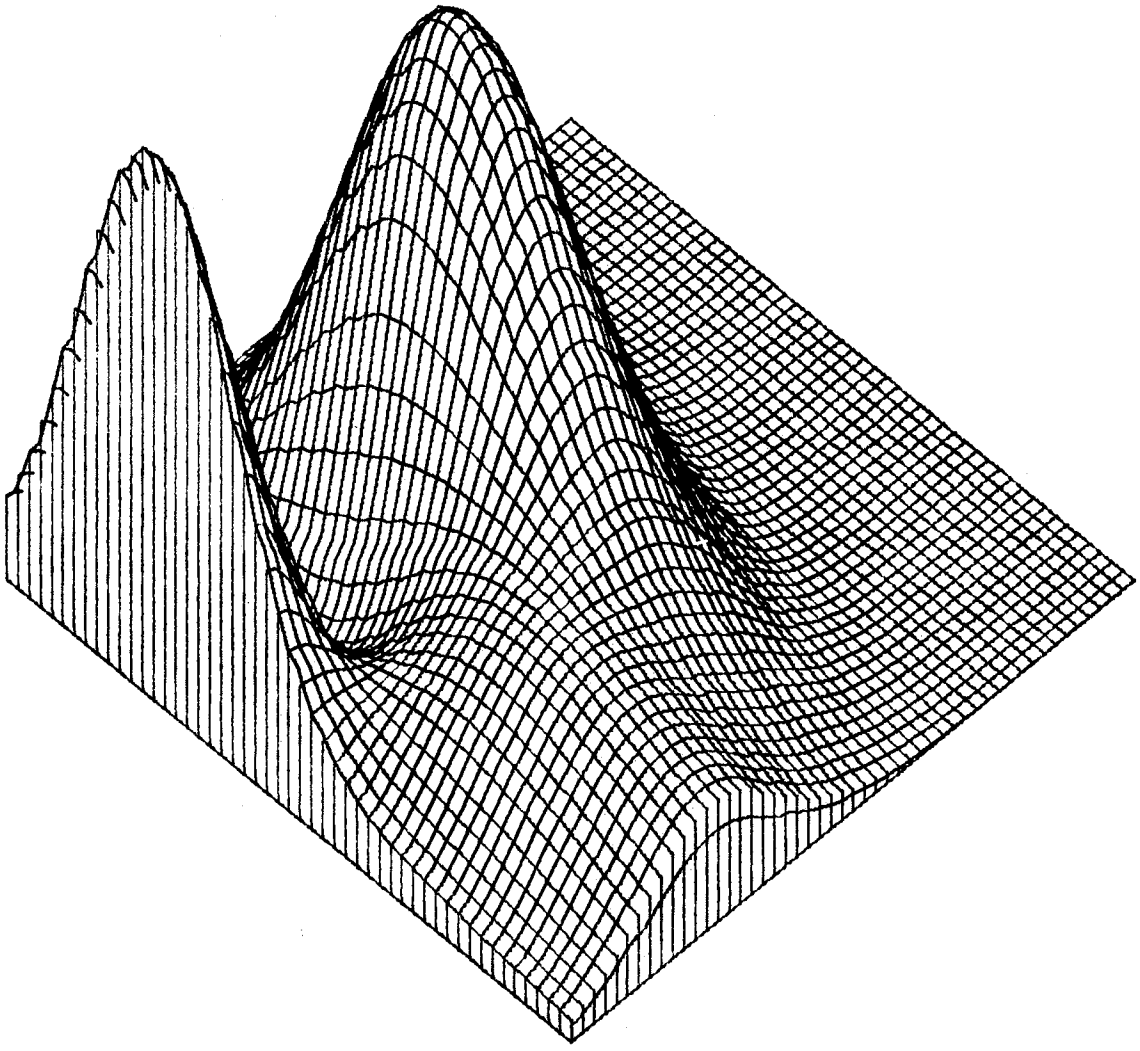

Figure 26. Calculation B, t = 135 Δt, FAC = 0.867

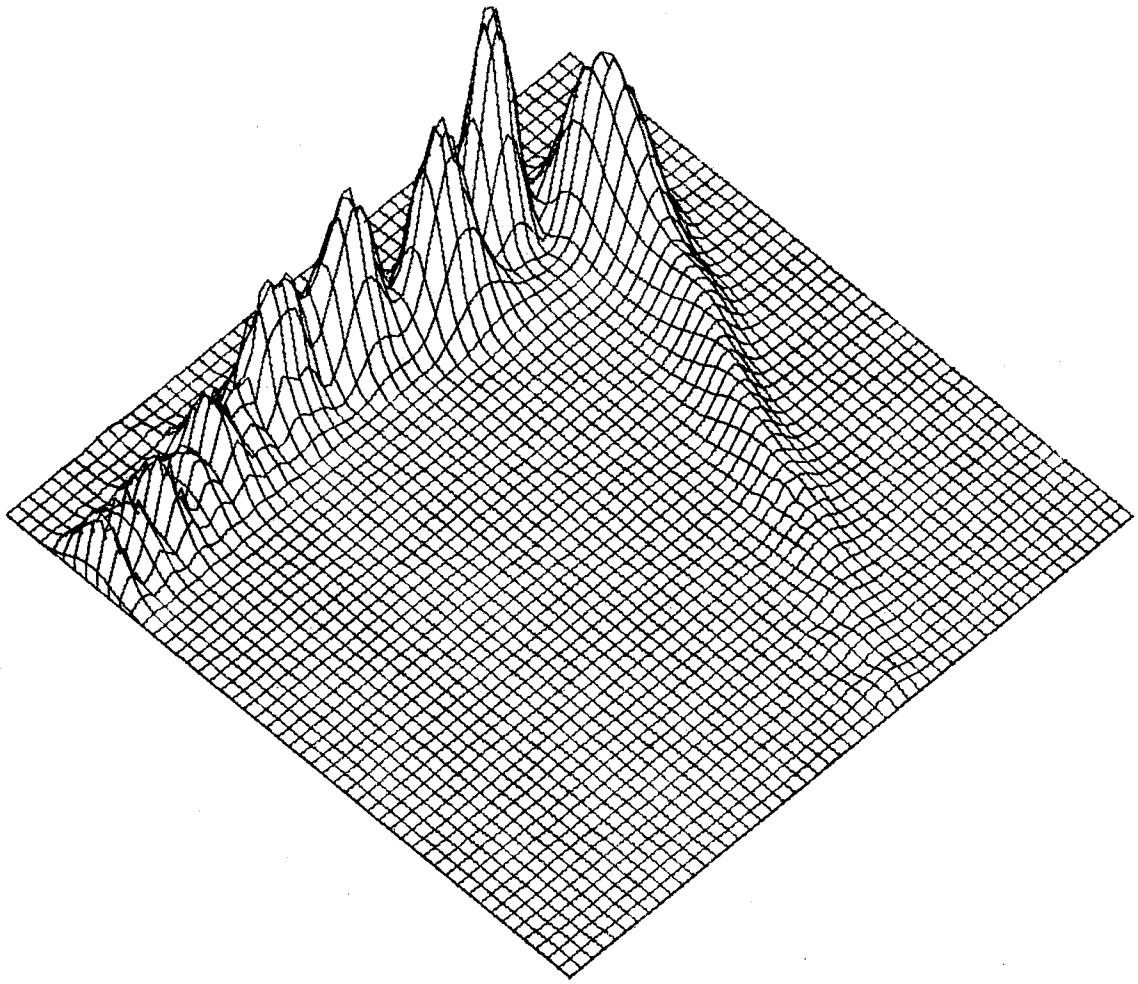

Figure 27. Calculation B, t = 165 Δt

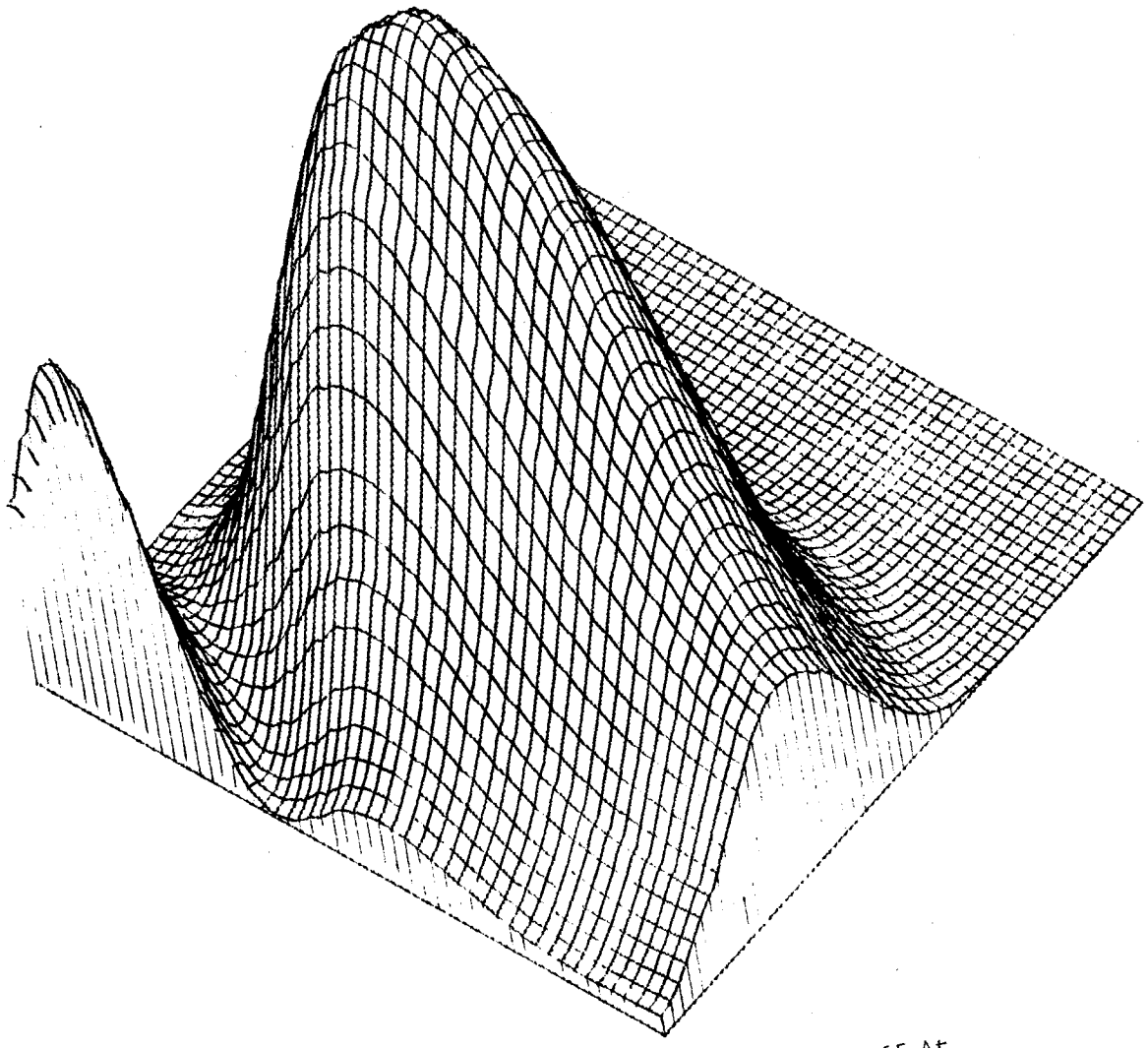

Figure 28. Calculation B, $t = 165\ \Delta t$

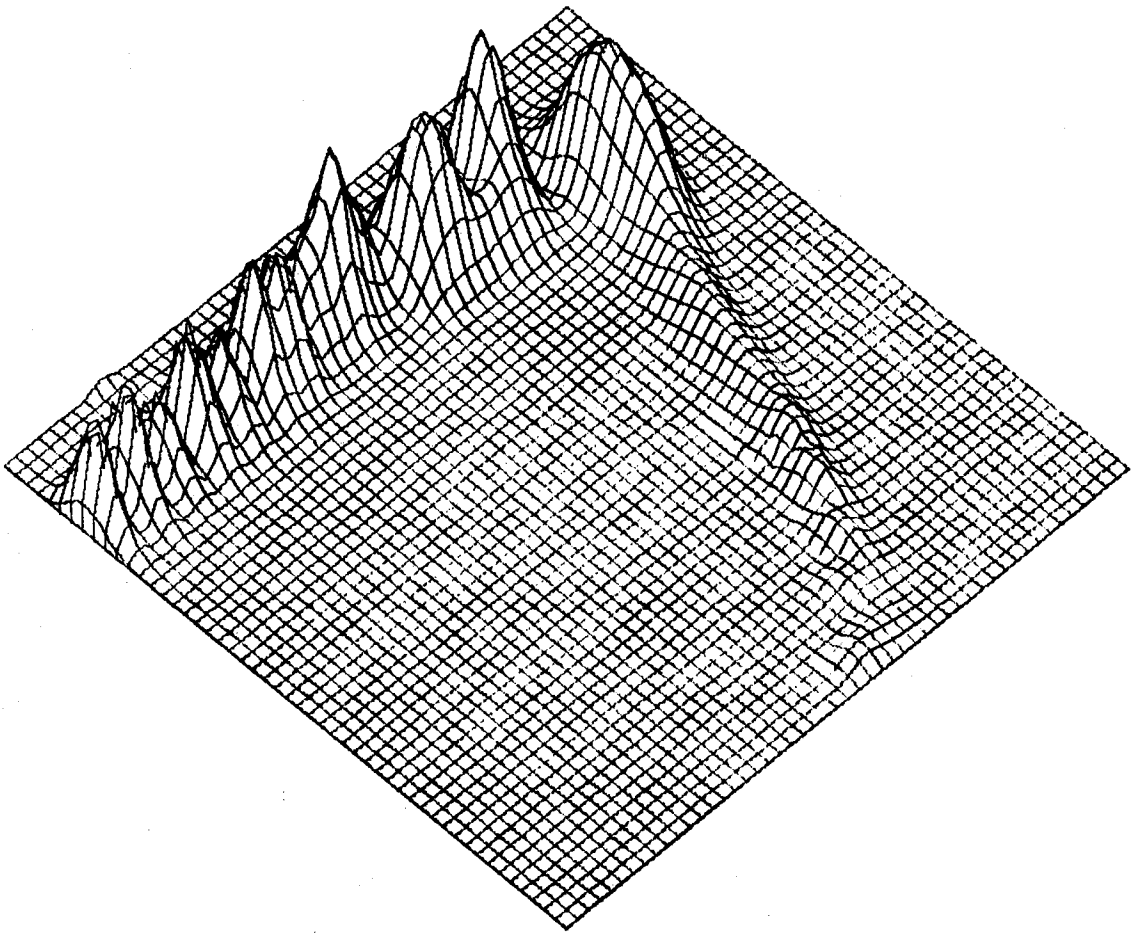

Figure 29. Calculation B, t = 172.5 Δt

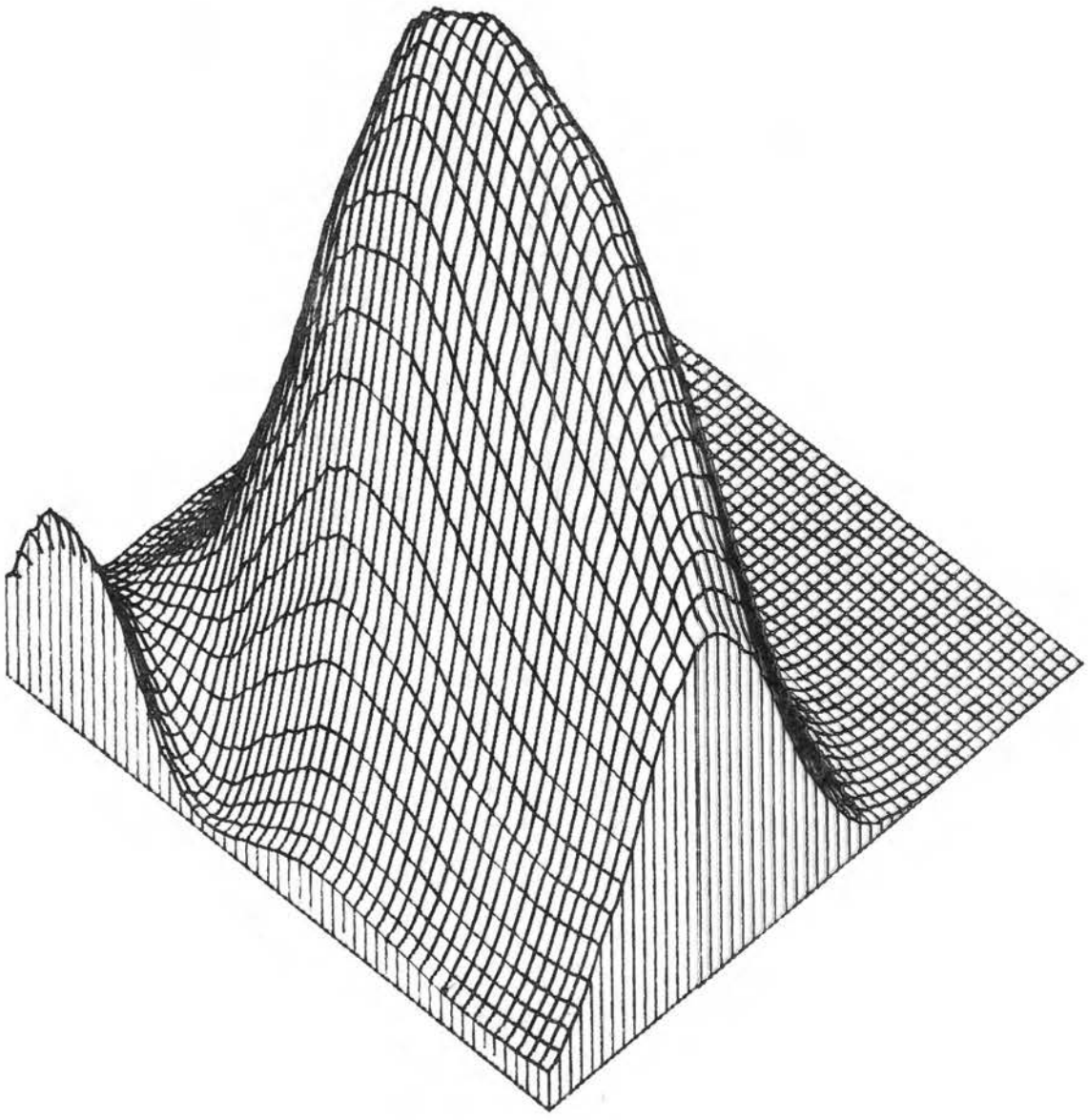

Figure 30. Calculation B, t = 172.5 Δt, FAC = 2.77

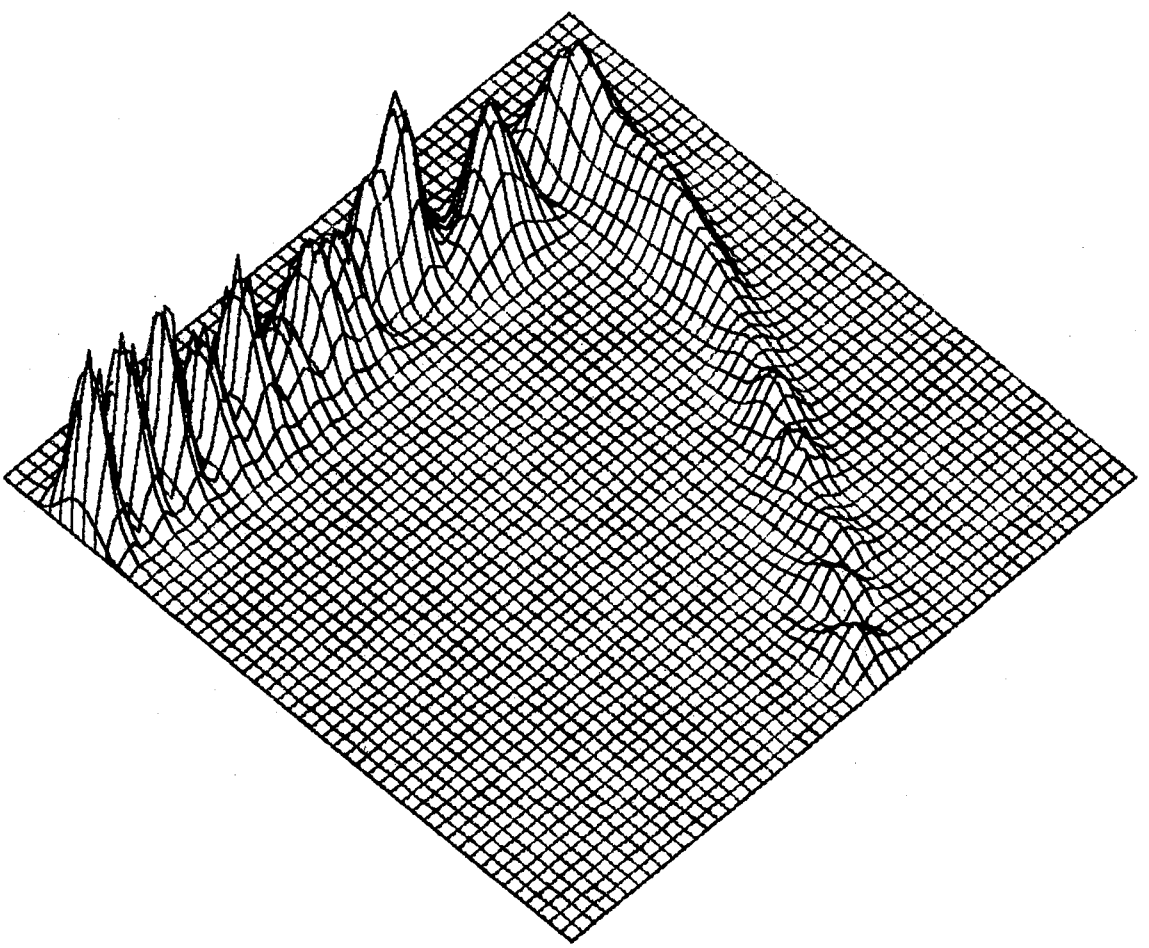

Figure 31. Calculation B, t = 187.5 Δt

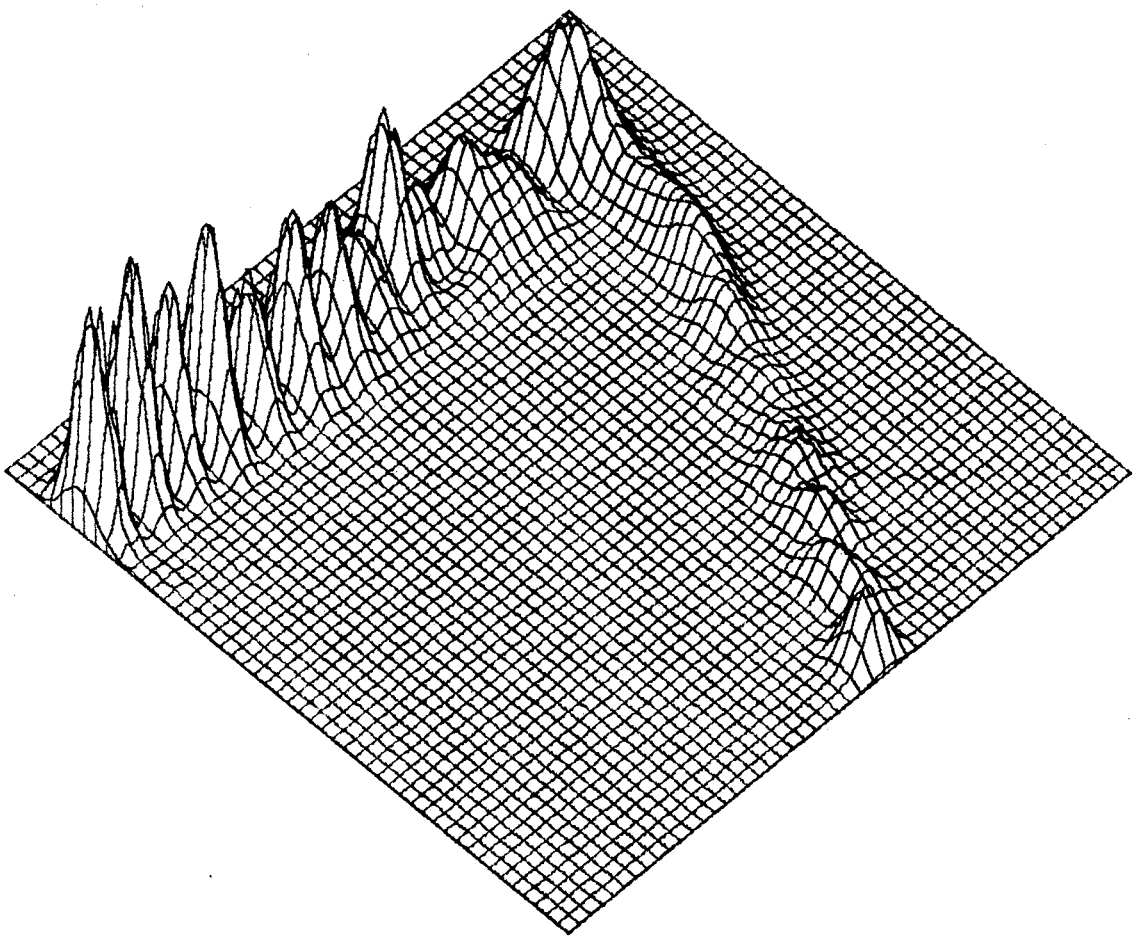

Figure 32. Calculation B, t = 197.5 Δt

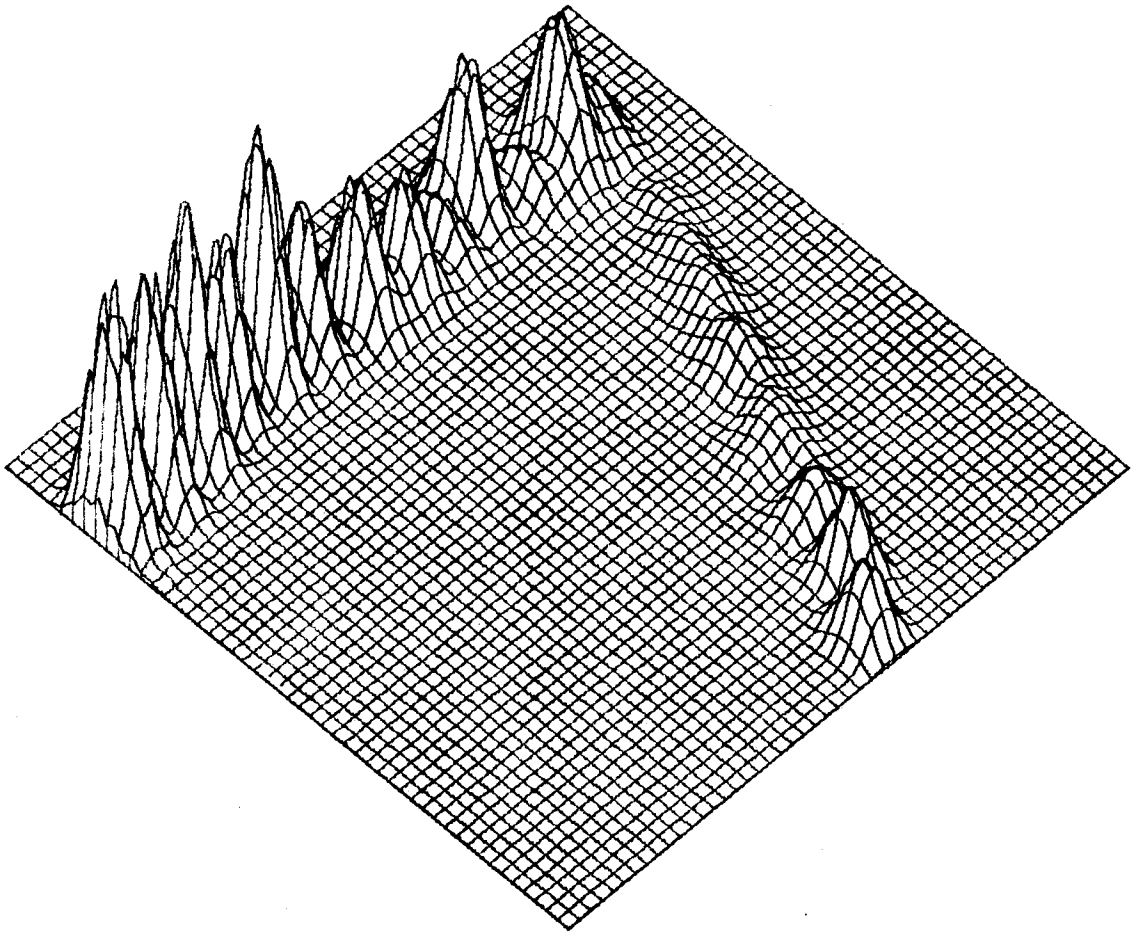

Figure 33. Calculation B, t = 217.5 Δt

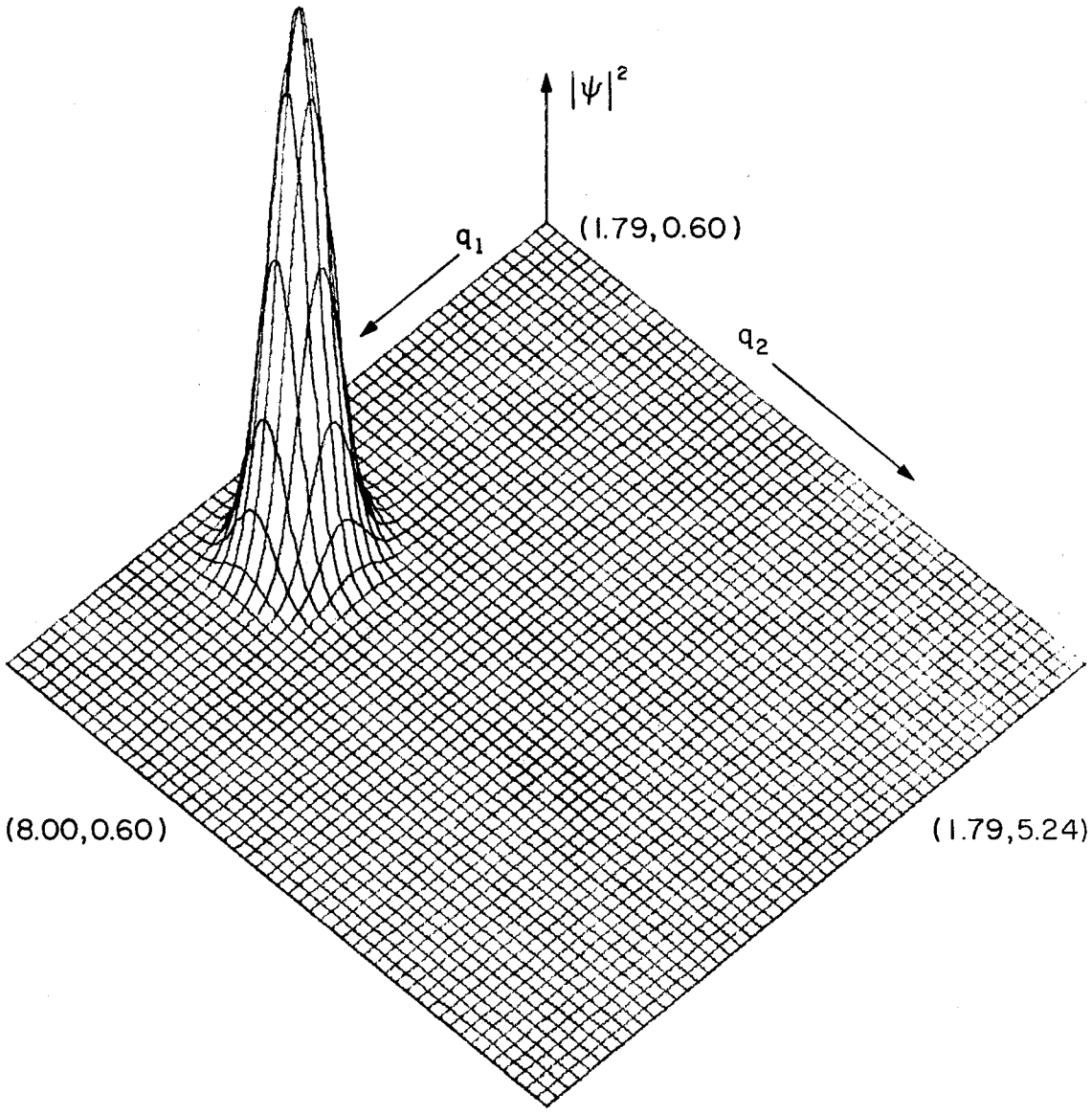

Figure 34. Calculation C, t = 0 Δt, FAC = 1.25

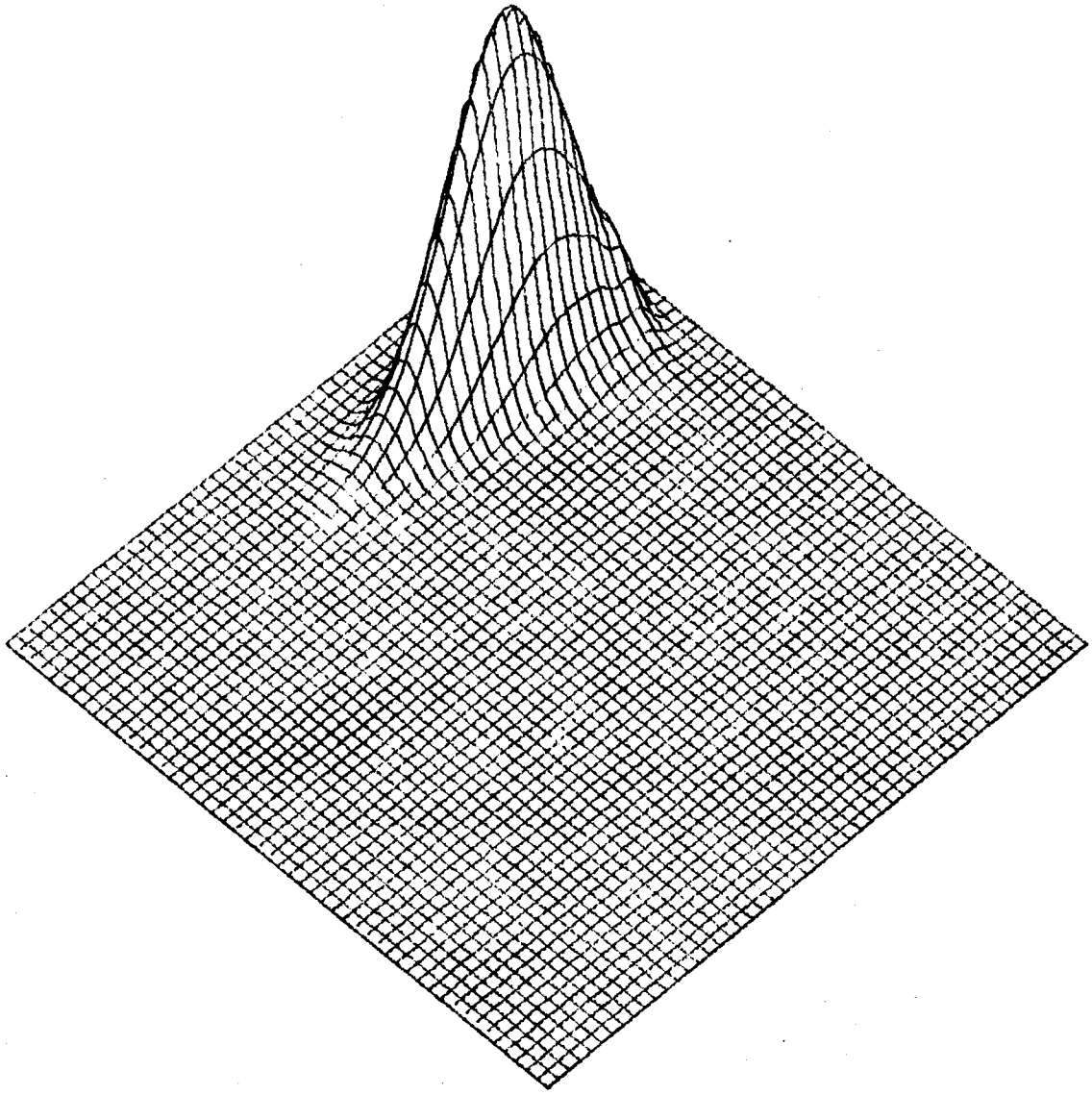

Figure 35. Calculation C, t = 45 Δt

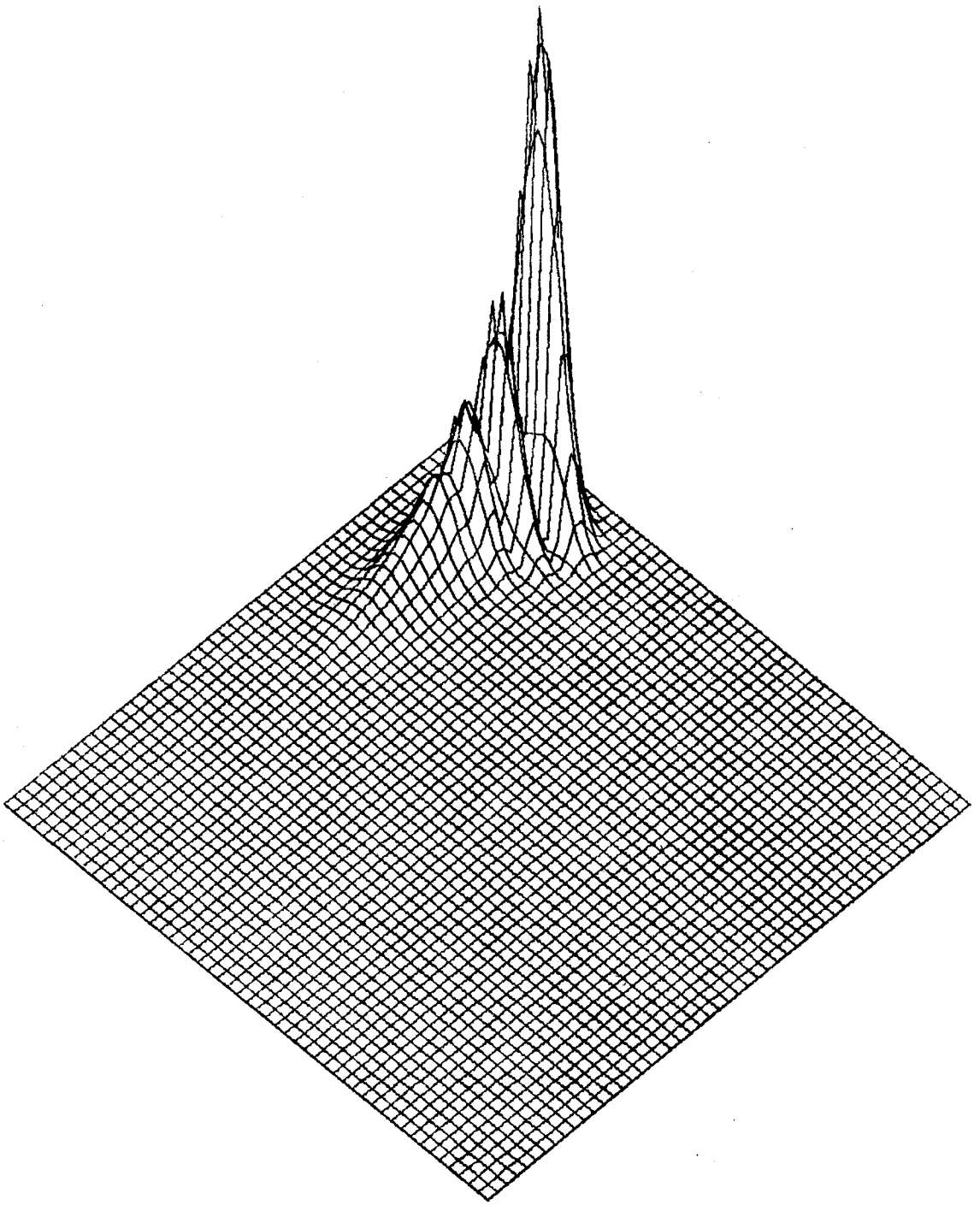

Figure 36. Calculation C, t = 60 Δt

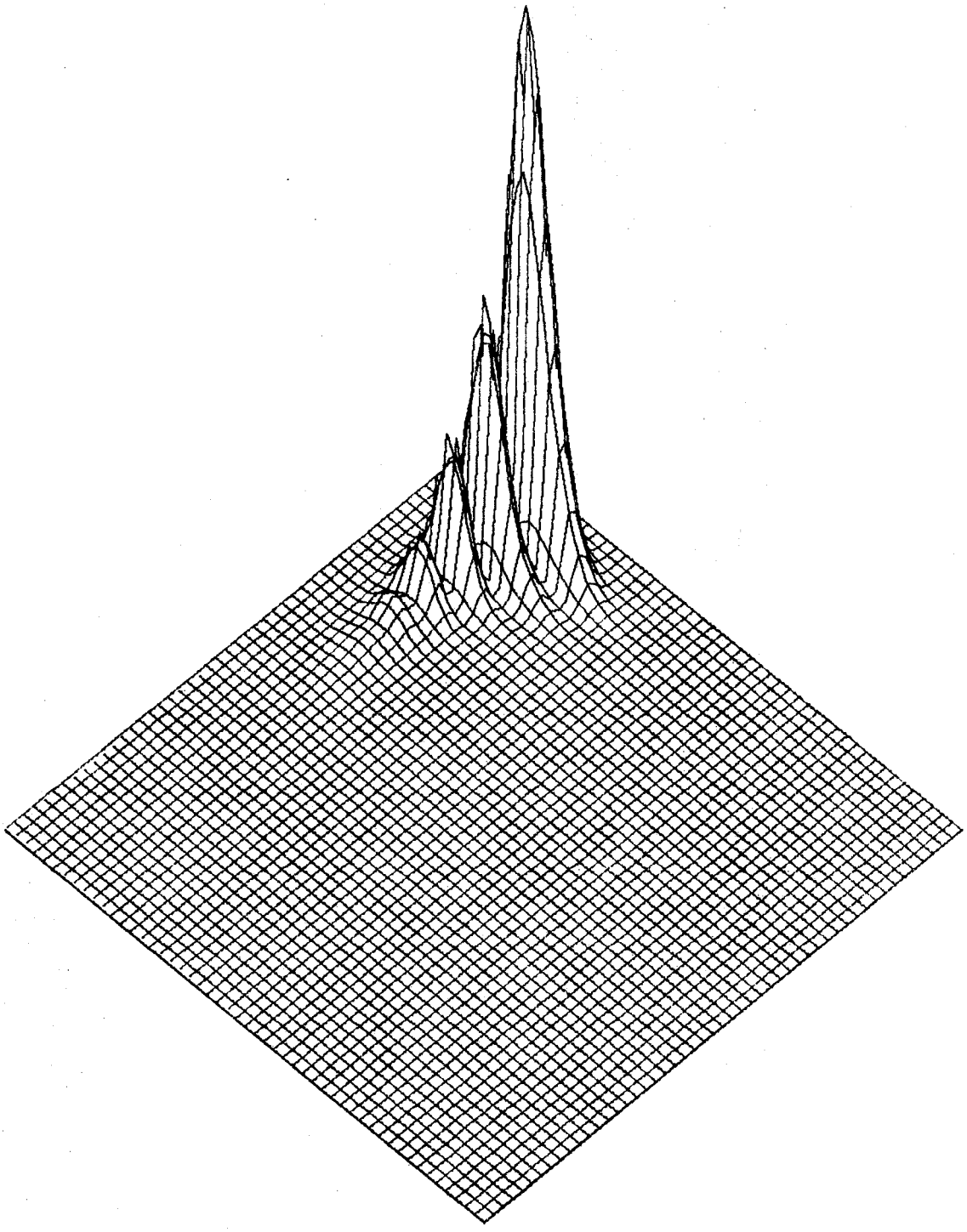

Figure 37. Calculation C, t = 67.5 Δt

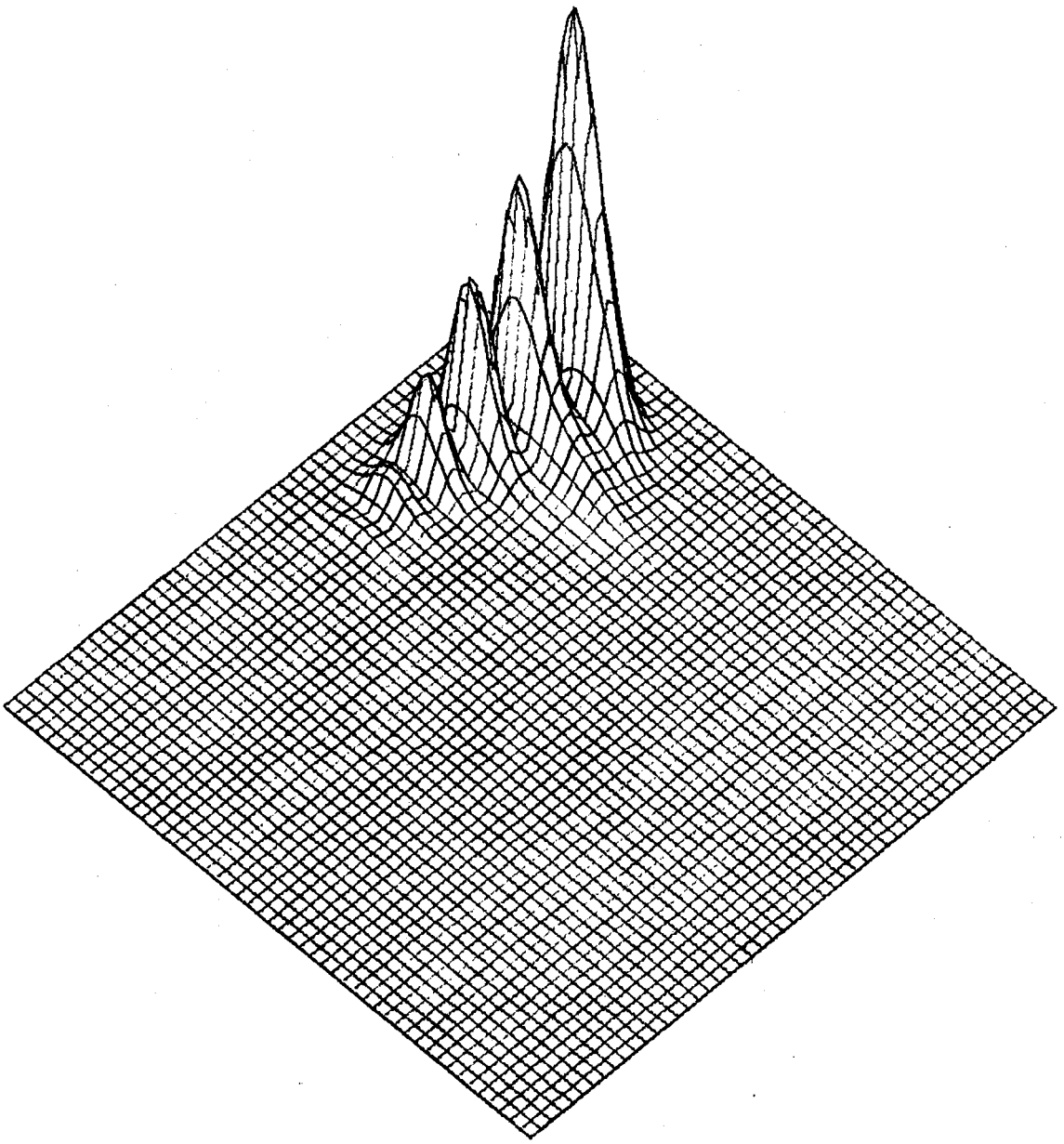

Figure 38. Calculation C, t = 80 Δt

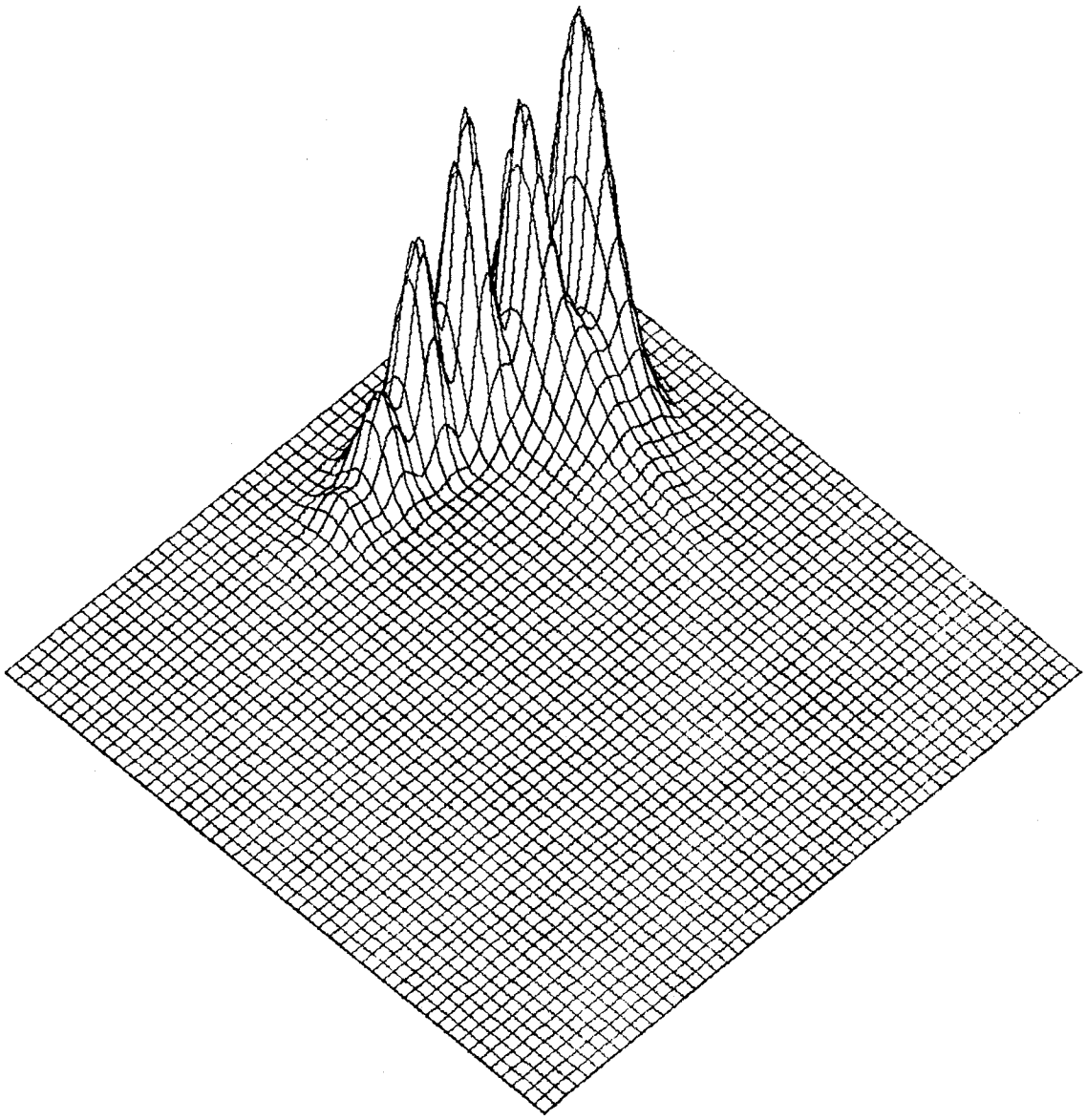

Figure 39. Calculation C, t = 90 Δt

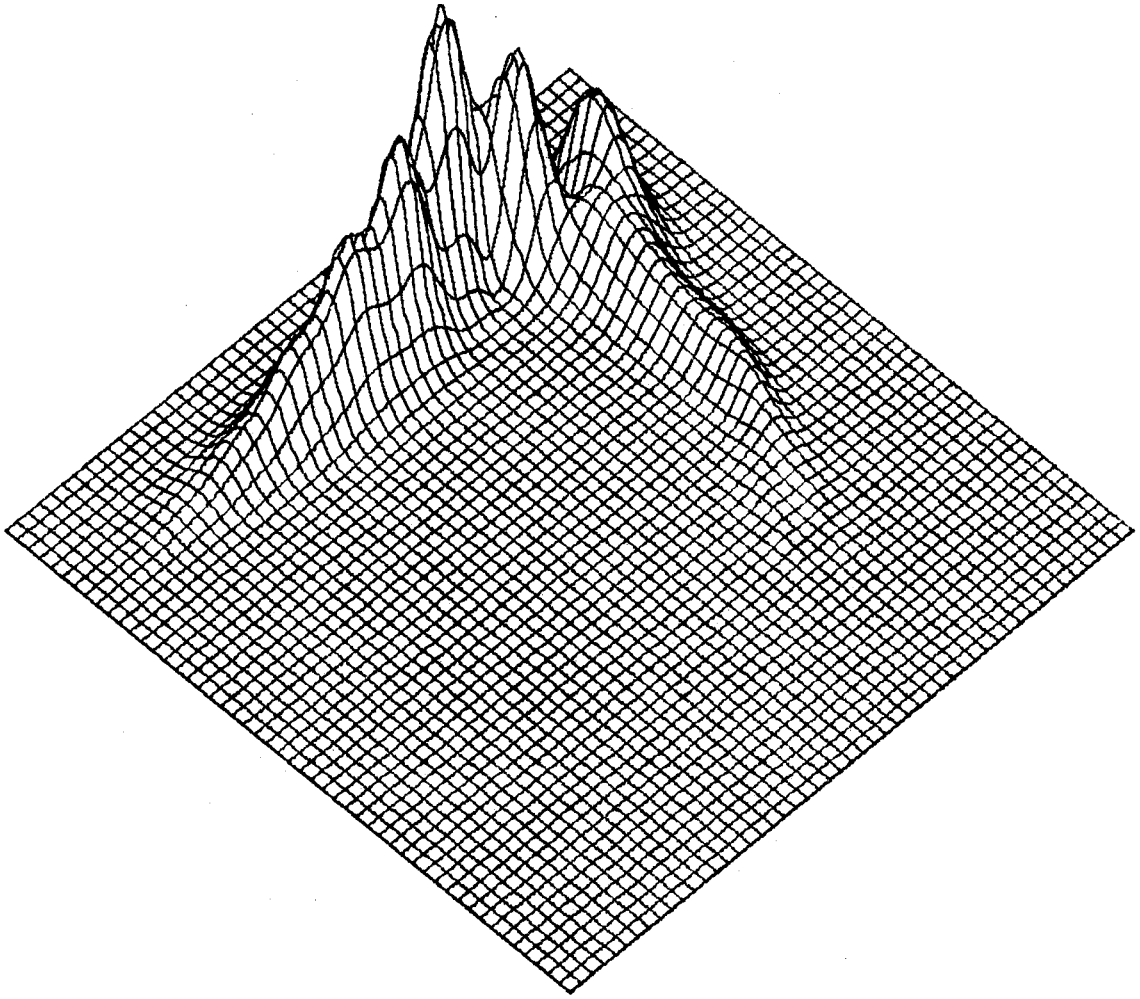

Figure 40. Calculation C, t = 110 Δt

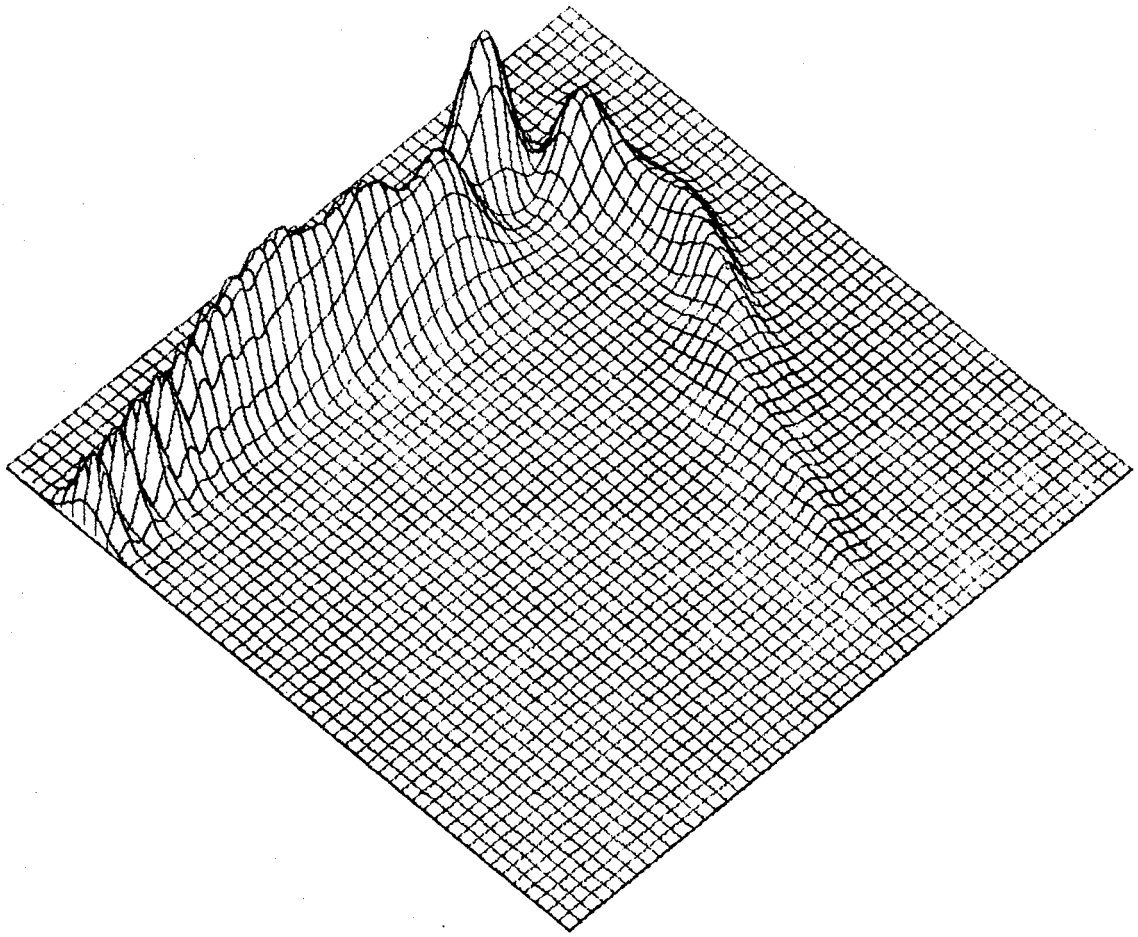

Figure 41. Calculation C, t = 130 Δt

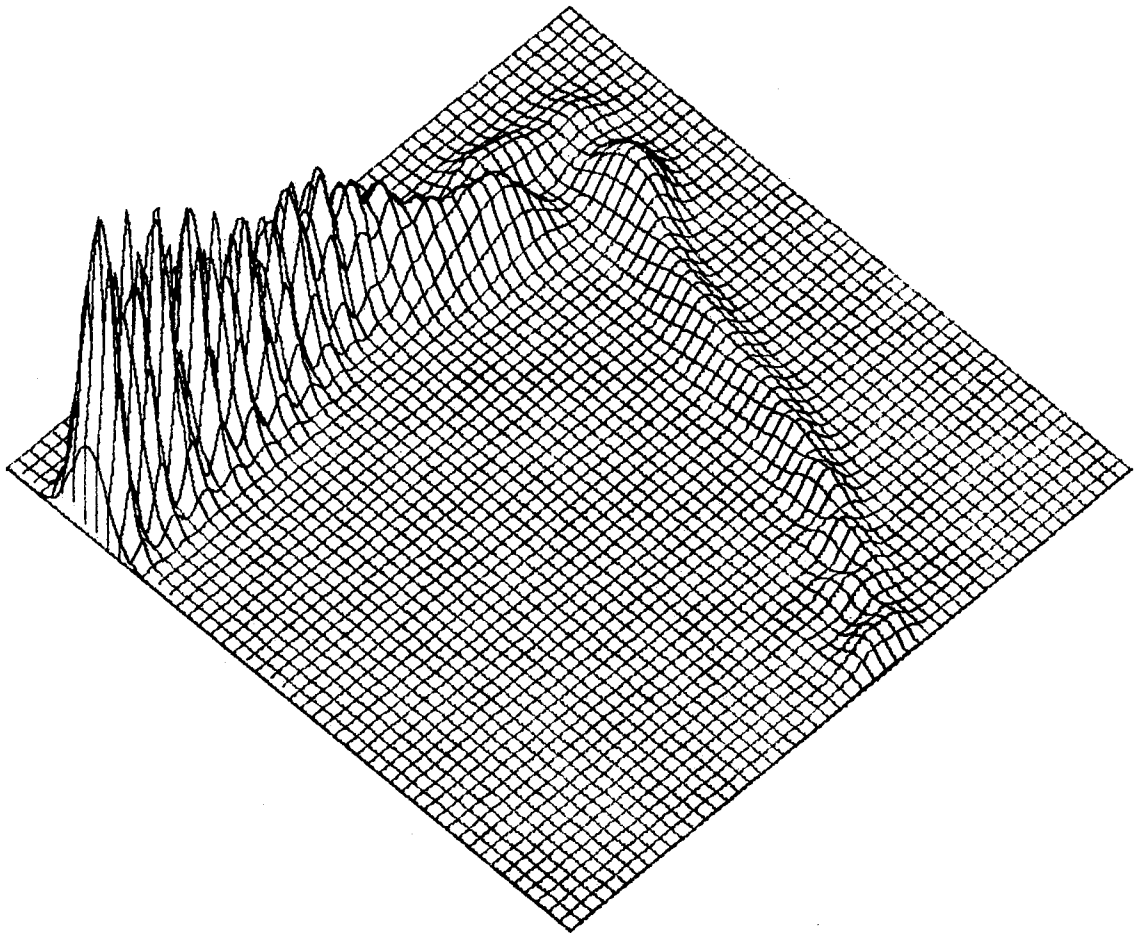

Figure 42. Calculation C, t = 150 Δt

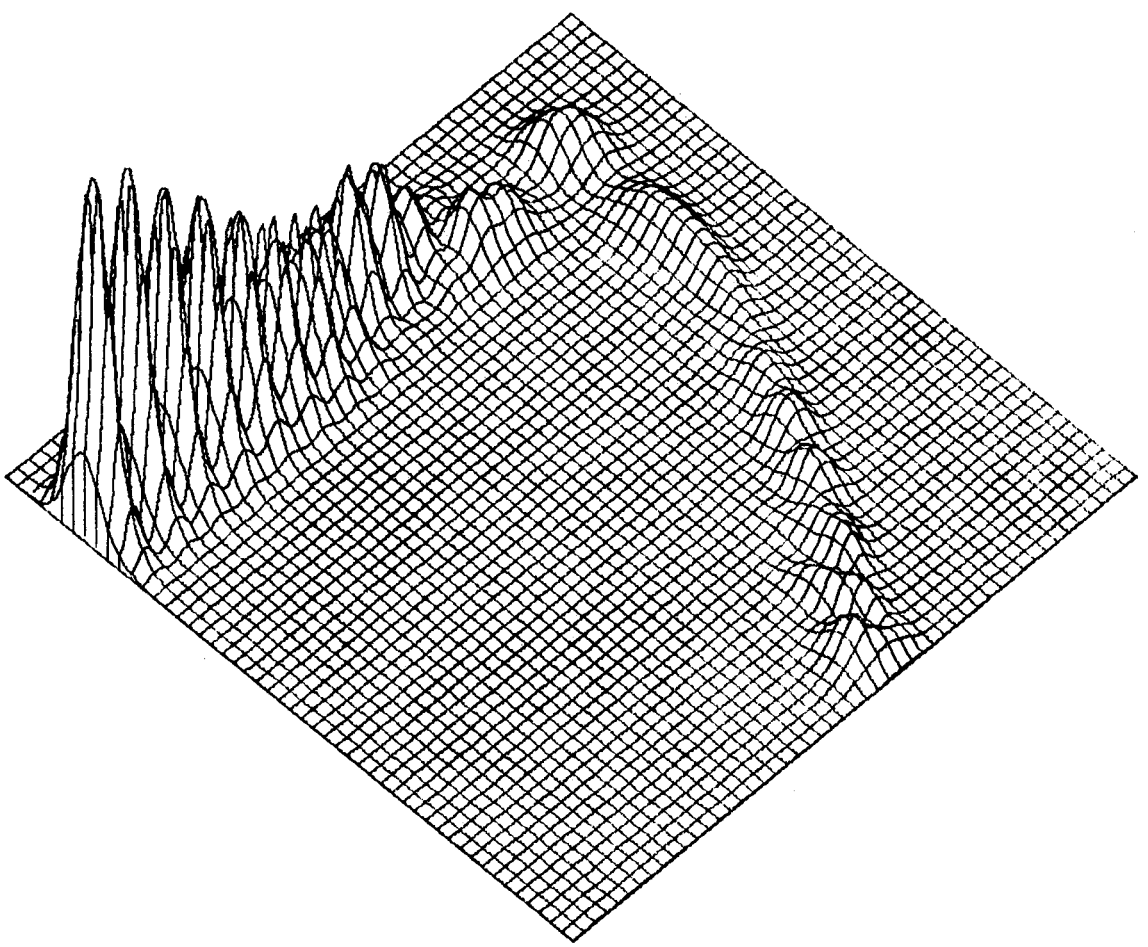

Figure 43. Calculation C, t = 162.5 Δt

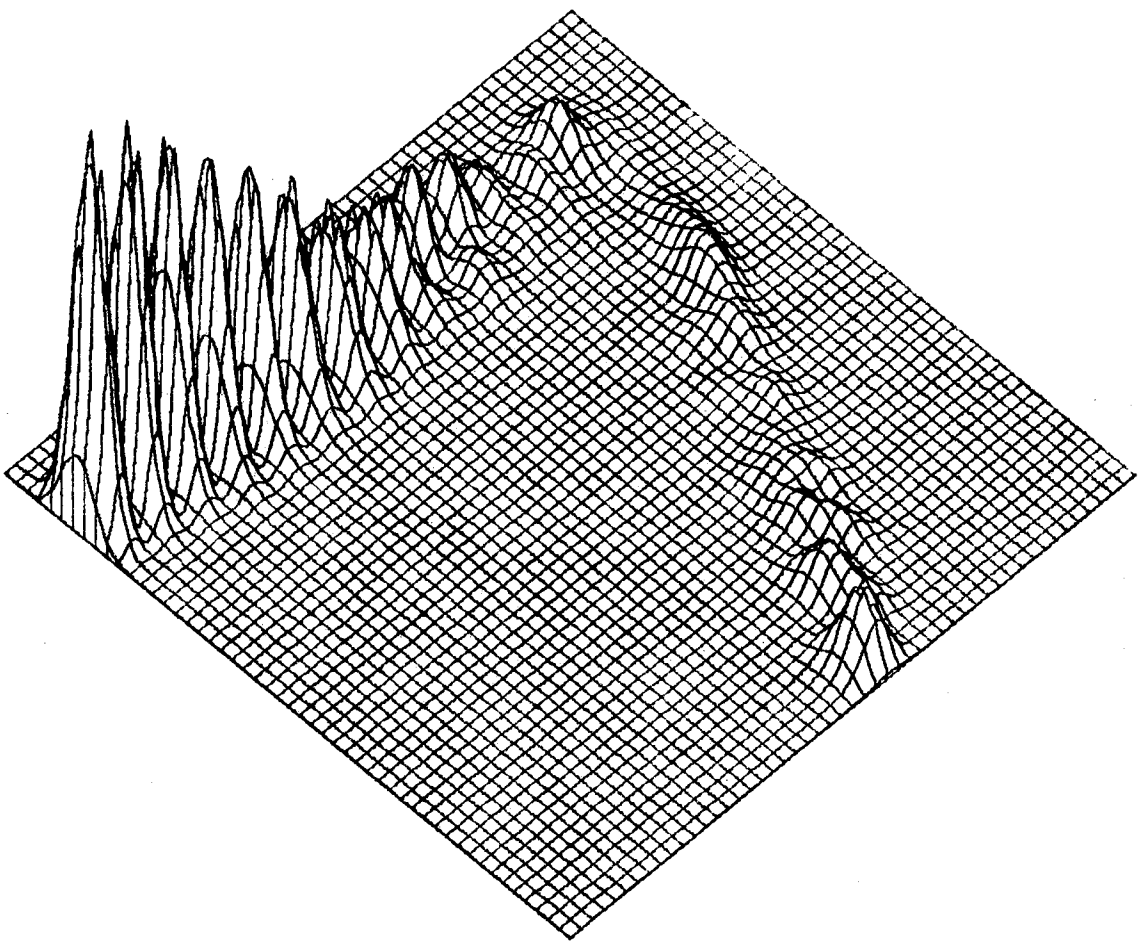

Figure 44. Calculation C, t = 175 Δt

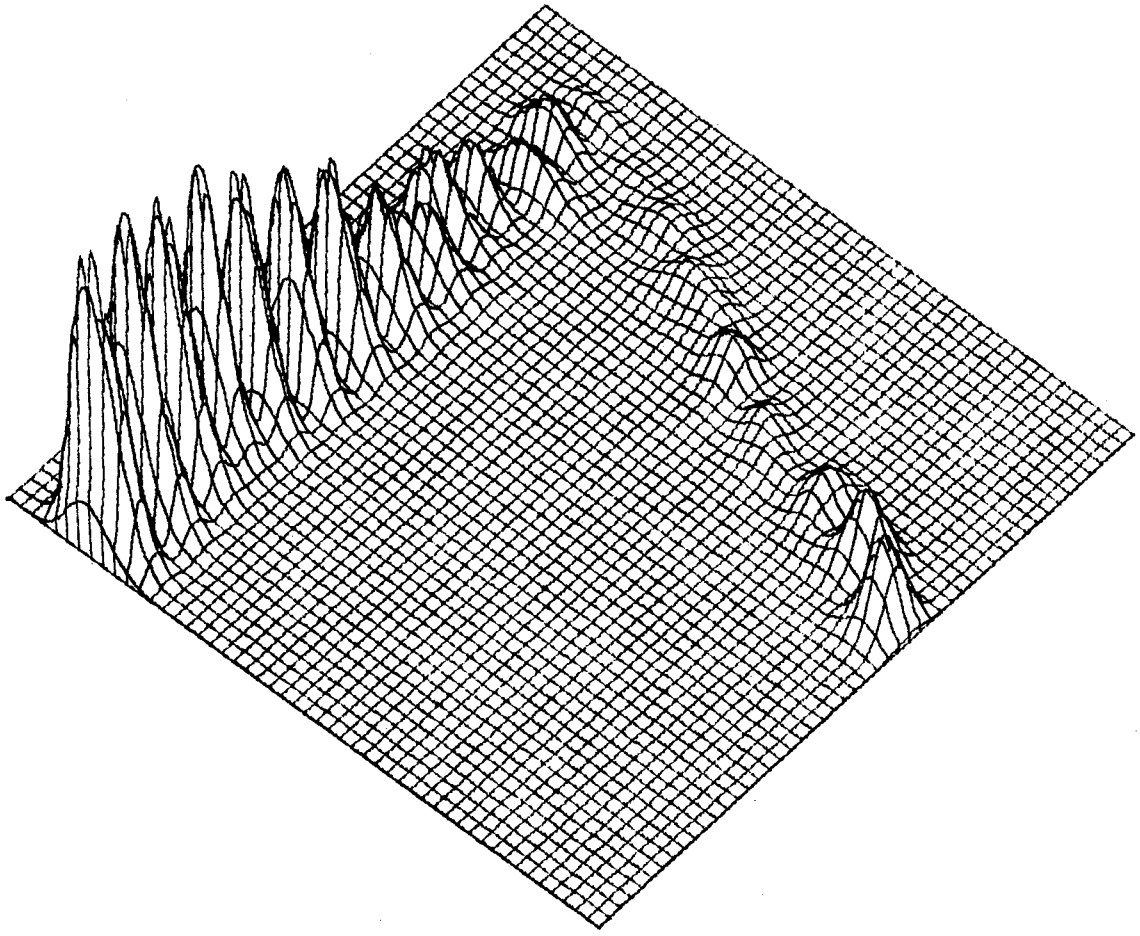

Figure 45. Calculation C, t = 187.5 Δt

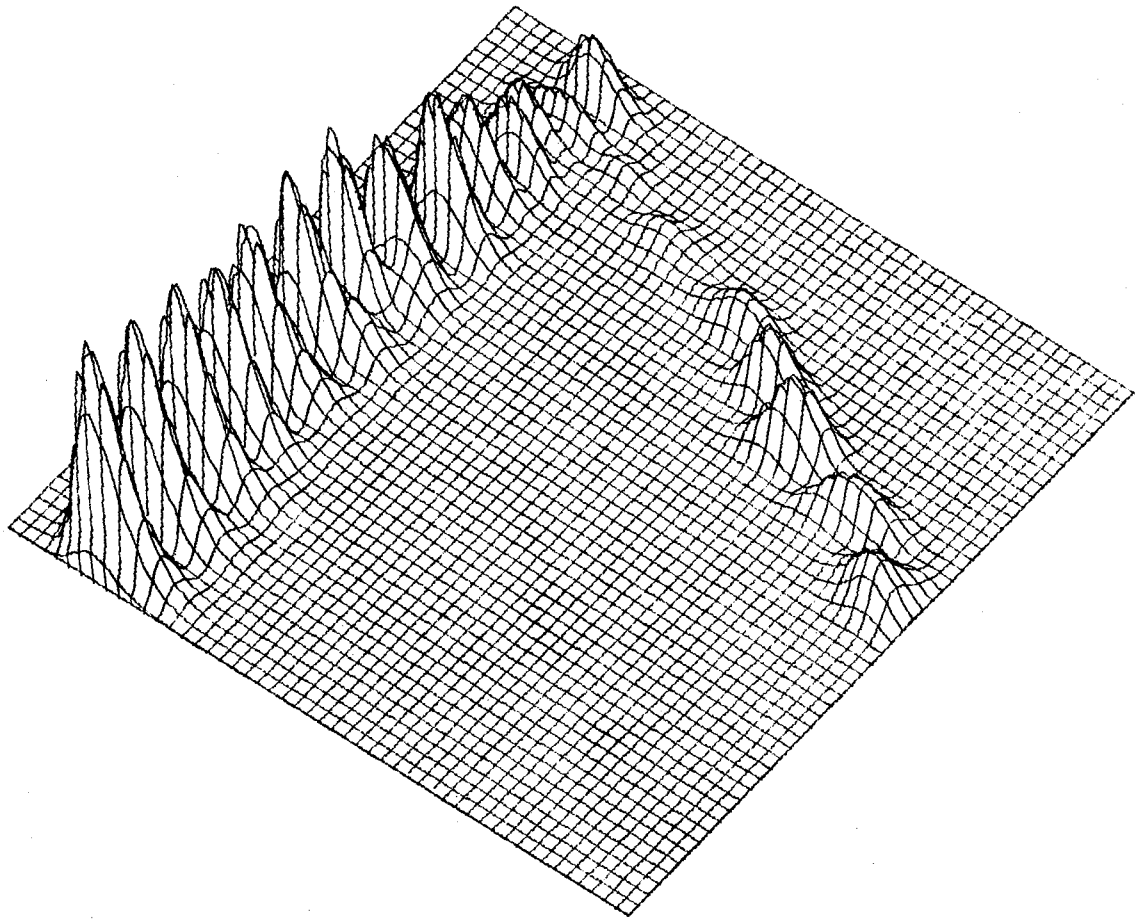

Figure 46. Calculation C, $t = 212.5\ \Delta t$

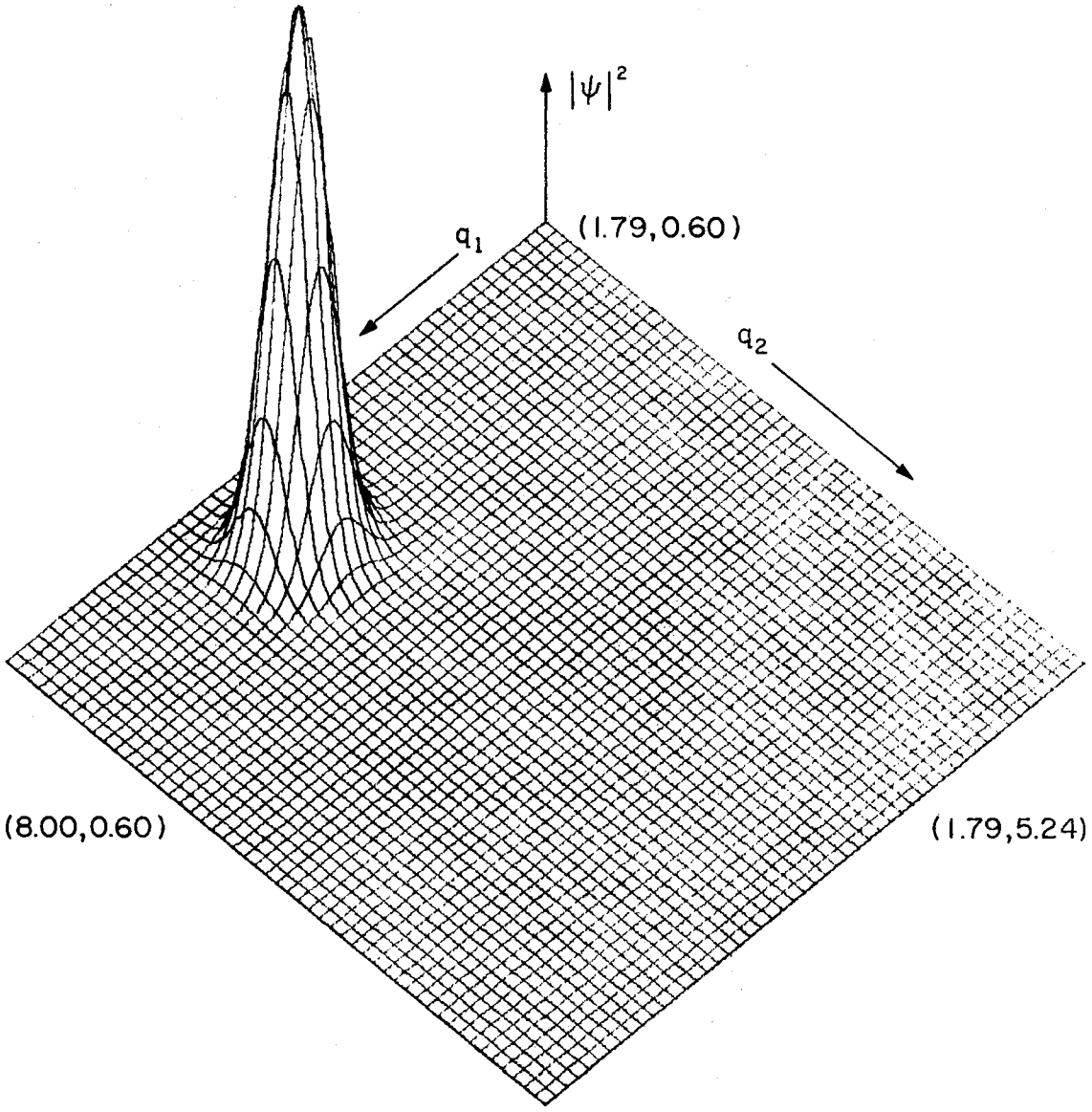

Figure 47. Calculation D, t = 0 Δt, FAC = 1.25

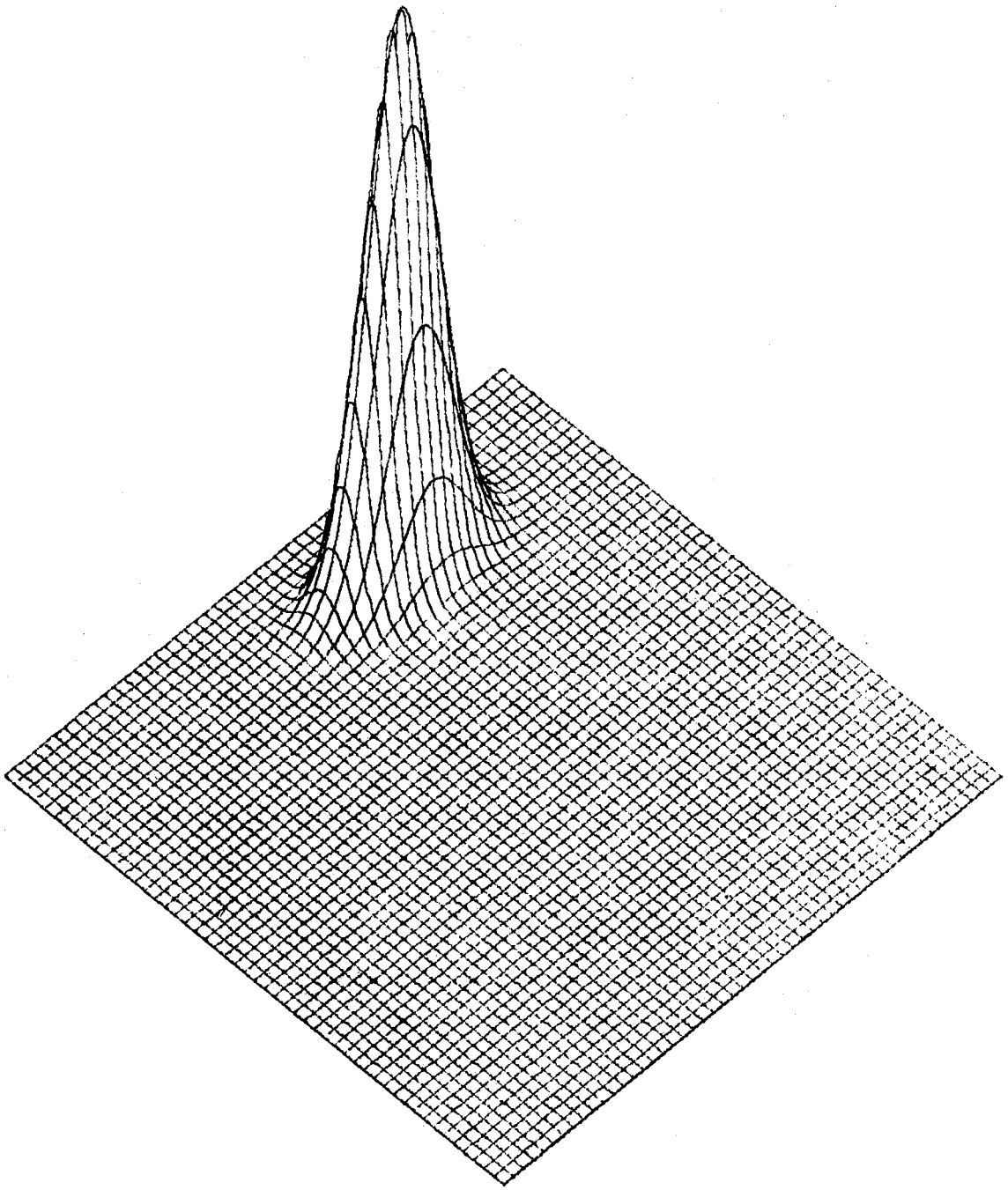

Figure 48. Calculation D, t = 25 Δt

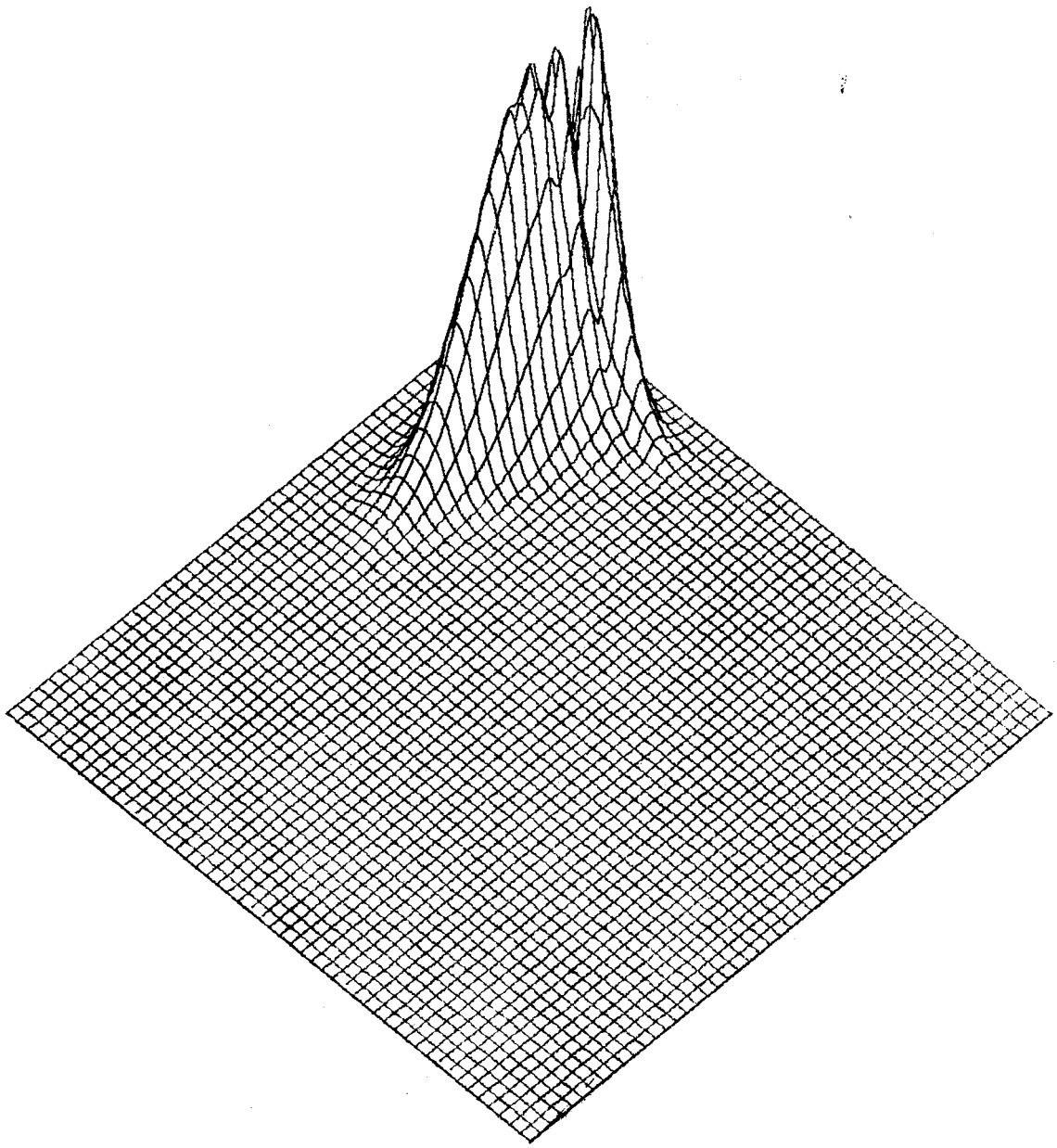

Figure 49. Calculation D, t = 45 Δt

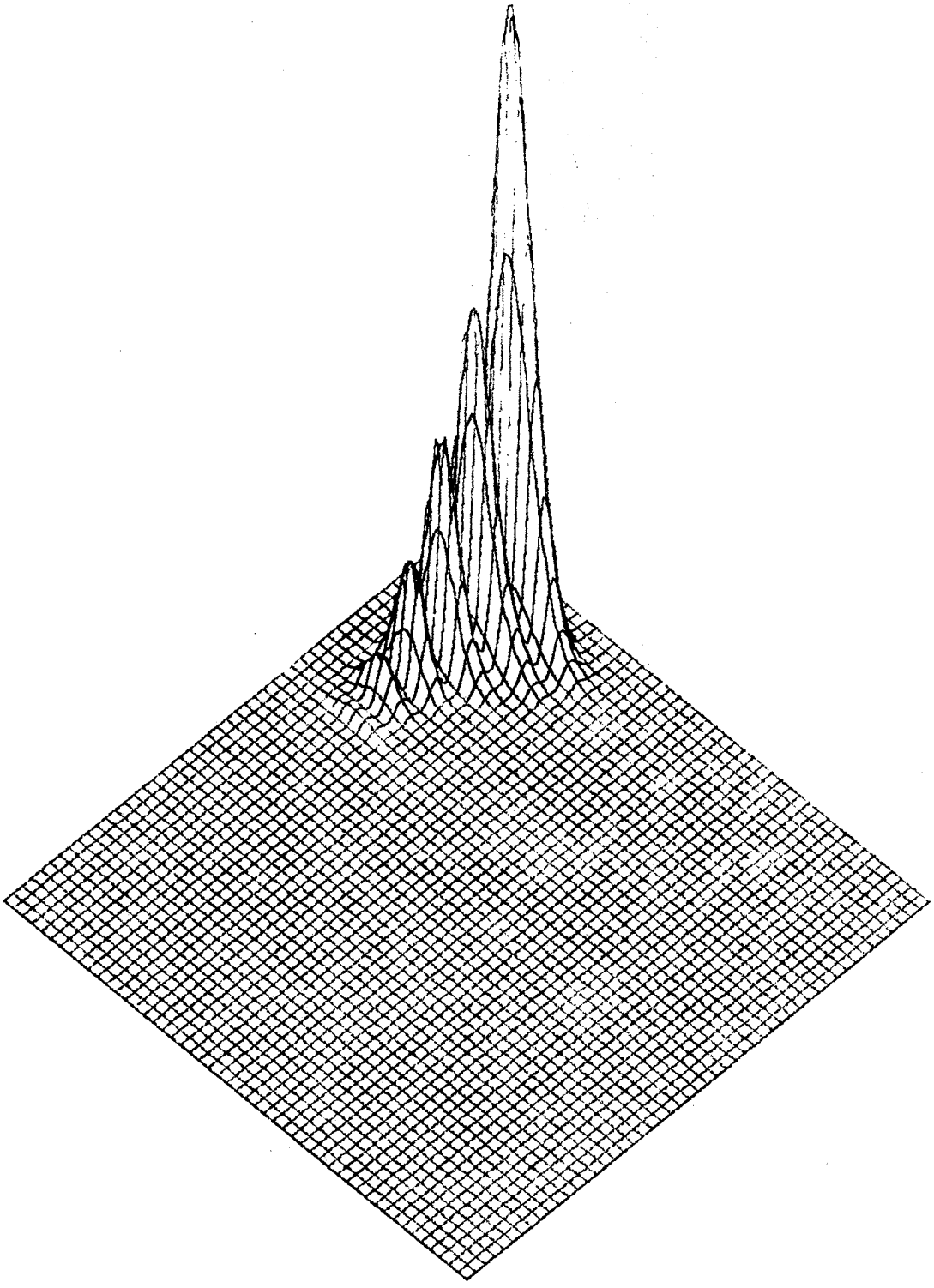

Figure 50. Calculation D, t = 65 Δt

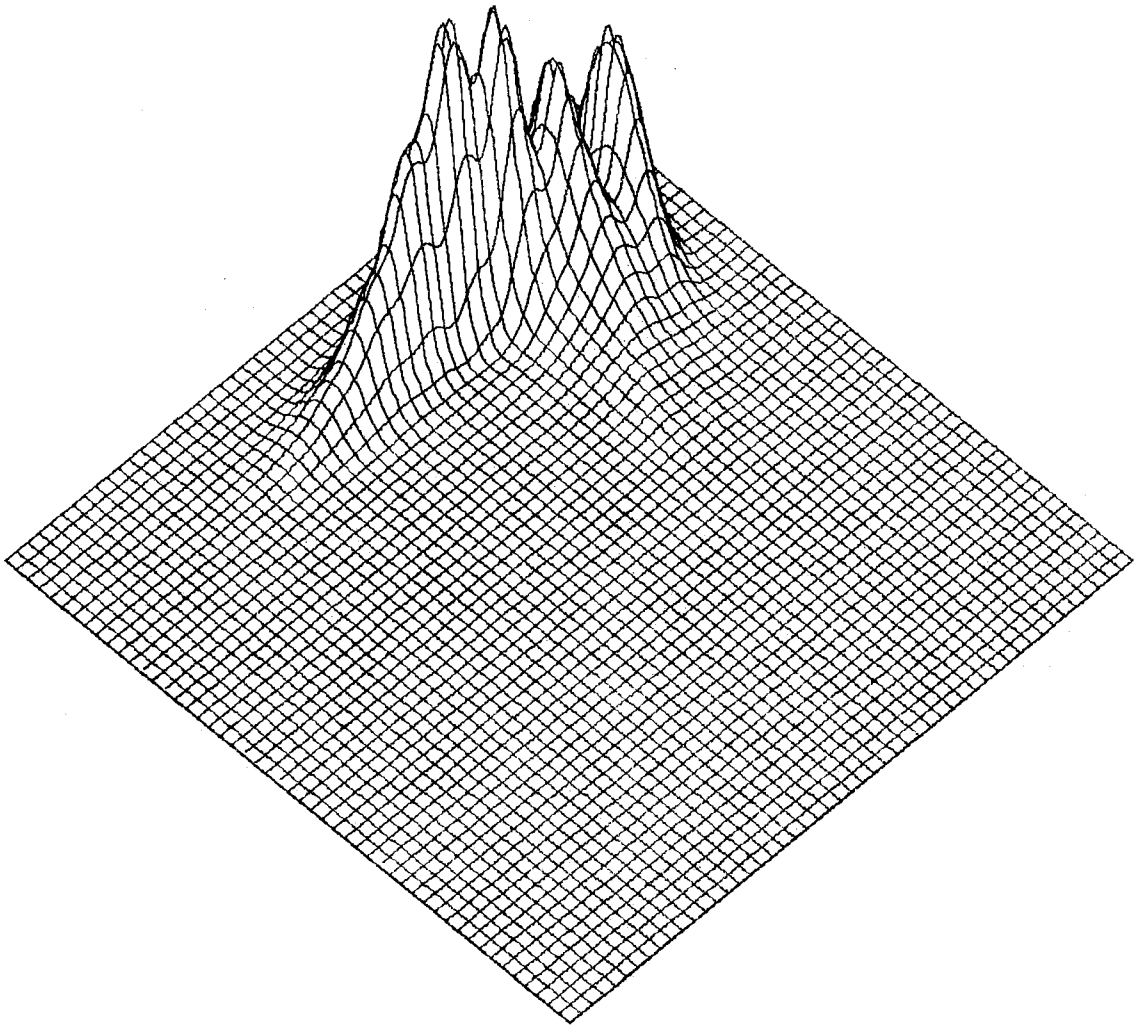

Figure 51. Calculation D, t = 85 Δt

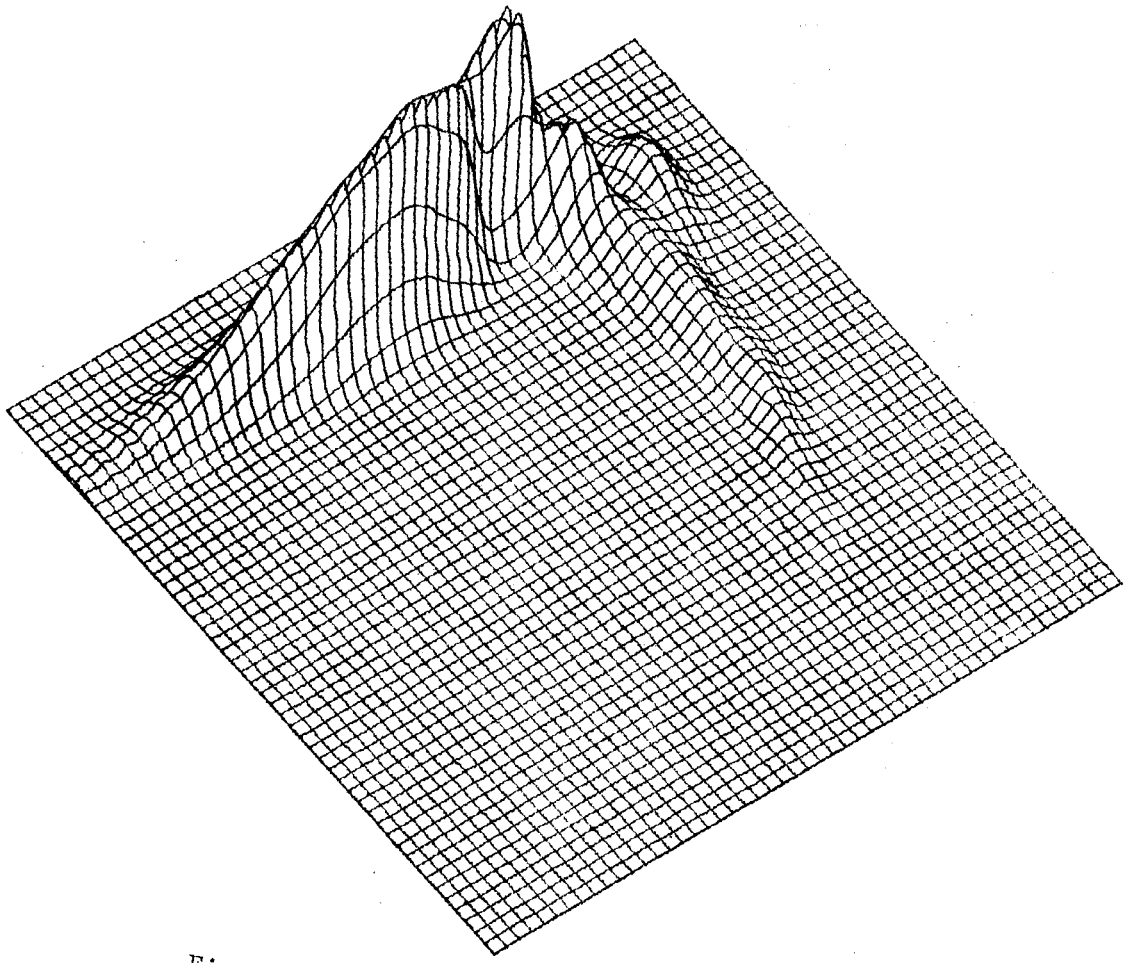

Figure 52. Calculation D, $t = 105\ \Delta t$

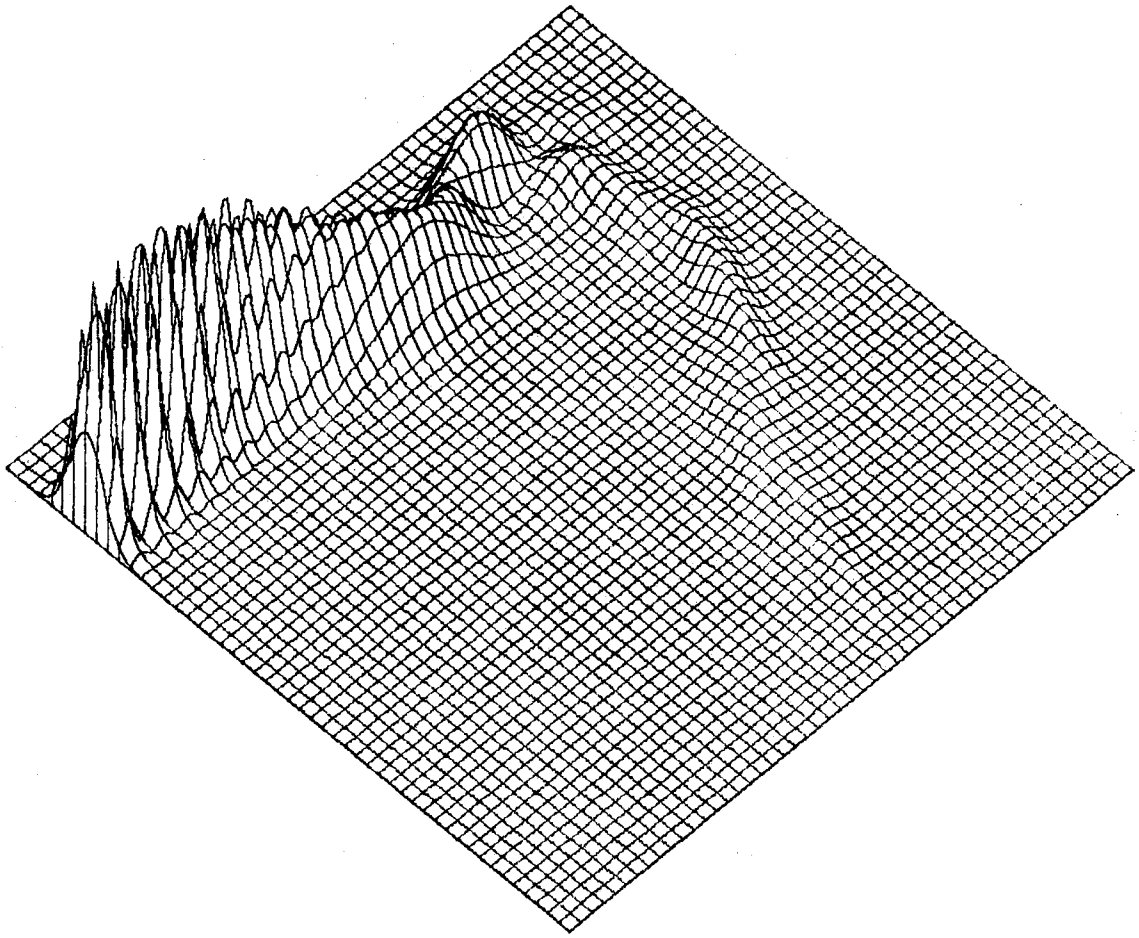

Figure 53. Calculation D, t = 125 Δt

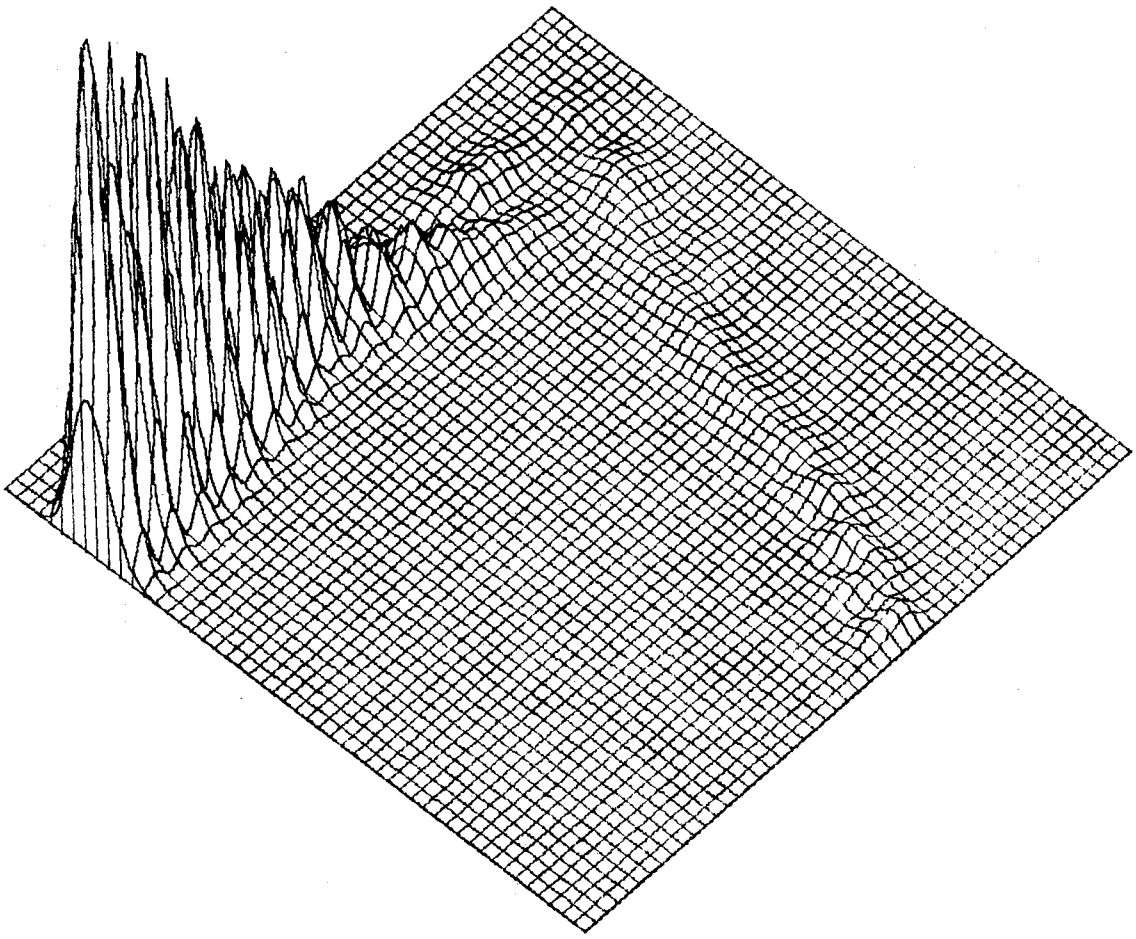

Figure 54. Calculation D, t = 145 Δt

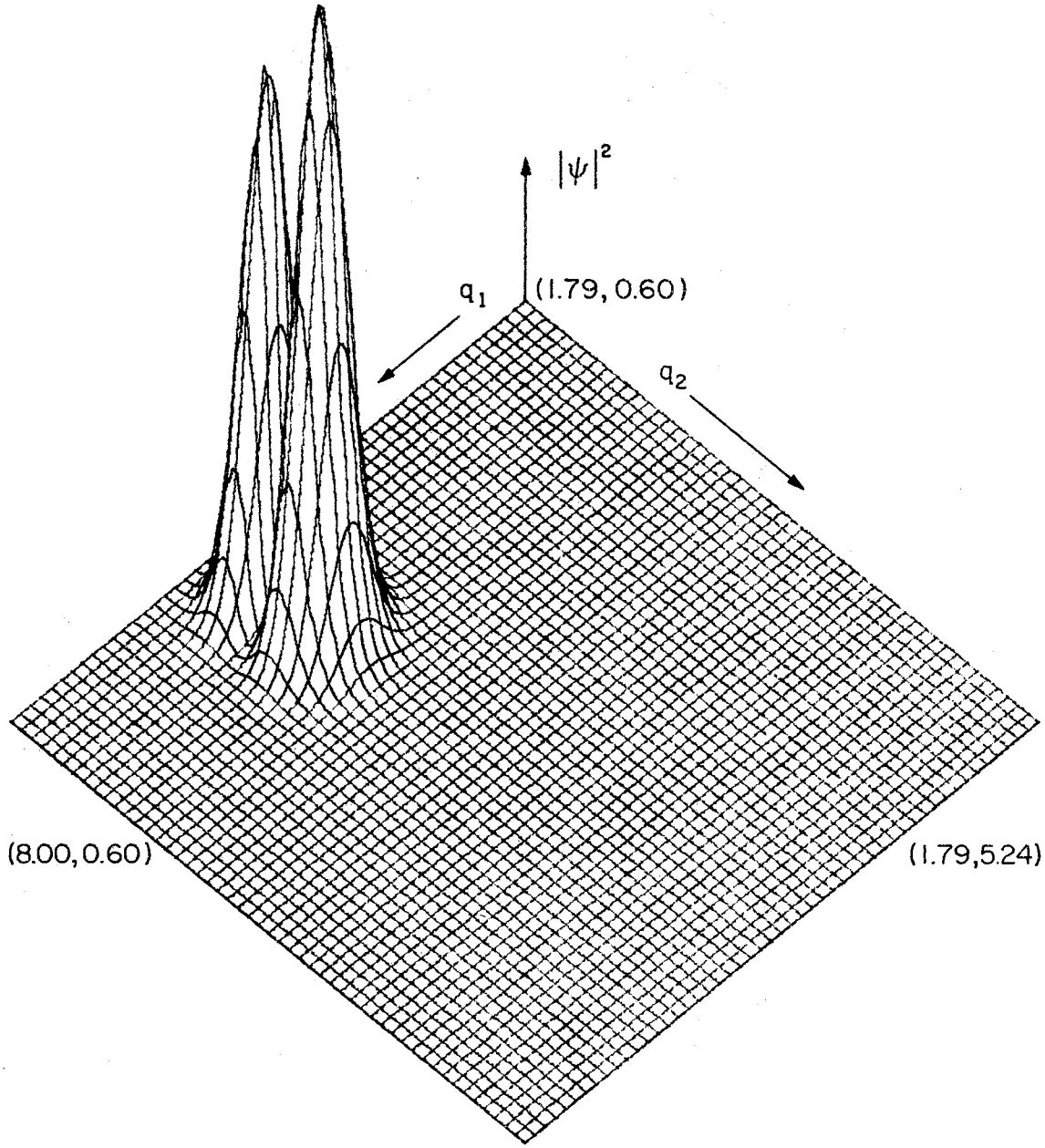

Figure 55. Calculation E, t = 0 Δt

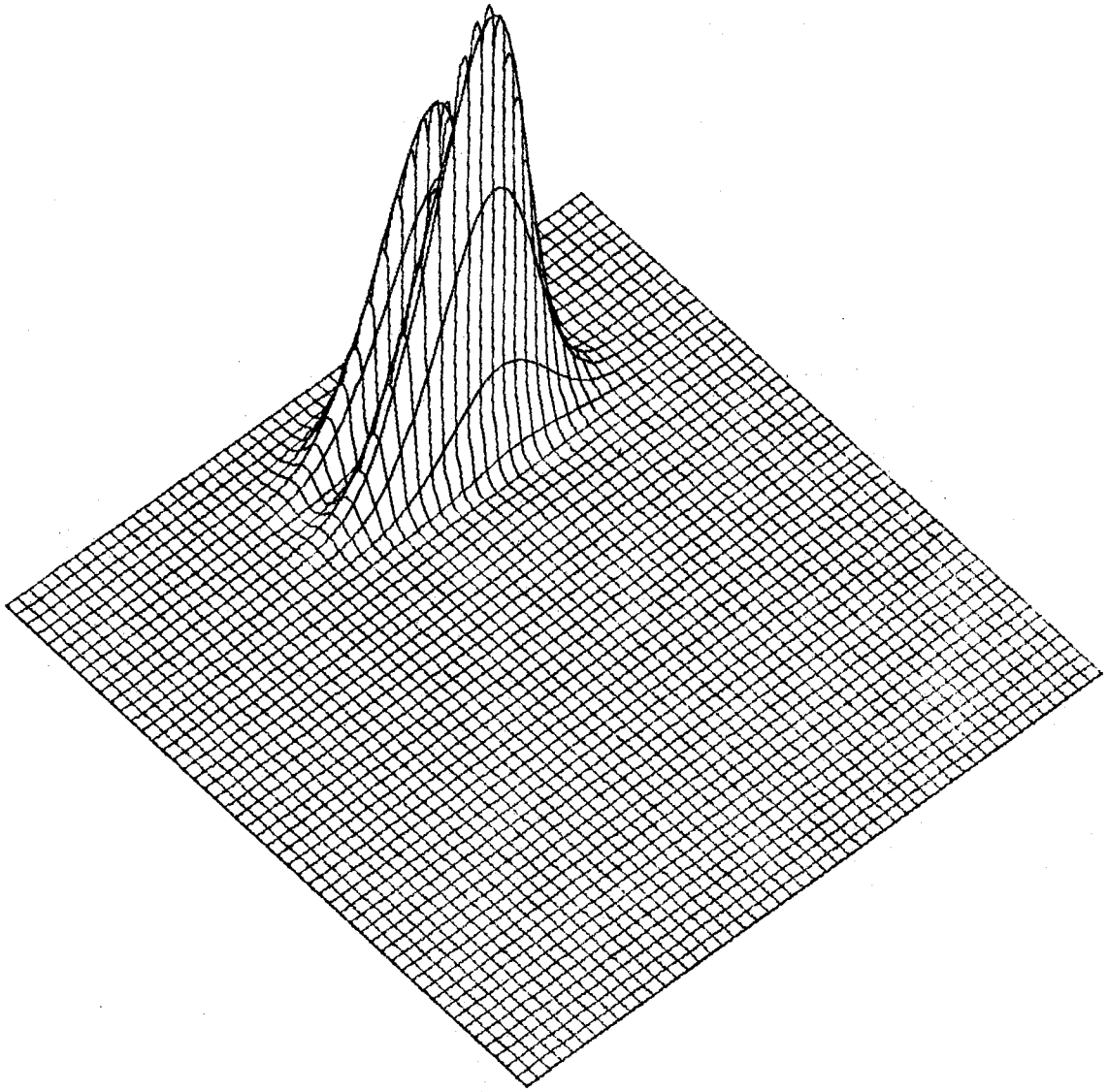

Figure 56. Calculation E, $t = 32.5\,\Delta t$

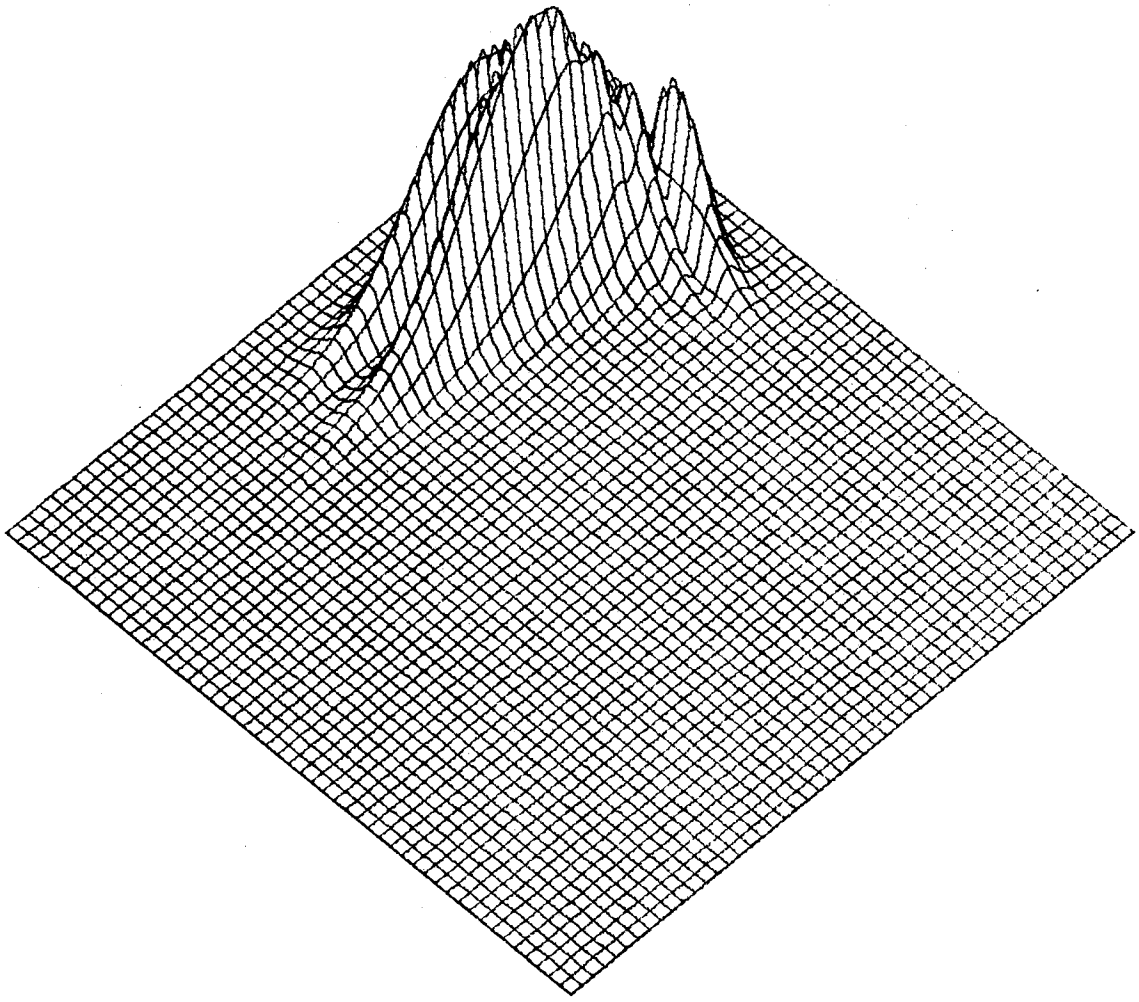

Figure 57. Calculation E, $t = 52.5\,\Delta t$

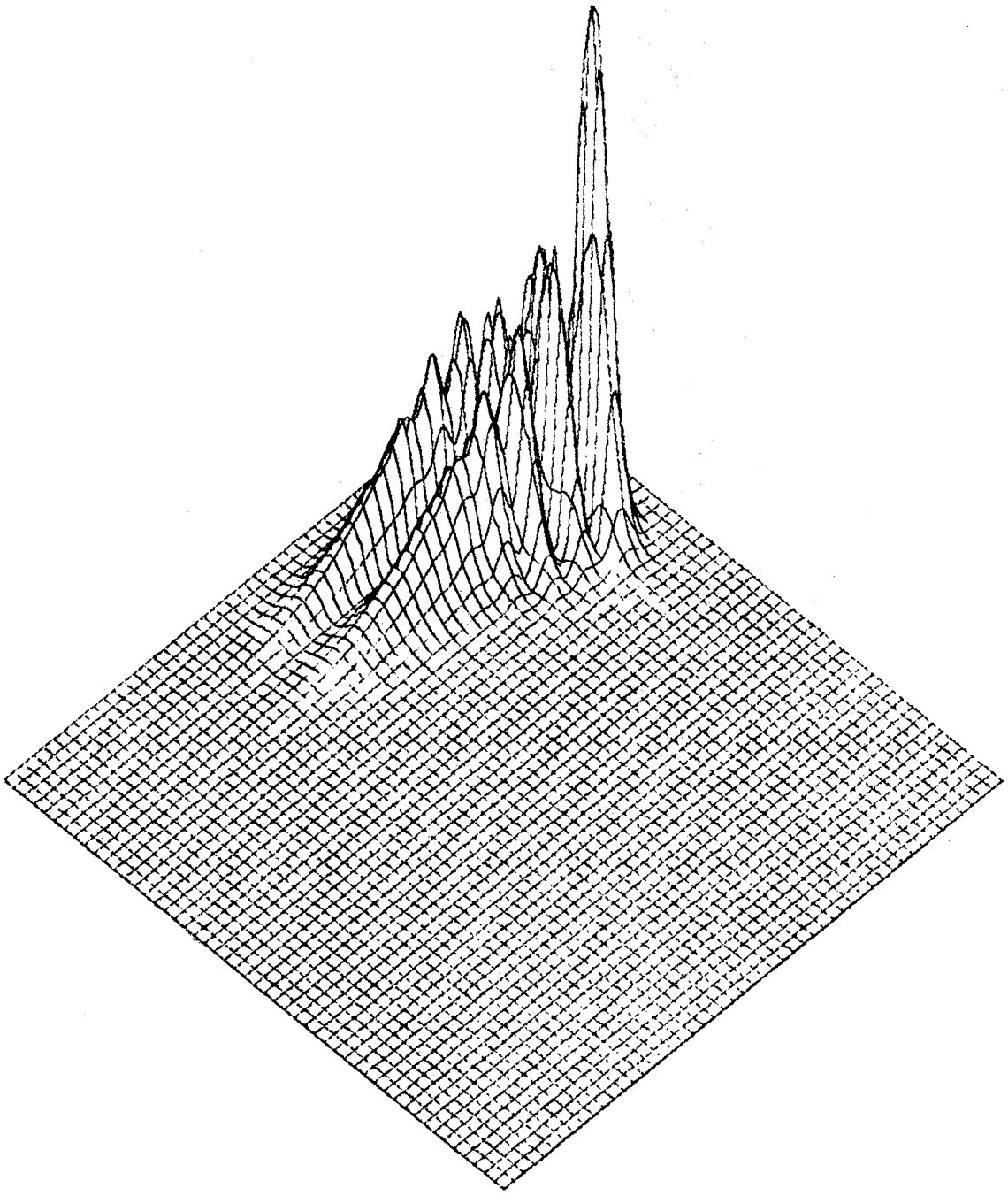

Figure 58. Calculation E, t = 62.5 Δt

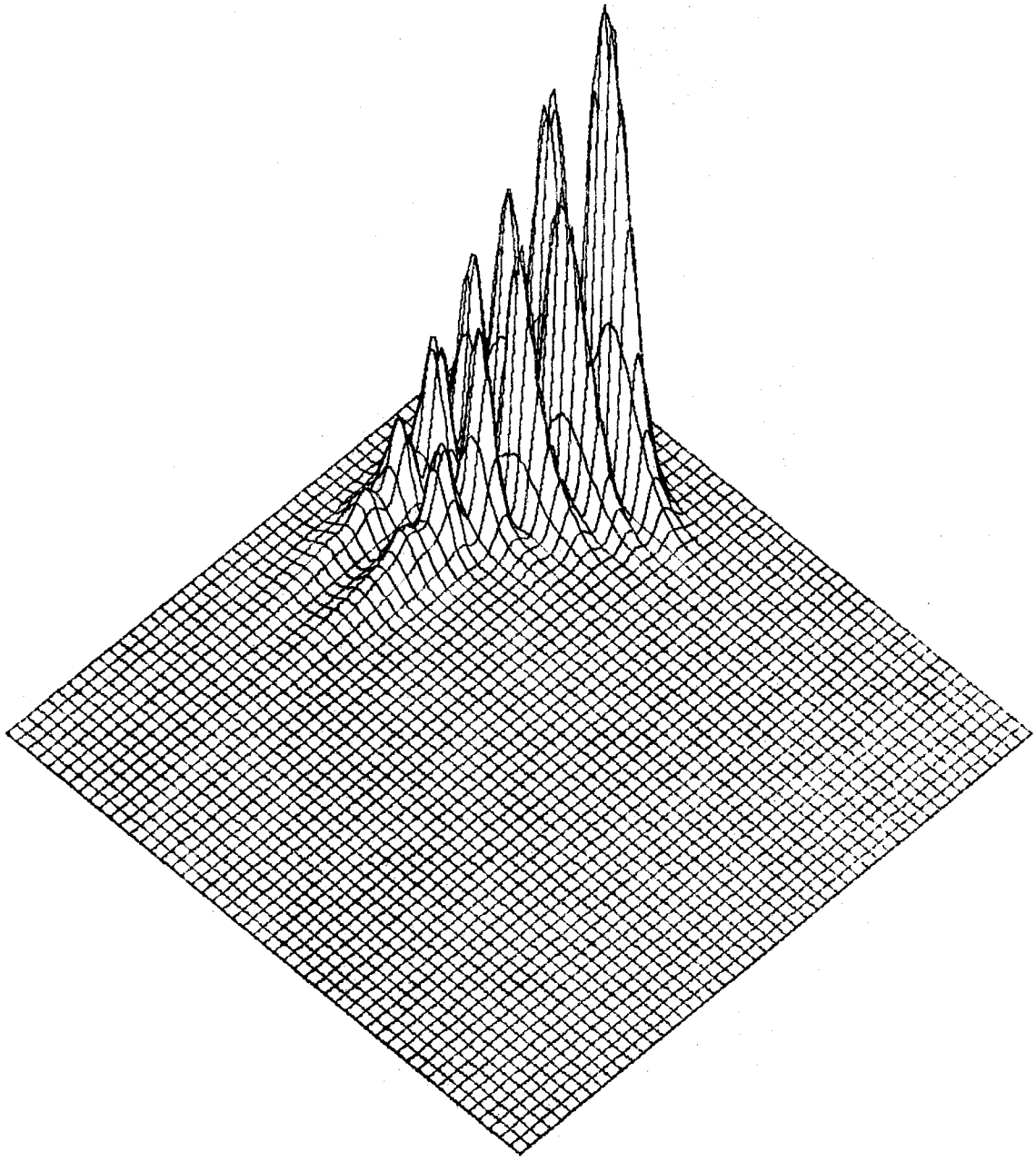

Figure 59. Calculation E, t = 72.5 Δt

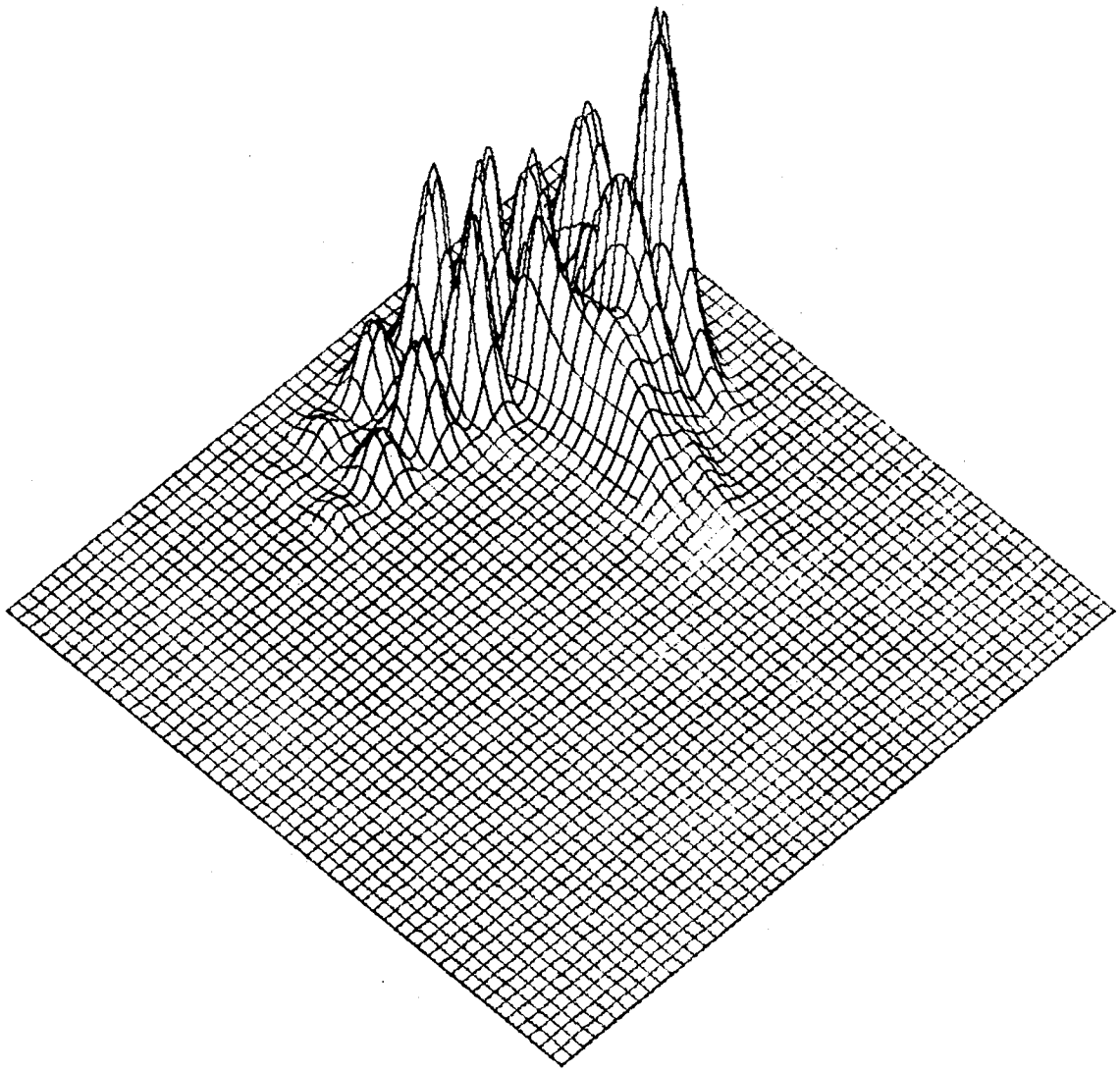

Figure 60. Calculation E, t = 92.5 Δt

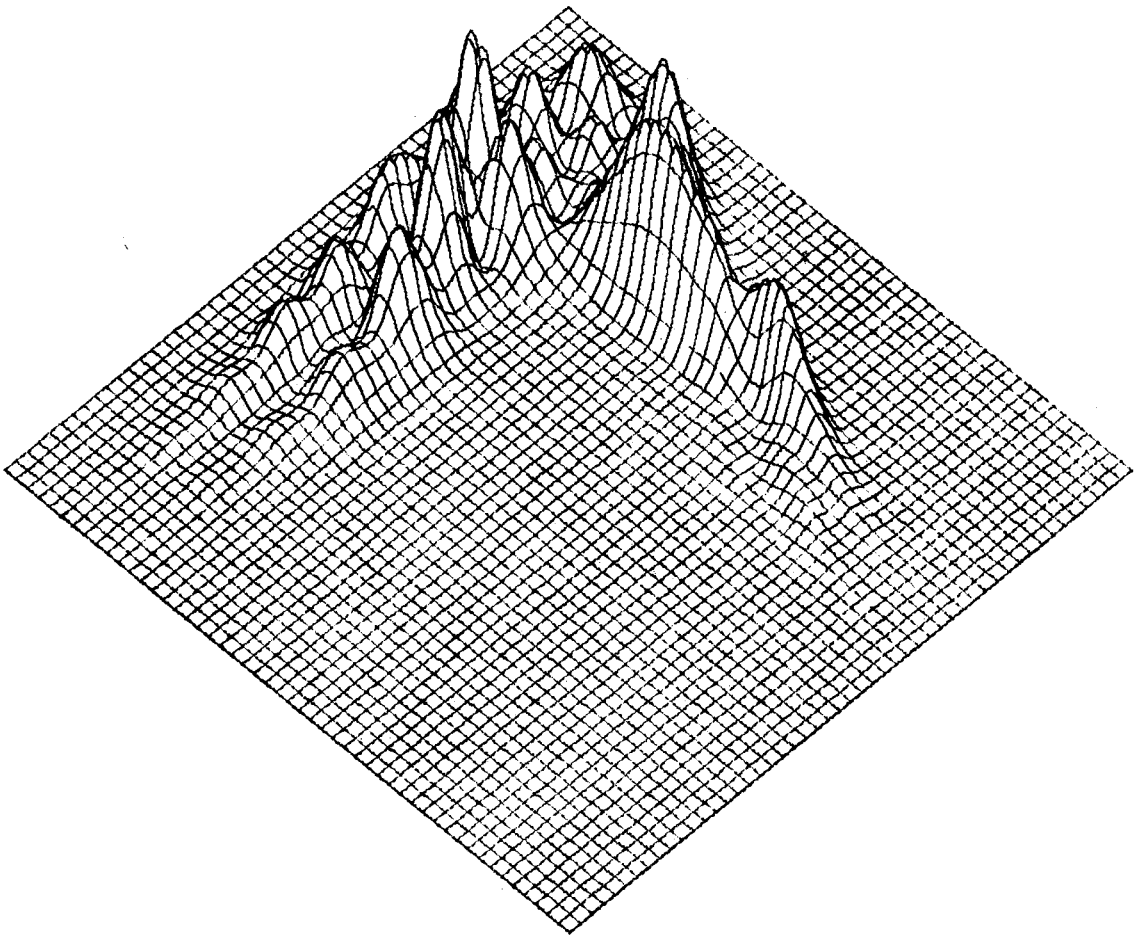

Figure 61. Calculation E, t = 112.5 Δt

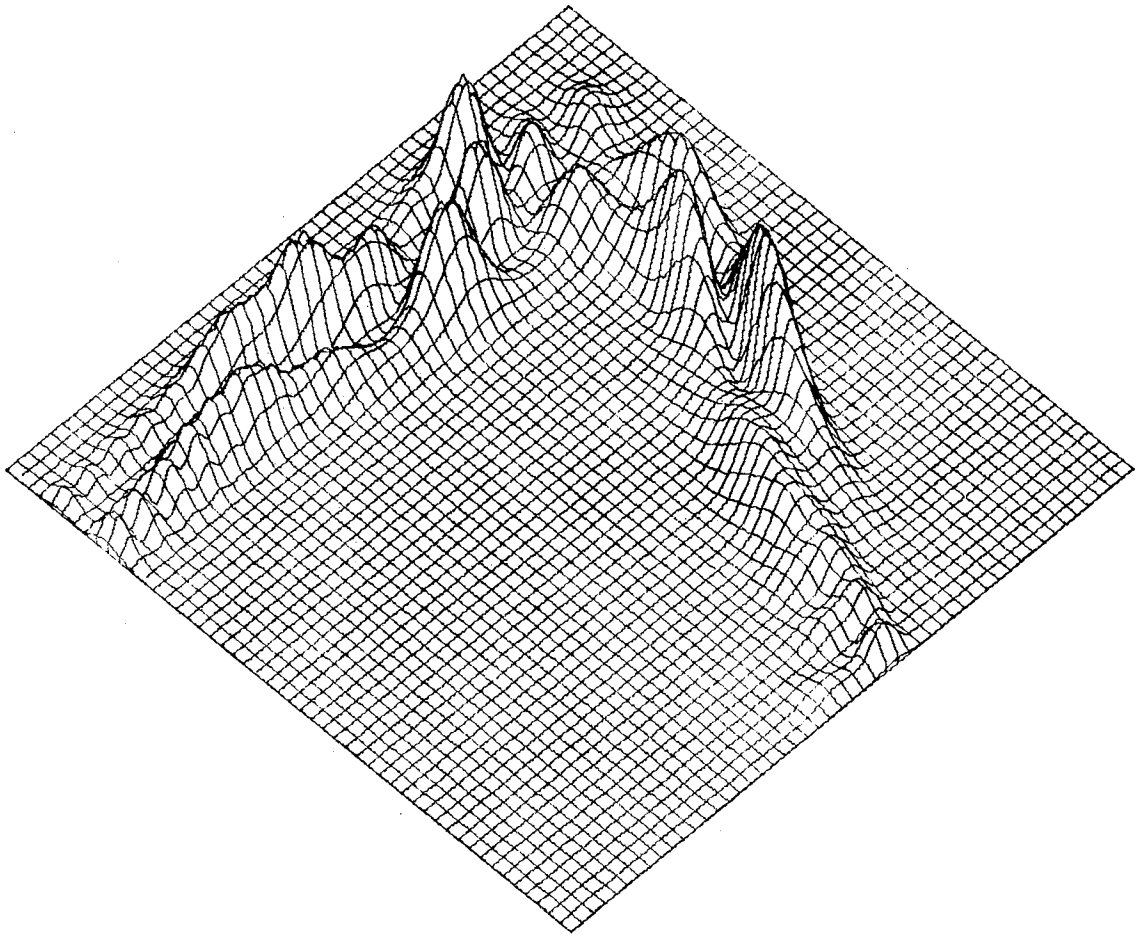

Figure 62. Calculation E, t = 132.5 Δt

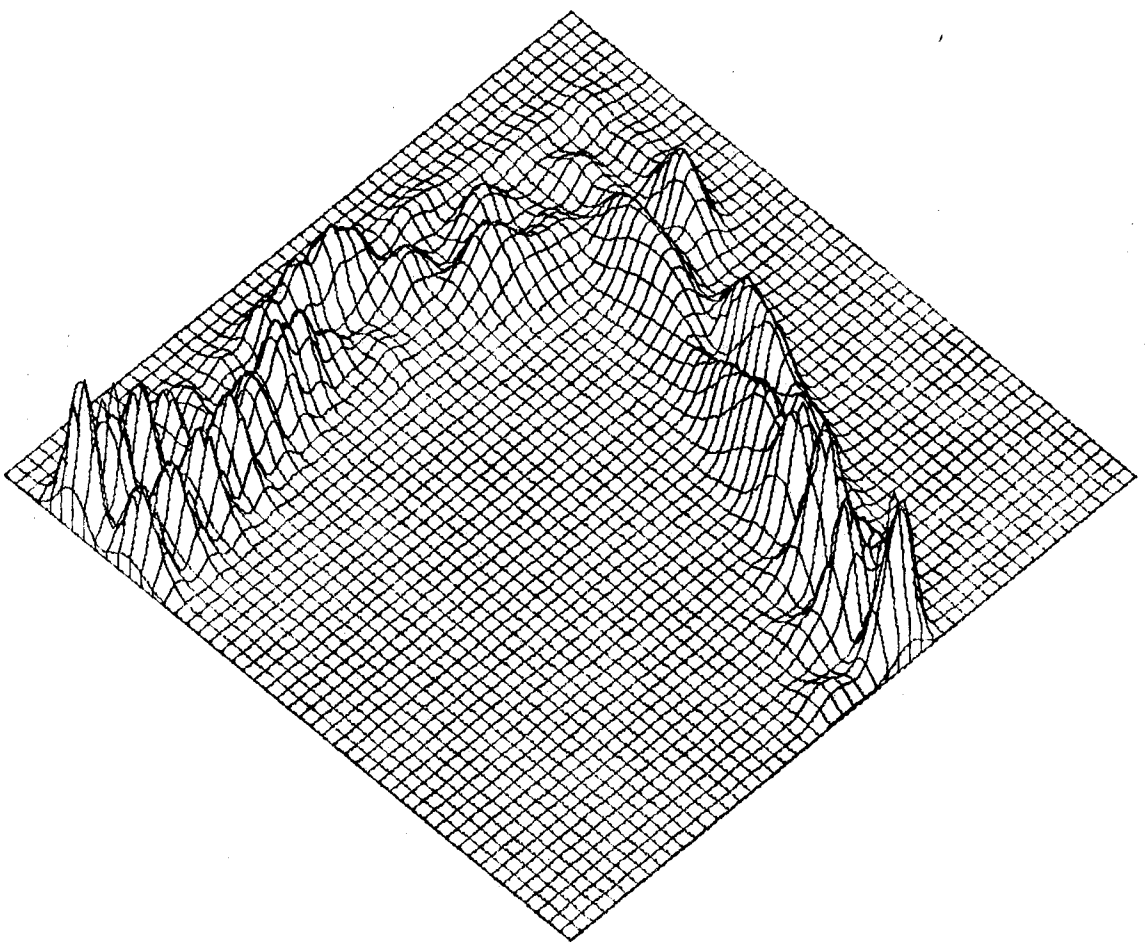

Figure 63. Calculation E, t = 152.5 Δt

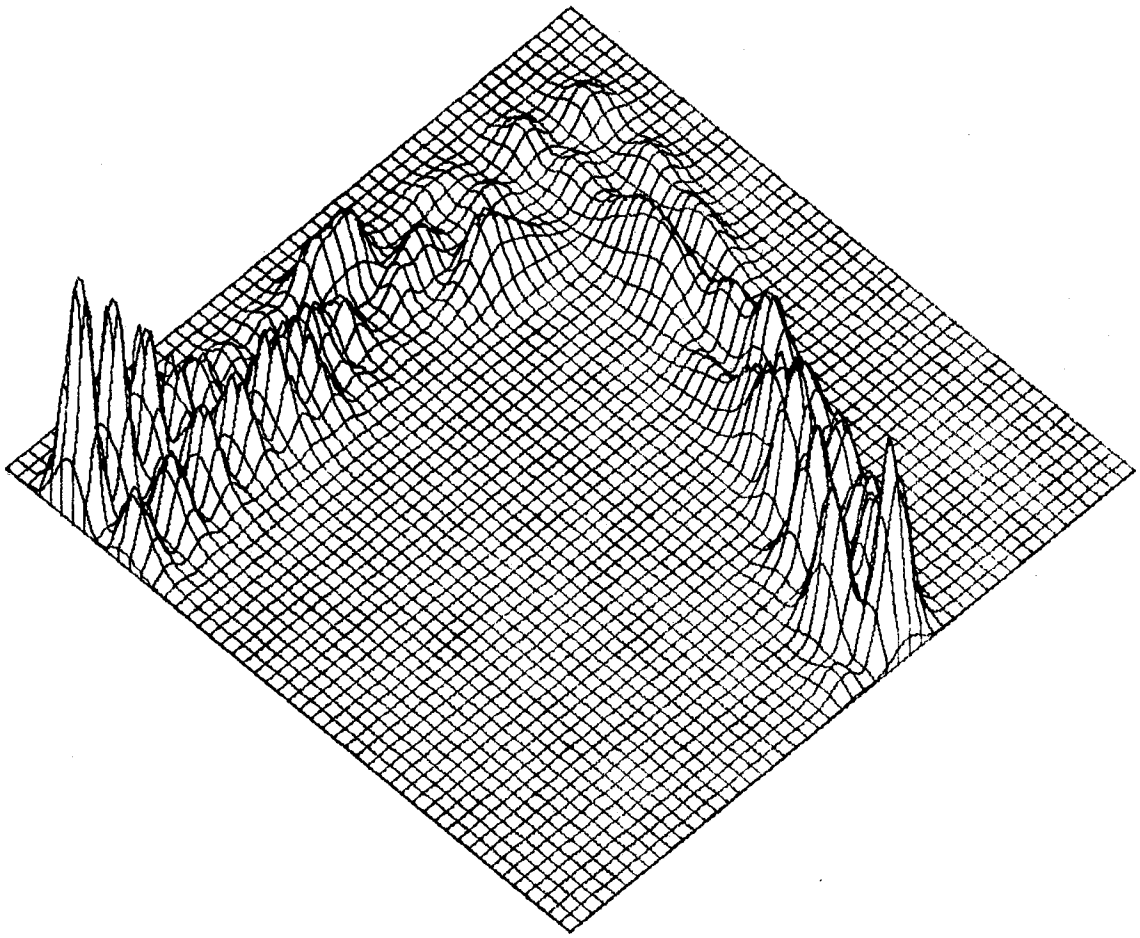

Figure 64. Calculation E, t = 162.5 Δt

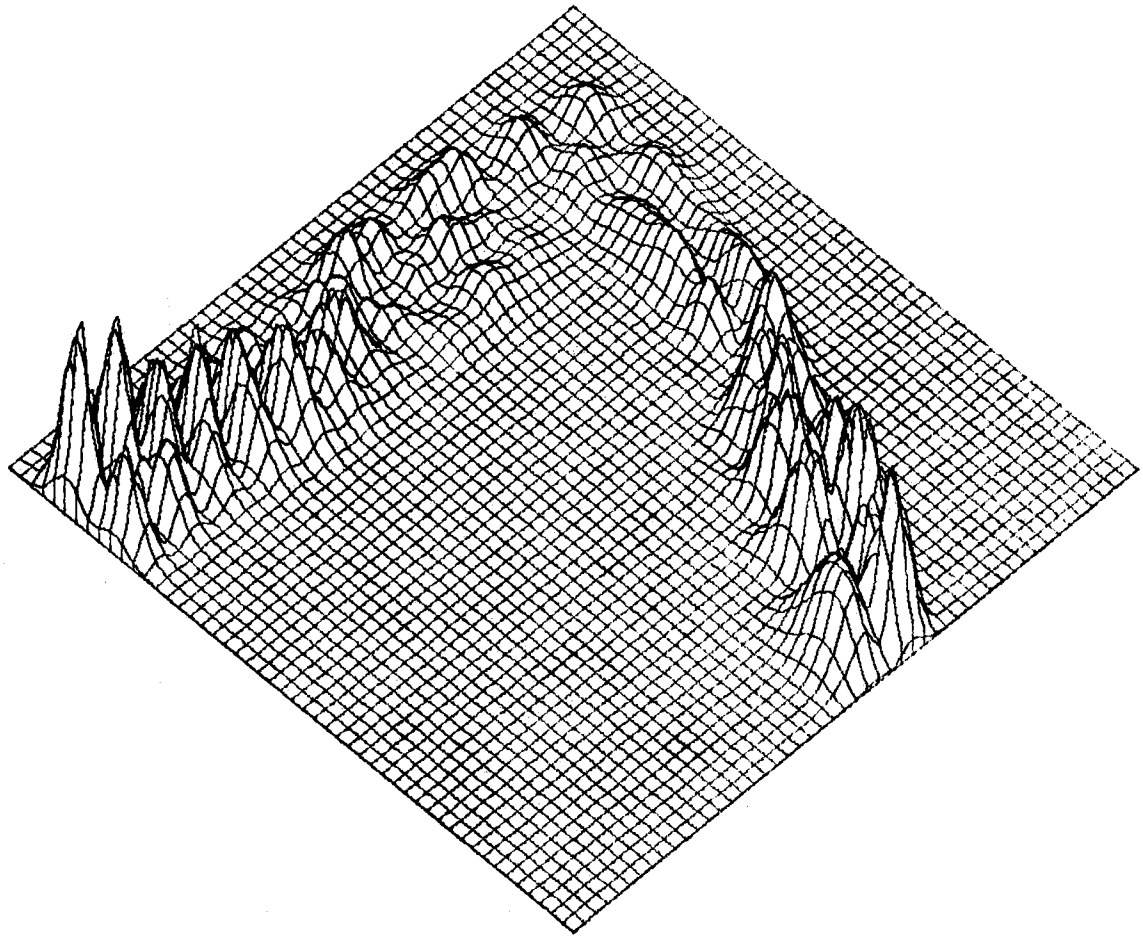

Figure 65. Calculation E, t = 172.5 Δt

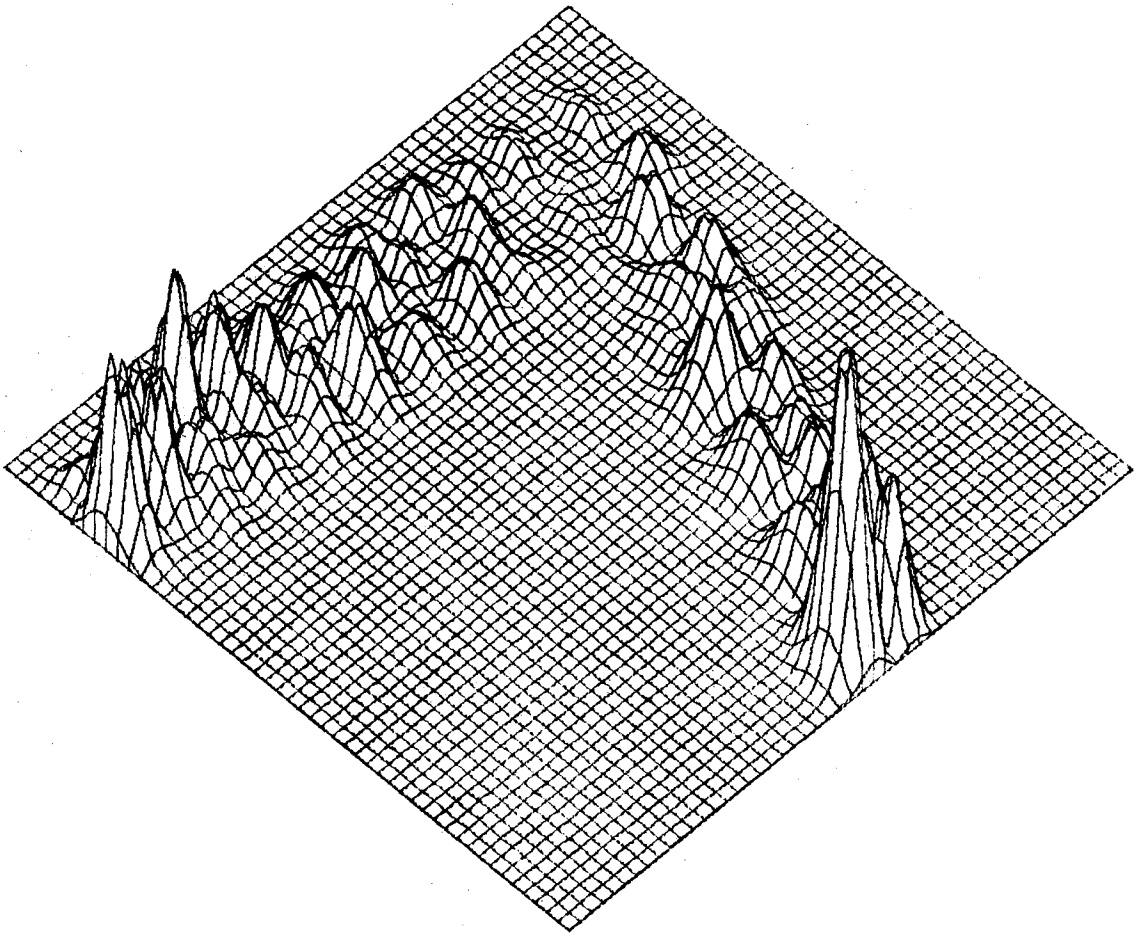

Figure 66. Calculation E, t = 192.5 Δt

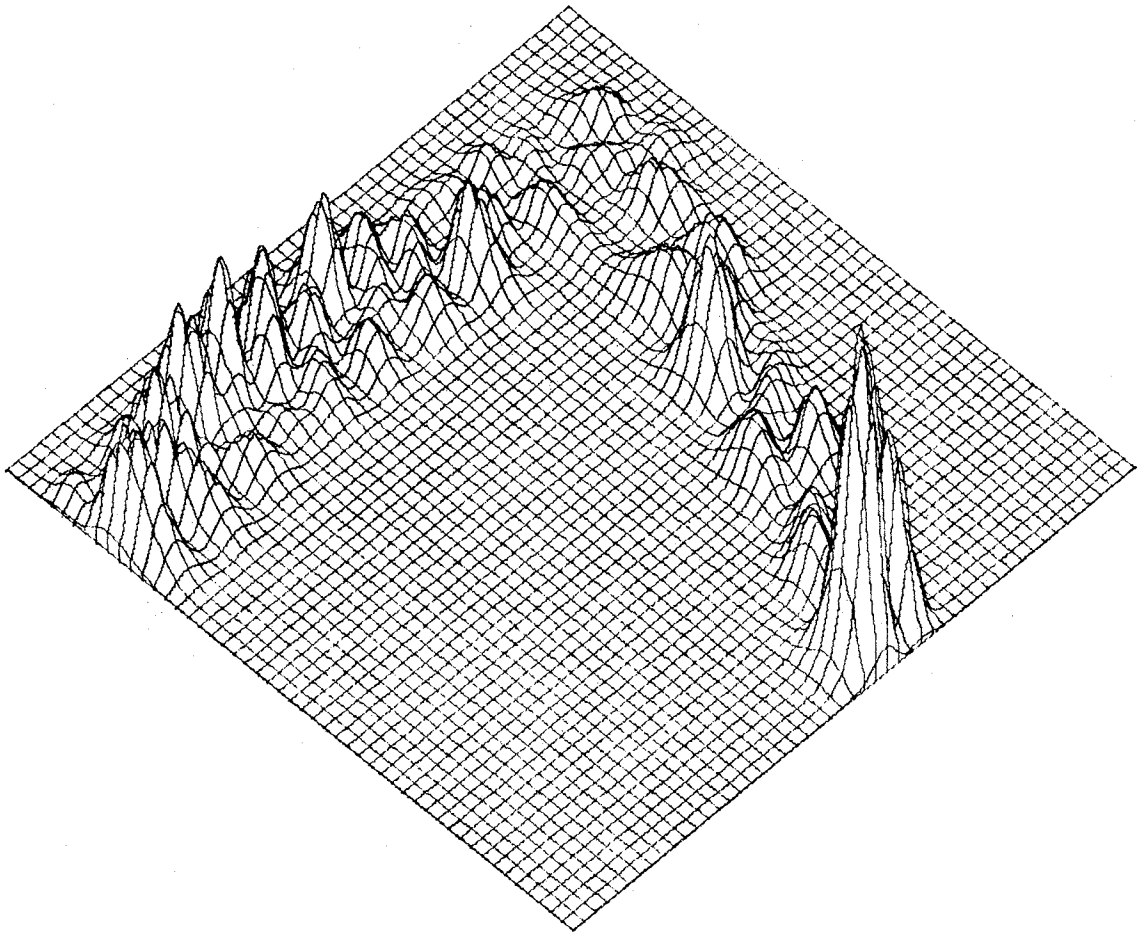

Figure 67. Calculation E, t = 202.5 Δt

dynamics, no vertical scale is provided for the figures, However, the perspective plotting routine does scale the z axis (height above the (x,y) or (q_1,q_2) plane exactly the same as the x axis (q_1 axis). For example, if 6 a.u. are represented by seven inches along the x axis (q_1 axis) then this same ratio prevails for the z direction. In order to produce a plot of more reasonable, eye pleasing proportions, it was necessary to change the height in the z direction by multiplying all z values by an appropriate factor. This factor is denoted by FAC and is equal to 2.00 for each figure unless otherwise stated. The time, t, given by $n\Delta t$ for each calculation is also given below each plot. The numerical value of Δt in each figure is 2.155×10^{-16} sec. even though the actual time step size used in carrying out the numerical procedures of Chapter II and obtain values of ρ displayed by the plot is quite often different from this value.

Figures 18, 19, 21, 23, 24, 26, 28, and 30 encompass only the interaction region, that part of the entire q-space grid in the vicinity of the saddle point. For these figures q_1 max (maximum q_1 value plotted) = 3.185 a.u., q_1 min (minimum q_1 value plotted) = 1.79 a.u., q_2 max (maximum q_2 value plotted) = 2.13 a.u., and q_2 min (minimum q_2 value plotted) = 1.005 a.u. As in the case of the other perspective plots the "tilt" angle is 45 degrees and the rotation angle is 135 degrees.

The perspective plots provide an excellent means of displaying the quantum probability density obtained directly from the numerical solution of the two-mathematical-dimension (q_1 and q_2) problem. The transient motion of the specially prepared wavepackets is vividly observable. In their subsequent motion the wavepackets spread and move toward the region of q-space where q_1 and q_2 are small (for example, see Figures 6-8). Along the path the potential energy is gradually

increasing but as yet the variation of the potential surface has had little observable effect. Eventually the wavepacket encounters a region of high potential, that is, a hard potential wall (Figures 9 and 10) and drastic changes occur. Large maxima rapidly form throughout the entire packet and extend back into the reactant region (Figure 11). These distrubance peaks result from the reflection of Ψ by the potential wall; the reflected portion is superimposed on the incoming packet giving rise to interference minima and maxima. The collision of the wavepacket with the potential wall is shown most dramatically in Figures 37 and 50. The large maximum remains almost stationary in a region of high potential (compare Figures 10, 11, and 12) but the decaying edge of the maximum clearly increases with time that is, the wavepacket partially negotiates the potential surface barrier, either passing over or tunneling through the barrier, and moves into the product (AB, C) region (Figures 12, 13, and 14). In each calculation the wavepacket eventually divides into two parts, one of which is reflected back into the reactant region and another part which moves out into the product region (reactive scattering). After a sufficient time has passed, the reflected and transmitted waves have died down in the neighborhood of the barrier, and the probability flow from reactants to products is essentially over. The presence of the interference peaks which propagate back into the (A, BC) region indicate that the reaction is not compatible with the idea that the packet passes smoothly around the corner. Comparing Figures 14 and 54, it is apparent qualitatively that an increase in the average relative translational energy is not an efficient means of increasing the probability density in the product region. The Figures indicate that the packet must remain in the interaction region a sufficient length of

time to enable probability density to round the corner, move to and surmount the barrier, and pass out into the product region. In essence, if the packet does not remain in the interaction region a long enough time, the packet is largely reflected back into the reactant region resulting in a small product probability density. Qualitatively the calculations indicate that the amount of vibrational energy in the reactant molecule is of utmost importance in determining how much probability density ends up in the product region. In both calculations D and E, the three atom system possesses the same total energy, but in calculation E the first excited Morse wavefunction was used to initially describe the molecule BC (see Table III). A comparison of Figures 54 and 67 reveals that an extraordinary larger amount of probability density reaches the product region in calculation E than for calculation D. In the vibrationally excited case, the probability density is much more spread out in the reaction valley (Figure 60) and an exceedingly large amount of probability density negotiates the barrier and eventually reaches the product region. This broad probability density prevails throughout the entire time of interaction. Scanning the two sets of figures representing calculations B and E allows comparison of two systems with the same average translational energy but which differ in the vibrational energy initially present in molecule BC.

The result of truncating the region of q-space considered by closing off the asymptotic reactant and product channels (setting the wavefunction to zero outside the L-shaped grid) is to produce nonphysical reflecting barriers which tend to reflect Ψ back toward the interaction region. Figures 31-33, 41-46, 53-54, and 63-67 clearly illustrate this reflection process. In fact the calculation represented by Figure 46

has been carried out to a time such that portions of the wave reflected from the closed off reactant channel have moved back into the interaction region. In general it is not necessary to carry out a calculation to such a long time and hence no problems are encountered since the reaction is essentially over before interference from reflected components occurs.

Reaction Probability

In order to quantitatively discuss the probability that the system which originated in the reactant (A, BC) region ends up in the product (AB, C) region, a dividing line is required between the two regions. In the saddle-point region the concept of reactants and products is ill-defined; a line drawn through the saddle-point region may be crossed several times by the system. Accordingly the reaction probability is a property of the system determined as $t \to \infty$. The dotted line in Figure 4 which passes through the saddle-point was used to divide reactants and products. The probability of finding the system on the (AB, C) side of this line after a sufficiently long time will be denoted P_r. Determination of P_r simply involves summing (integrating) the probability density on the product side of the dividing line. In the actual calculation (step 9 of the computer program description) the probability density on the reactant side of the line was summed and P_r obtained by subtracting this value from the value of the integral $\langle \Psi | \Psi \rangle$. The numerical values of P_r obtained for each calculation will be presented after a classical mechanical treatment of the (A, BC) system is given.

Classical Dynamics

Classically, the motion of particles obeys Hamilton's equations,

$$\frac{\partial H}{\partial p_i} = \dot{q}_i$$
$$\frac{\partial H}{\partial q_i} = -\dot{p}_i \qquad [61]$$

where H is the classical Hamiltonian function of the system given by equation [5] and q_i, p_i ($i = 1$ or 2) are the conjugate positions and momenta. Given the initial positions and initial momenta, the solution of the simultaneous, first-order equations (specification of p_i and q_i for all i) for all time of interest defines a trajectory.

Dropping the center of mass motion, the separation of atoms B and C for the general three-dimensional case can be represented by a vector (pointing toward C) with components Q_1, Q_2, and Q_3. The distance from atom A to the center of mass of BC is described by a vector (pointing toward A) with components Q_4, Q_5, and Q_6. For the collinear study one can write (referring to Figure 1)

$$Q_6 = r_1 + [m_c/(m_b + m_c)]r_2$$
$$Q_4 = Q_5 = 0 \qquad [62]$$

and for the (H, H_2) system,

$$Q_6 = r_1 + r_2/2 \ . \qquad [63]$$

The BC internuclear separation is given by

$$Q_3 = r_2, \text{ and } Q_1 = Q_2 = 0. \qquad [64]$$

Carrying out the process described in Chapter II yields

$$2T = \mu_{A,\,BC}\,\dot{Q}_6^2 + \mu_{BC}\,\dot{Q}_3^2 \qquad [65]$$

where $\mu_{A,\,BC}$ is the reduced mass of the (A, BC) system given after Equation [4] and μ_{BC} is the reduced mass of the BC molecule, $m_b m_c/(m_b + m_c)$. The classical Hamiltonian function for the internal motion is

$$H = \left(\mu_{A,\,BC}/2\right)\dot{Q}_6^2 + (\mu_{BC}/2)\,\dot{Q}_3^2 + V(Q_6, Q_3)\,. \qquad [66]$$

In terms of the conjugate momenta we have,

$$H = P_6^2/2\,\mu_{A,\,BC} + P_3^2/2\,\mu_{BC} + V(Q_6, Q_3)\,. \qquad [67]$$

The equations of motion were integrated from the initial to the final state by means of a computer program obtained from Dr. Lionel M. Raff, Department of Chemistry, Oklahoma State University. The program was modified to study the one-dimensional (A, BC) system. The potential energy subroutine was changed to correspond exactly to the extended LEPS surface described in Chapter II and used in the quantum claculations. In the initial configuration for each collision, the atom A, is far removed from BC, a distance at which the interaction between the atom and molecule is negligible. A value of 10 a.u. was assumed for the initial separation (initial Q_6) of atom and molecule. The atom and molecule approach each other along their line of centers at a chosen relative translational energy. The relative translational energies used were identical to those of the quantum calculations given in Table III. The initial vibrational energy of BC was chosen to be the quantum mechanically allowed value corresponding to the ground or first vibrational excited state. The initial Q_3 value corresponded to the separation of atoms B and C to the classical turning points (points at

which the total energy is equal to the potential energy). The vibrational energy also corresponded to the values in Table III. Since the molecular energy is quantized, these calculations are more properly referred to as quasiclassical trajectory calculations rather than classical in which all values of vibrational energy are allowed. The reaction probability for the particular initial conditions is simply the number of collisions which result in the formation of AB divided by the total number of trajectories computed.

An additional variable was utilized to average over the vibrational phase of BC. This was accomplished by adding to the preselected minimum starting separation (10 a.u.) a number $\Delta x = V_r \tau / N$, for each trajectory computed. V_r is the relative velocity, N is the total number of trajectories to be computed in a particular batch run, and τ is the vibrational period of BC calculated using the harmonic oscillator approximation to the Morse function,

$$\tau = (2\mu/D)^{\frac{1}{2}} (\pi/\alpha) \qquad [68]$$

where μ is the reduced mass of BC, and D and α are given for BC in Table I. Another method of selecting the vibrational phase of the molecule has recently been used (146). In this study the two methods of selection proved to give equivalent averages.

Approximately 200 calculations (trajectories) were run for each of the initial conditions in Table III. The integration time step size was varied from 1.0775×10^{-16} sec on the higher-energy runs to 2.155×10^{-16} sec on the low-energy trajectories. The integration technique employed was the Runge-Kutta-Gill procedure (147) with the accuracy of the integration tested by changes in the step size and by integration backwards

along selected trajectories. As an additional verification of numerical accuracy, trajectories were checked for conservation of total energy. Computation time for a single trajectory was dependent on the initial conditions but was on the average about 8 seconds per trajectory on the IBM 360/65. The classical and quantum reaction probabilities are given in Table IV. $P_r(Q)$ represents the quantum probability as defined previously and $P_r(C)$ the classical reaction probability. One additional classical calculation corresponding to initial conditions different from any of the quantum calculations was performed. This batch had relative translational energy of 2.00 kcal/mole and BC in the ground vibrational state. The resulting reaction probability was 0.36. Figure 68 is a plot of reaction probability versus relative translational energy. The upper curve corresponds to the classical results; the lower curve the quantum results. The Δ and 0 represent respectively the quantum and classical results for calculation E. Straight lines were drawn between points to distinguish the classical and quantum results. Values of the reaction probability for energies between the plotted points are not given by the present calculations.

An estimation of the reaction time for the quantum calculations can be obtained from Figures 5-67 (and from the computer output). For Calculation A the packet is entering the interaction region at about time, $t = 50\,\Delta t$. At approximately time, $t = 165\,\Delta t$, the interaction is essentially over. The reaction time is therefore about $115\,\Delta t \simeq 2.5 \times 10^{-14}$ sec. Classical interaction times of $1\text{-}3 \times 10^{-14}$ sec. were found on the Porter-Karplus potential surface (117) by Karplus, et al. (29). The following reaction times are estimated for the other quantum calculations: Calculation B: 2.7×10^{-14} sec., Calculation C: 2.0×10^{-14}

sec., Calculation D: 1.8×10^{-14} sec., and Calculation E: 2.6×10^{-14} sec. These times are of the same order of magnitude as the time required for a free atom to pass the reactant molecule in the absence of interaction (80). The results support the conjecture that the reaction proceeds by way of a direct interaction mechanism.

TABLE IV

QUANTUM AND CLASSICAL REACTION PROBABILITIES

Calculation	n*	E_T** kcal/mole	$P_r(Q)$	$P_r(C)$
A	0	9.689	0.092	0.470
B	0	15.683	0.188	0.380
C	0	21.189	0.152	0.110
D	0	27.521	0.082	0.000
E	1	27.522	0.493	0.585

* n denotes the vibrational quantum number.

** The total system energy.

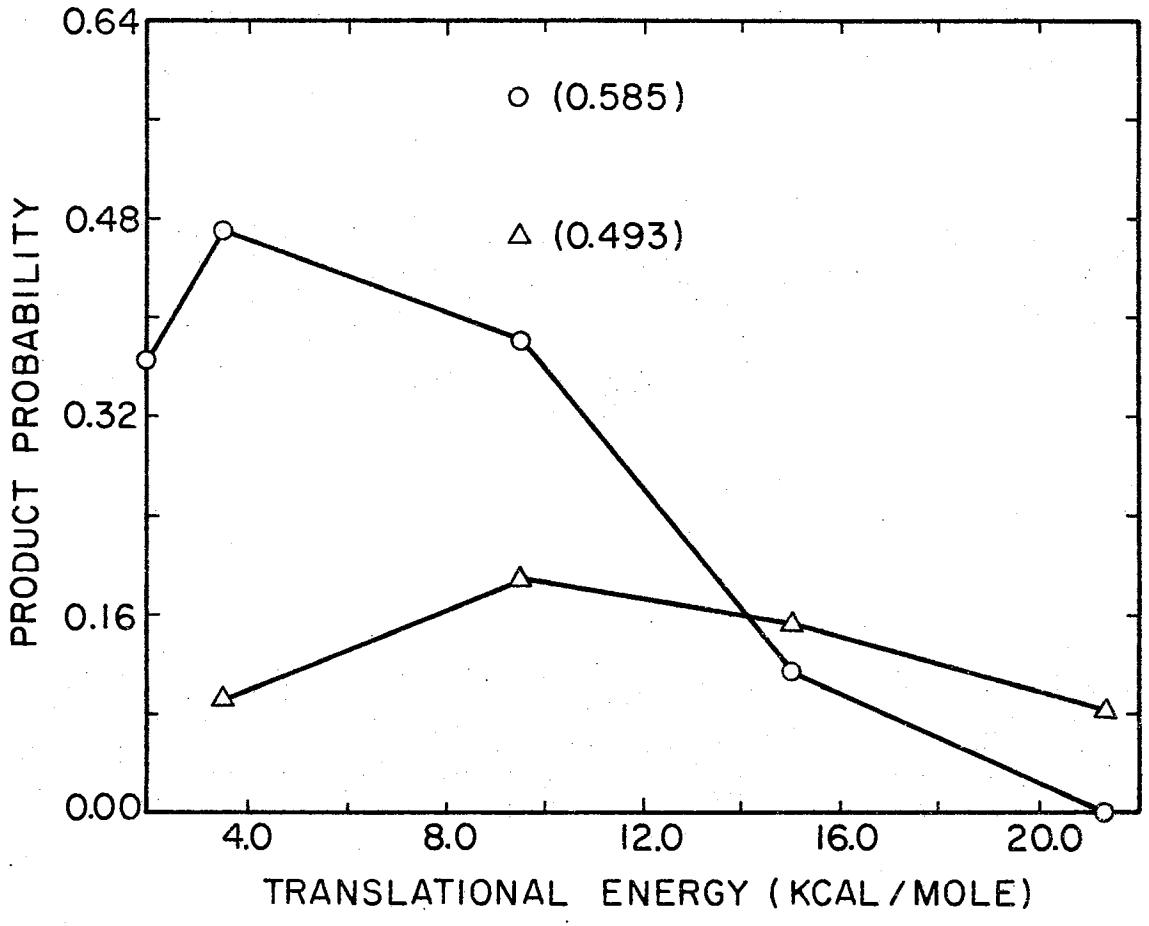

Figure 68. Reaction Probability Versus Relative Translational Energy

CHAPTER IV

DISCUSSION AND CONCLUSION

Discussion of Results

The results of this study, as displayed by Figure 68, clearly show a large discrepancy between the two methods of calculation. No previous comparison studies between classical and quantum mechanical treatments of the (H, H_2) system on symmetrical potential-energy surfaces have exhibited such a large discrepancy.

The calculation by McCullough and Wyatt (80), whose calculational procedure was followed in this quantum study, showed classical mechanics to give a good description of the reaction dynamics. They studied the (H, H_2) system using the Porter-Karplus (117) potential-energy surface, hereafter referred to as PK surface. This surface has a barrier height of 0.396 eV (9.132 kcal/mole). Initial translational energies of 0.32, 0.38, 0.44, and 0.51 eV were used and, they found the classical reaction probability to be lower than their quantum counterparts by amounts ranging from 23% at 0.32 eV to 15% at 0.51 eV. The author estimates from their figures the following reaction probabilities: 0.32 eV: $P_r(C) = 0.45$, $P_r(Q) = 0.58$, 0.38 eV: $P_r(C) = 0.53$, $P_r(Q) = 0.66$, 0.44 eV: $P_r(C) = 0.59$, $P_r(Q) = 0.70$, and 0.51 eV: $P_r(C) = 0.62$, $P_r(Q) = 0.73$ where C and Q represent classical and quantum mechanically calculated results, respectively. Although energies of this study do not correspond exactly to their calculations, it is apparent that both

the classical and quantum reaction probabilities lie below their values. At an everage translational energy of 0.4117 eV (Calculation B) $P_r(C)$ is 0.38. Interpolating one might guess their classical probability at this energy to be 0.56, a considerable difference. The corresponding interpolated $P_r(Q)$ is 0.68 opposed to the present calculated value of 0.188. Obviously one expects differences between the two calculations due to the difference in barrier heights of the two surfaces but intuitively the difference between the classical and quantum reaction probabilities is expected to be approximately the same. The classical reaction probability is about 68% of their value: the quantum probability approximately 28% of their value. Even calculation E, where molecule BC is initially in the first excited vibrational level, results in a quantum reaction probability much lower than any of the values obtained when the PK surface is used. However, the striking difference between the two calculations is that their quantum values are larger than their corresponding classical values whereas the reverse is true in this study.

The literature contains other values for the collinear quasi-classical reaction probabilities using the same PK surface. Morokuma and Karplus (148) in their Table II give $P_r(C) = 0.65$ for an initial relative translational energy of 0.32 eV and $P_r(C) = 0.71$ for 0.38 eV. Values for the classical reaction probabilities on the PK surface at higher relative translational energy can be estimated from the work by Wu and Marcus (149), who carried out collinear calculations up to about 23.8 kcal/mole initial relative translational energy (IRTE). From their Figure 15 the author estimates that $P_r(C) = 1.0$ at 0.44 eV IRTE and $P_r(C) = 0.85$ at 0.51 eV IRTE. These $P_r(C)$ values at 0.32, 0.38, 0.44,

and 0.51 eV IRTE all lie above the corresponding quantum reaction probabilities calculated by McCullough and Wyatt. Furthermore the results of the above references are in qualitative agreement with the findings of Mortensen (9) who studied the collinear (H, H_2) system using the potential surface of Weston (150).

The reason for the differences in the classical reaction probabilities using the same potential surface is due to the different calculational procedures used to obtain the reported values. McCullough and Wyatt followed the motion of an ensemble consisting of 3000 phase points by solving Hamilton's equations to find the trajectory of each phase point. The initial quantum conditions state that the vibrational energy of the reactant molecule is quantized. They abandoned strict quantization and chose a four-dimensional phase space probability density function and generated an ensemble of phase points having this density function. Morokuma and Karplus and Wu and Marcus, on the other hand, carried out their classical calculations as described in Chapter III of this work. The important point is that the choice of the classical mechanical initial conditions may result in quite different results for the classical reaction probability. Comparing the above classical reaction probabilities calculated by Morokuma, Karplus, Wu, and Marcus to the quantum probabilities of McCullough and Wyatt shows the classical reaction probability curve for the PK surface to lie above the quantum curve. This result is similar to the findings of this study. Furthermore, in this study both curves lie below the values for the symmetrical PK surface. These data lead one to conclude that the position of the barrier occurring late in the reaction coordinate is responsible for the smaller reaction probabilities. Perplexing, however, is the fact that

the quantum reaction probabilities are lowered by a larger amount than the classical reaction probabilities (for IRTE up to 0.51 eV) as the barrier shifts to the exit channel. At higher initial relative translational energies the quantum reaction probabilities are larger (see Calculation C) than the corresponding classical probabilities. It is certainly desirable to have quantum reaction probabilities for higher IRTE for the PK surface than those available from the McCullough and Wyatt study. Their largest IRTE is 0.1139 eV above the barrier height of the PK surface. An IRTE of 0.1139 eV above the barrier on our asymmetric surface corresponds to an IRTE of 0.4196 eV (9.67 kcal/mole) which lies in the region where the quantum curve has reached a maximum. At higher IRTE it is possible that the quantum curve would exhibit a similar crossing of the classical curve for the PK surface.

For the energies considered in this study, both the classical and quantum calculations appear to exhibit an upper-energy bound for reaction. That is, $P_r(C)$ is equal to zero for Calculation D and the corresponding $P_r(Q)$ has decreased from 0.188 for calculation B down to 0.082. The existence of an upper-energy bound for the classical calculation is not new and has been reported by Wall, et al. (23) (24) in their early collinear-classical trajectory studies. The upper-energy bound seems to indicate that high-energy systems encounter a virtually vertical wall in the interaction region and are reflected back out into the reactant valley. For systems which have upper bounds it is expected that the bound is so high that it would not be experimentally detected in thermal reactions unless the temperature were so high as to cause considerable electronic excitation of the reacting species. In this case the adiabatic assumption of a single potential-energy surface for

a given reaction would be invalid. Furthermore, the aforementioned argument is presented under the assumption of a collinear reaction.

Morokuma and Karplus (148) compared transition-state theory results with collinear-quasiclassical trajectory calculations for the same potential surface. In the study of one of their systems they employed an extended LEPS potential surface identical to the one employed in the present calculations. They list surface parameters in their Table VII and give reaction probabilities in Table VIII. At a total system energy of 0.5064 eV (11.677 kcal/mole) they obtained a reaction probability of 0.43. This total system energy corresponds to an initial relative translational energy of 5.488 kcal/mole. Their reaction probability at this energy appears to correspond exactly with the classical result of Figure 68. Morokuma and Karplus found that displacement of the well-defined barrier from its symmetric position to an asymmetric position in the exit channel was the dominant factor in deviations between transition-state theory and the classical-trajectory technique. The deviations support the findings of Polanyi and Wong (122) that vibrational energy is more effective than translational energy in increasing the reaction probability when the barrier lies in the exit channel. The results of quantum and classical calculations D and E of this work clearly support these findings.

Previous studies have exhibited large discrepancies between quantum mechanics and classical mechanics but in these instances the calculations were performed on model potential surfaces that were aphysical in nature. Mazur and Rubin (101) applied time-dependent quantum mechanics and classical mechanics to the infinite-walled square corner potential surface and concluded that classical mechanics was grossly inadequate

for reactions on this surface. Their classical reaction probability was about a factor of five larger than the quantum probability. Kleinman and Tang (94) also reported serious discrepancies between time-independent quantum reaction probabilities and exact classical probabilities on a similar surface. One is led to conclude that this type of surface and others with sharp edges accentuate the discrepancy between quantum and classical mechanics. These types of surfaces seem perhaps to have dynamic eccentricities which cannot be extrapolated safely to smooth surfaces. Hence the model calculations are probably not helpful in explaining the present results which were carried out on a more realistic potential surface.

Recently (1969 to present), time-independent quantum mechanical studies on the (H, H_2), (F, H_2), (Cl, H_2), and (H, Cl_2) systems have been reported in the literature. Most of these studies have employed one of two independent methods applicable to a collinear, electronically adiabatic model: the finite-difference boundary-value method (FDBVM), developed by Diestler and McKoy (97) or a close-coupling method (CCM), first presented by Diestler (99).

Since these two methods have been extensively used, a brief outline of the methods will be attempted. Both the FDBVM and CCM involve the solution of the time-independent Schrödinger equation describing the collision. By requiring the asymptotic form of the collision wavefunction to satisfy the proper scattering boundary conditions, namely an incident wave in one channel plus outgoing waves in all open channels and decaying exponentials in the included closed channels, one obtains the scattering matrix and subsequently the matrices of nonreactive and reactive probabilities. In these matrices the first row (or column) is

labelled 0 and corresponds to the ground final (or initial) vibrational state, and the second row (or column) is labelled 1 and corresponds to the first excited final (or initial) vibrational state. In both the FDBVM and CCM the wavefunction is expressed as a linear combination of members of a set of linearly independent solutions of the full Schrödinger equation. The difference between the two techniques is the manner in which the set of linearly independent solutions (lis) is determined. In the FDBVM the lis's are generated by solving the finite-difference analogue of the Schrödinger equation with a set of physically motivated linearly independent boundary conditions specified on channel surfaces in the asymptotic regions. The boundary conditions label the lis's. The accuracy of the FDBVM depends primarily on the number of lis's included in the expansion of the wavefunction (or equivalently the number of channels taken into account) and also on the mesh size of the finite-difference grid. In practice the matrices of scattering probabilities are obtained for a series of mesh sizes h, and then extrapolated to h = 0. In the CCM, on the other hand, each linear solution itself is further expanded as a sum (over internal states of both arrangements) of products of internal wavefunctions (of the diatomic) and translational wavefunctions (f's). Substitution of the expansion into the Schrödinger equation and subsequent projection with each internal state leads to a set of coupled differential equations for the f's. Specification of a set of linearly independent initial conditions on the f's allows one to generate a set of lis's by integrating the close-coupled equations. The lis's are now labelled by the initial conditions and their accuracy is determined by the number of states included in the expansion of each lis (or equivalently the number of

channels taken into account) and by the integration step size. The FDBVM is described by Truhlar (151) and a computer program which performs calculations by this method is available from Quantum Chemistry Program Exchange (Program No. 203). The finite difference approximation for the second derivative of the Hamiltonian operator used in this program is the same as the one employed in the quantum calculations reported here.

Some of the numerous studies on the aforementioned reactive systems will now be mentioned. The purpose is three-fold: a) present evidence of the large amount of research being done in the field of chemical dynamics, and in particular, the large number of applications of FDBVM and CCM to reactive systems, b) supplement the introductory chapter with more recent references for the interested reader, and c) present results of another calculation performed on an unsymmetrical potential-energy surface and compare with this work. Of these goals, the third is the most relevant and if so desired, the reader can simply move ahead to the last paragraph on page 134.

Employing the FDBVM, Truhlar and Kuppermann (82) (152) obtained quantum reaction probabilities for $H + H_2$ on the parameterized potential surface of Wall and Porter (24). Classical reaction probabilities for the collinear (H, H_2) system on the same potential surface were determined by Bowman and Kuppermann (48). They compared their classical results to the quantum results of Truhlar and Kuppermann (82). Diestler (112) (126) applied his CCM to a series of parameterized Wall and Porter potential surfaces and obtained quantum reaction probabilities for the collinear (H, H_2) system. Diestler and Karplus (81) used the CCM on the $H + H_2$ reaction using the PK surface. It has been

published (153) that the FDBVM and CCM yield quantum reaction probabilities in very good agreement. Levine and Wu (154) studied the collinear (H, H_2) system on the PK surface using the CCM. The collinear $H + H_2$ reaction on the PK surface in the energy range 0-1.5 eV was studied by Johnson (155) using the CCM along a reaction coordinate of unique computational simplicity. Russell and Light (156) studied the collinear $H + H_2$ reaction by transforming the two-mathematically dimensional problem into an equivalent one-dimensional problem. Saxon and Light (157) investigated the ($H + H_2$) reactive scattering system using as their potential an analytic fit to the quantum mechanical surface obtained by Shavitt, et al. (158). Quantum reaction probabilities for the collinear $H + H_2$ reaction on the PK surface using the FDBVM were recently reported by Duff and Truhlar (159). Mortensen and Gucwa (98) investigated the collinear (H, H_2) system using the Sato potential-energy surface as described by Weston (150). Truhlar and Kuppermann (82) found good agreement between their results and the Mortensen and Gucwa results even though the potential surfaces used were different but similar (both were symmetrical). Truhlar, et al. (160) have carried out calculations on the isotopically substituted $H + H_2$ reactions. Recently Wolken and Karplus (83) applied the CCM in <u>three</u> dimensions to study the $H + H_2$ reactive scattering problem. They used the PK surface.

Schatz, Bowman, and Kuppermann (63) used the CCM to obtain quantum mechanical reaction probabilities for the collinear (F, H_2) reaction using the semiempirical (LEPS) potential surface of Muckerman (44). For the (F, H_2) potential surface the barrier lies in the reactant valley. Koeppl (161) compared Transition State Theory and quantum mechanical reaction probabilities for the $H_2 + F$ reaction on the Muckerman surface.

Baer (162) used CCM to study the collinear (Cl, H_2) and (H, Cl_2) reactive systems. The unsymmetrical potential surface used in the calculations was a LEPS type. Light and co-workers (108) (109) had previously studied the (H, Cl_2) system using a different calculational procedure. The above studies have recently been reviewed by Porter (163).

Truhlar and Kuppermann (82) (152) obtained good agreement in their comparison of quantum and quasiclassical reaction probabilities for the H + H_2 reaction. However, using the same calculational method, the quasiclassical reaction probabilities differed considerably from the quantum reaction probabilities for the (F, H_2) system (as mentioned in Chapter I) where the potential is unsymmetrical. The barrier is located in the reactant valley. They studied the system for the range of initial relative translational energies from 0.0-0.4 eV. In the relative translational energy range 0.025-0.075 eV, the quasiclassical reaction probability is more than 2.5 times greater than the quantum probability. The barrier height on the Muckerman (44) F + H_2 surface is 0.0471 eV (1.086 kcal/mole). Hence, the range of energies where the large disagreement between their quantum and classical mechanical reaction probabilities occurs is at relative translational energies ranging from 0.022 eV below the barrier to 0.028 eV above the barrier. Their results are in agreement (both show a large disagreement) with those reported here. The present studies indicate a large discrepancy between the two reaction probabilities in a range of initial relative translational energies from 0.086 eV (2 kcal/mole), 0.2197 eV below the barrier to about 0.564 eV (13 kcal/mole), 0.258 eV above the barrier. Their results are quite interesting since the quantum and classical curves

agreed quite well for the (H, H_2) reaction which would be expected to show greater quantum effects. Due to the good agreement between classical and quantum reaction probabilities found (160) on the isotopically substituted $H + H_2$ reactions, one cannot attribute all of their large disagreement to the effects of the larger F-atom mass. In summary both studies display a large discrepancy in the relative translational energy range approximately centered about the barrier height. Comparing their two quantum calculations, the quantum reaction probabilities were lower for the (F, H_2) system than for the (H, H_2) system where the potential surface is symmetrical. This is in exact accord with the results obtained here when a comparison is made with the McCullough and Wyatt study using the symmetrical PK surface. Reference (63) is the only comparison study (other than this work) between classical and quantum mechanical methods carried out an asymmetric potential surface known to the author.

Conclusion, Summary, and Suggestions for Future Work

A large amount of time (human and computer) and effort was expended on applying the equations of Chapter II on the reaction represented by Equation [1] where the mass of A is equal to the mass of an iodine atom and BC represents the hydrogen molecule. As mentioned earlier, the (I, H_2) system exhibits dynamic effects when studied by classical trajectory techniques. A semiempirical potential-energy surface (164) with a barrier height of 35.87 kcal/mole was used. A skewed grid (angle between q_1 and q_2 axes was 45 degrees) was used to more aptly cover the region of q-space appropriate for the (I, H_2)

system. A broad spectrum of problems was encountered for this system. Since this barrier height is approximately five times larger than for the (A, BC) system studied, the potential changes much more rapidly as the atoms approach one another. Accordingly, the second derivative of the wavefunction with respect to coordinate space, which is contained in the Hamiltonian operator, can be expected to vary rapidly. Furthermore for a given time increment the (I, H_2) system wavefunction is expected to exhibit a more drastic change than the (A, BC) system wavefunction. In order to numerically describe accurately the more complicated system, more grid points and a smaller time step are required. The availability of computer time and computer storage limit the extent to which these two quantities can be refined. In summary the author feels that if a much larger number of grid points were used (perhaps 40,000-50,000) and a quite small time step that a quantum calculation as outlined could be performed on realistic and more difficult systems such as (I, H_2).

An analysis of the results of this comparison study leads to the conclusion that the nature of the potential-energy surface is of great importance in determining the details of reaction dynamics. The effects of the asymmetric potential-energy surface are evident from the lower quantum and classical reaction probabilities than for similar symmetric potential surfaces. Quite peculiar is the fact that the quantum probabilities are lowered a larger degree than the classical reaction probabilities as the barrier of the potential surface moves to an asymmetric location. In a mysterious fashion the asymmetric potential surfaces possess inherent dynamic features producing unexpected, strange, presently unexplainable results. As revealed by calculation E,

vibrational excitation of the molecule under attack enhances the quantum probability as in the case of quasiclassical studies when the barrier lies in the product valley.

Tow possible future calculations immediately come to mind. One could carry out a comparison study identical to this investigation on 1) a symmetric extended LEPS potential surface and 2) an asymmetric extended LEPS surface whose barrier lies in the entrance valley. The first study would allow a direct comparison using the same calculational procedure on potential surfaces with identical barrier heights and differing only in the location of the barrier. These two calculations in conjunction with this study would reveal the effects on the classical and quantum reaction probabilities as the barrier location is changed on otherwise identical potential surfaces. Perhaps a rule could be formulated relating the results to the barrier location.

Application of the FDBVM or CCM to determine quantum reaction probabilities on the surface used in this study would serve to expose differences, if any, between the different computational approaches. As mentioned above a computer program (QCPE No. 203) employing the FDBVM is available. It would be relatively easy to order this program (it's only 1000 cards) and perform calculations on the present surface and the two previously mentioned surfaces. The results would be interesting. (The calculations mentioned would probably consume the computer time allocation for the next 2 or 3 years also). Attention could be focused on quantum calculations of the first order as defined by Dr. Hirschfelder (165) and attempt to calculate an ab initio potential surface for a chemical system of interest and study the dynamics.

Biological developments have shown that DNA (deoxyribonucleic acid)

is the hereditary substance which carries the genetic message in the cell. These giant organic molecules (DNA) govern the cell duplication and protein synthesis and are important in the problem of normal growth and aging. The method of calculation described in this thesis could possibly be used to study the proton transfer process between the base pairs in DNA (165). It has been proposed (166) that the proton may tunnel from one base pair to another altering the genetic code and give rise to a mutation. A similar tunneling effect in a multi-cellular organism may lead to a loss of genetic information which may be the primary cause of aging (166).

Potential curves to describe the interaction of the proton as it moves from one base pair to another, include 1) the superposition (167) of two equivalent single Morse potentials with their original minima a chosen distance apart, 2) the double-well potentials according to Ladik (168), 3) the double-well potential curve given by Rein and Harris (169), and 4) the elaborate (8 days of computer time) calculation by Clementi, et al. (170). The latter calculation did not yield a double-well potential. The choice of potentials would be limited to one which is reasonable and compatible with the facilities available (8 days is too long). The initial conditions could consist of a well-prepared wavepacket (with average translational energy less than the barrier height) located in one of the double-well potentials. The calculations would consist of the evolution of the wavepacket in one dimensional coordinate space (one mathematical dimension also). Part of the wavepacket is transmitted (tunneling) and part reflected from the potential barrier. One could compute the portion of the packet which reaches the second well and hence the probability of tunneling. Various average translational energies could be used.

A SELECTED BIBLIOGRAPHY

(1) Eyring, H. and M. Polanyi, Zeitschrift fur Physikalische Chemie, B12, 279 (1931), translated from the German in Laidler, K. J., Selected Readings in Chemical Kinetics, Pergamon Press, New York, 41-67 (1967).

(2) London, F., Z. Elecktrochem., 35, 552 (1929).

(3) Schrödinger, E., Ann. Physik., 79, 361, 489 (1929); 80, 437 (1926); 81, 109 (1926).

(4) Elaison, M. A. and J. O. Hirschfelder, J. Chem. Phys., 30, 1426 (1959).

(5) McCullough, E. A., Jr., Doctoral dissertation, The University of Texas at Austin, 1970.

(6) Born, M. and J. R. Oppenheimer, Ann. d. Physik, 84, 457 (1927).

(7) Westhaus, P. A., personal communication and see also S. Golden, J. Chem. Phys., 17, 620 (1949).

(8) Levine, R. D., Quantum Mechanics of Molecular Rate Processes, Oxford University Press, Elly House, London, 241 (1969).

(9) Mortensen, E. M., J. Chem. Phys., 49, 3526 (1968).

(10) Hirschfelder, J. O., C. F. Curtiss, and R. B. Bird, Molecular Theory of Gases and Liquids, John Wiley and Sons, Inc., New York, 921-928 (1954).

(11) Hopper, D. G., Doctoral dissertation, Oklahoma State University, Stillwater, Oklahoma, 1971.

(12) Laidler, K. J., Theories of Chemical Reaction Rates, McGraw-Hill Book Company, New York, 13-40 (1969).

(13) Montroll, E. W. and K. E. Shuler, Advances in Chemical Physics, Vol. 1, John Wiley and Sons, Inc., New York, 361 (1958) and B. J. Widom, J. Chem. Phys., 55, 44 (1971).

(14) Wynne-Jones, W. F. K. and H. Eyring, J. Chem. Phys., 3, 492 (1935) and H. Eyring, J. Chem. Phys., 3, 107 (1935).

(15) Reference 12, 153.

(16) Johnston, H. S., Gas Phase Reaction Rate Theory, The Ronald Press Company, New York, 190 (1966).

(17) Hirschfelder, J. O., H. Eyring, and B. Topley, Chem. Phys., 4, 170 (1936).

(18) Hirschfelder, J. O. and E. Wigner, J. Chem. Phys., 7, 616 (1939).

(19) Glasstone, S., K. J. Laidler, and H. Eyring, The Theory of Rate Processes, Chap. V, McGraw-Hill Book Company, Inc., New York (1941).

(20) Eyring, H., J. Amer. Chem. Soc., 53, 2537 (1931).

(21) Wheeler, A., E. Topley, and H. Eyring, J. Chem. Phys., 4, 178 (1936).

(22) Arrhenius, S., Z. Physik. Chem., 4, 226 (1889).

(23) Wall, F. T., L. A. Hiller, and J. Mazur, J. Chem. Phys., 29, 255 (1958); 35, 1284 (1961).

(24) Wall, F. T. and R. N. Porter, J. Chem. Phys., 39, 3112 (1963).

(25) Bunker, D. L., J. Chem. Phys., 37, 393 (1962).

(26) Blais, N. C. and D. L. Bunker, J. Chem. Phys., 37, 2713 (1962).

(27) Polanyi, J. C. and S. D. Rosner, J. Chem. Phys., 38, 1028 (1963).

(28) Bunker, D. L. and N. C. Blais, J. Chem. Phys., 39, 315 (1963).

(29) Karplus, M., R. N. Porter, and R. D. Sharma, J. Chem. Phys., 40, 2033 (1964); 43, 3259 (1965); 45, 3871 (1966).

(30) Karplus, M. and L. M. Raff, J. Chem. Phys., 41, 1267 (1964).

(31) Raff, L. M. and M. Karplus, J. Chem. Phys., 44, 1212 (1966).

(32) Bunker, D. L. and N. C. Blais, J. Chem. Phys., 41, 2377 (1964).

(33) Raff, L. M., J. Chem. Phys., 44, 1202 (1966).

(34) Kuntz, P. J., E. M. Nemeth, J. C. Polanyi, S. D. Rosner, and C. E. Young, J. Chem. Phys., 44, 1168 (1966).

(35) Blais, N. C., J. Chem. Phys., 49, 9 (1968).

(36) Godfrey, M. and M. Karplus, J. Chem. Phys., 49, 3602 (1968).

(37) Kuntz, P. J., E. M. Nemeth, and J. C. Polanyi, J. Chem. Phys., 50, 4607 (1969).

(38) Brown, N. J. and R. J. Munn, J. Chem. Phys., 56, 1983 (1972).

(39) Russell, D. and J. C. Light, J. Chem. Phys., 51, 1720 (1969).

(40) Raff, L. M., L. B. Sims, D. L. Thompson, and R. N. Porter, J. Chem. Phys., 53, 1606 (1970).

(41) Porter, R. N., D. L. Thompson, L. B. Sims, and L. M. Raff, J. Amer. Chem. Soc., 92, 3208 (1970).

(42) Anderson, J. B., J. Chem. Phys., 52, 3849 (1970).

(43) Jaffe, R. L. and J. B. Anderson, J. Chem. Phys., 54, 2224 (1971).

(44) Muckerman, J. T., J. Chem. Phys., 54, 1155 (1971).

(45) Borne, T. B. and D. L. Bunker, J. Chem. Phys., 55, 4861 (1971).

(46) Thompson, D. L., J. Chem. Phys., 56, 3570 (1972).

(47) George, T. F. and W. H. Miller, J. Chem. Phys., 56, 5722 (1972).

(48) Bowman, J. M. and A. Kuppermann, Chem. Phys. Letters, 12, 1 (1971).

(49) Saxon, R. P. and J. C. Light, J. Chem. Phys., 57, 2758 (1972).

(50) George, T. F. and W. H. Miller, J. Chem. Phys., 57, 2458 (1972).

(51) Miller, W. H. and T. F. George, J. Chem. Phys., 56, 5668 (1972) and references cited therein.

(52) Thompson, D. L., J. Chem. Phys., 57, 4164 (1972).

(53) Thompson, D. L., J. Chem. Phys., 57, 4170 (1972).

(54) Parr, C. A., J. C. Polanyi, and W. H. Wong, J. Chem. Phys., 58, 5 (1973).

(55) Hodgson, B. A. and J. C. Polanyi, J. Chem. Phys., 55, 4745 (1971).

(56) Blais, N. C. and D. G. Truhlar, J. Chem. Phys., 58, 1090 (1973).

(57) Kwei, G. H., J. Chem. Phys., 58, 1722 (1973).

(58) Wilkins, R. L., J. Chem. Phys., 58, 2326 (1973).

(59) Anderson, J. B. and R. T. V. Kung, J. Chem. Phys., 58, 2477 (1973).

(60) Porter, R. N., L. B. Sims, D. L. Thompson, and L. M. Raff, J. Chem. Phys., 58, 2855 (1973).

(61) Wilkins, R. L., J. Chem. Phys., 58, 3038 (1973).

(62) Henry, J. M., J. B. Anderson, and R. L. Jaffe, Chem. Phys. Letters, 20, 138 (1973).

(63) Schatz, G. C., J. M. Bowman, and A. Kuppermann, J. Chem. Phys., 58, 4023 (1973).

(64) White, J. M., J. Chem. Phys., 58, 4482 (1973).

(65) Anderson, J. B., J. Chem. Phys., 58, 4684 (1973).

(66) Wilkins, R. L., J. Chem. Phys., 57, 912 (1972).

(67) Wilkins, R. L., J. Chem. Phys., 59, 698 (1973).

(68) Jaffe, R. L., J. M. Henry, and J. B. Anderson, J. Chem. Phys., 59, 1128 (1973).

(69) Preston, R. K. and R. J. Cross, Jr., J. Chem. Phys., 59, 3616 (1973).

(70) LaBudde, R. A. and R. B. Bernstein, J. Chem. Phys., 59, 3687 (1973).

(71) McLaughlin, D. R. and D. L. Thompson, J. Chem. Phys., 59, 4393 (1973).

(72) LaBudde, R. A., P. J. Kuntz, R. B. Bernstein, and R. D. Levine, J. Chem. Phys., 59, 6286 (1973).

(73) Kuntz, P. J. and A. C. Roach, J. Chem. Phys., 59, 6299 (1973).

(74) Chapman, S. and R. J. Suplinskas, J. Chem. Phys., 60, 248 (1974).

(75) Valencich, T. and D. L. Bunker, Chem. Phys. Lett., 20, 50 (1974).

(76) Chapman, S., T. Valencich, and D. L. Bunker, J. Chem. Phys., 60, 329 (1974).

(77) Raff, L. M., J. Chem. Phys., to be published.

(78) Duff, J. W. and D. G. Truhlar, Abstracts of papers, American Physical Society Meeting, Philadelphia, PA., March, 1974.

(79) Reference 12, p. 160, reference 16, pp. 184-204; Steinfeld, J. I. and Kinsey, J. L., Progress in Reaction Kinetics, Vol. 5, Pergamon Press, New York, 3 (1970); K. J. Laidler and J. C. Polanyi, Progress in Reaction Kinetics, Vol. 3, Pergamon Press, New York, 3 (1965); R. D. Levine, International Journal of Chemical Kinetics, Vol. 1, John Wiley and Sons, Inc., New York, 353 (1969); and D. L. Bunker, International Encyclopedia of Physical Chemistry and

Chemical Physics, Vol. 1, topic 19, Pergamon Press, New York (1966).

(80) McCullough, E. A., Jr. and R. E. Wyatt, J. Chem. Phys., 54, 3578 (1971).

(81) Diestler, D. J. and M. Karplus, J. Chem. Phys., 55, 5832 (1971).

(82) Truhlar, D. G. and A. Kuppermann, J. Chem. Phys., 56, 2232 (1972).

(83) Wolken, G. and M. Karplus, J. Chem. Phys., 60, 351 (1974).

(84) Light, J. C., Advances in Chemical Physics, Vol. 19, John Wiley and Sons, Inc., New York, 1 (1971).

(85) Micha, D., J. Chem. Phys., 50, 722 (1969).

(86) Karplus, M. and K. T. Tang, Disc. Faraday Soc., 44, 56 (1967).

(87) Tang, K. T. and M. Karplus, J. Chem. Phys., 49, 1676 (1968).

(88) Walker, R. B. and R. E. Wyatt, Chem. Phys. Lett., 16, 52 (1972).

(89) Mott, N. F. and H. S. W. Massey, The Theory of Atomic Collisions, Chapt. II, Oxford University Press, London, (1965).

(90) Bernstein, R. B., J. Chem. Phys., 33, 795 (1960).

(91) Lester, W. A., Jr., and R. B. Bernstein, J. Chem. Phys., 48, 4896 (1965).

(92) Hulbert, H. and J. O. Hirschfelder, J. Chem. Phys., 11, 276 (1943).

(93) Tang, K., B. Kleinman, and M. Karplus, J. Chem. Phys., 50, 1119 (1969).

(94) Kleinman, B. and K. Tang, J. Chem. Phys., 51, 4587 (1969).

(95) Mortensen, E. M. and K. S. Pitzer, The Transition State, Chem. Soc. (London), Spec. Publ., 16, 57 (1962).

(96) Mortensen, E. M., J. Chem. Phys., 48, 4029 (1968).

(97) Diestler, D. J. and V. McCoy, J. Chem. Phys., 48, 2941 (1968); 48, 2951 (1968).

(98) Mortensen, E. M. and L. D. Gucwa, J. Chem. Phys., 51, 5695 (1969).

(99) Diestler, D. J., J. Chem. Phys., 50, 4746 (1969); 54, 4547 (1971).

(100) Diestler, D. J. and P. Feuer, J. Chem. Phys., 54, 4626 (1971).

(101) Mazur, J. and R. J. Rubin, J. Chem. Phys., 31, 1395 (1959).

(102) Park, Y. R. L. and C. T. Yahk, and D. J. Wilson, J. Chem. Phys., 53, 786 (1970).

(103) Weiner, J. H. and A. Askar, J. Chem. Phys., 54, 3534 (1971).

(104) Weiner, J. H. and Y. Partom, Phys. Rev. B1, 1533 (1970).

(105) Marcus, R. A., J. Chem. Phys., 45, 4493 (1966).

(106) Marcus, R. A., J. Chem. Phys., 49, 2610 (1968).

(107) Reference 12, p. 10 and reference 16, p. 181.

(108) Rankin, C. C. and J. C. Light, J. Chem. Phys., 51, 1701 (1969).

(109) Miller, G. and J. C. Light, J. Chem. Phys., 54, 1635 (1971); 54, 1643 (1971).

(110) Saxon, R. P. and J. C. Light, J. Chem. Phys., 55, 455 (1971).

(111) Reference 12, p. 10.

(112) Diestler, D. J., J. Chem. Phys., 56, 2092 (1972).

(113) Wyatt, R. E., J. Chem. Phys., 51, 3489 (1969).

(114) Crawford, O. H., J. Chem. Phys., 55, 2571 (1971).

(115) Miller, W. H., Accounts of Chemical Research, 4, 161 (1971).

(116) Goldberg, A., H. M. Schey, and J. L. Schwartz, Am. J. Phys., 35, 177 (1967).

(117) Porter, R. N. and M. Karplus, J. Chem. Phys., 40, 1105 (1964).

(118) Raff, L. M., D. L. Thompson, L. B. Sims, and R. N. Porter, J. Chem. Phys., 56, 5998 (1972).

(119) Sullivan, J. H., J. Chem. Phys., 39, 3001 (1963); 46, 73 (1967).

(120) Kondrat'ev, V. N., Chemical Kinetics of Gas Reactions, Addison-Wesley Publishing Company, Inc., Reading, Mass., 349 (1964).

(121) Noyes, R. M., J. Chem. Phys., 48, 323 (1968); 49, 3741 (1968).

(122) Polanyi, J. C., J. Chem. Phys., 31, 1338 (1959); J. C. Polanyi and W. H. Wong, J. Chem. Phys., 51, 1439 (1969).

(123) Mok, M. H. and J. C. Polanyi, J. Chem. Phys., 51, 1451 (1969); 53, 4588 (1970).

(124) Anlauf, K. G., D. H. Maylotte, J. C. Polanyi, and R. B. Bernstein, J. Chem. Phys., 51, 5716 (1969).

(125) Muckerman, J. T., J. Chem. Phys., 56, 2997 (1972).

(126) Fong, K. P. and D. J. Diestler, J. Chem. Phys., 56, 3200 (1972).

(127) Reference 19, p. 101.

(128) Messiah, A., Quantum Mechanics, Vol. 1, John Wiley and Sons, Inc., New York, 68 (1968).

(129) Morse, P. M., Phys., Rev., 34, 57 (1929).

(130) Sato, S., J. Chem. Phys., 23, 592, 2465 (1955).

(131) Reference 12, p. 20.

(132) Westhaus, P. A., Handout notes for Line Spectra Class, Oklahoma State University, Fall, 1971.

(133) Löwdin, Per-Olov, Preprint No. 78, "Quantum Theory of Time-Dependent Phenomena Treated by the Evolution Operator Technique", June 15, 1965, p. 38. Quantum theory project for research in atomic, molecular and solid state chemistry and physics, University of Florida, Gainsville, Florida.

(134) Reference 133, p. 39.

(135) Smyser, W. E. and D. J. Wilson, J. Chem. Phys., 50, 182 (1969), E. B. Alterman, C. T. Yahk, and D. J. Wilson, J. Chem. Phys., 44, 451 (1966), R. C. Baetzold, C. T. Yahk, and D. J. Wilson, J. Chem. Phys., 45, 4209 (1966), and reference 102.

(136) Varga, R. S., Matrix Iterative Analysis, Chap. 8, Prentice-Hall, Inc., Englewood Cliffs, New Jersey (1962).

(137) Crank, J. and P. Nicholson, Proc. Camb. Phil. Soc., 43, 50 (1947).

(138) Acton, F. S., Numerical Methods That Work, Harper & Row Publishers, New York, 436-447 (1970).

(139) Ralston, A., A First Course in Numerical Analysis, McGraw-Hill Book Co., New York, 84 (1965).

(140) Reference 136, Chapter 4.

(141) Carnahan, B., H. A. Luther, and J. O. Wilkes, Applied Numerical Methods, John Wiley and Sons, Inc., New York, 446 (1969) and reference 136, p. 195.

(142) Brabson, G. D., J. Chem. Ed., 50, 397 (1973).

(143) Merzbacher, E., Quantum Mechanics, John Wiley and Sons, Inc., New York, 19 (1970).

(144) Kaplan, W., Advanced Calculus, Addison-Wesley Publishing Co., Inc., Reading, Mass., 191-193 (1963) and T. R. McCalla, Introduction to Numerical Methods and Fortran Programming, John Wiley and Sons, Inc., New York, 270-271, 277-279 (1967).

(145) Hamming, R. W., Numerical Methods for Scientists and Engineers, McGraw-Hill Book Company, New York, 318-319 (1962).

(146) Suzukawa, H. H., Jr., D. L. Thompson, V. B. Cheng, and M. Wolfsberg, J. Chem. Phys., 59, 4000 (1973).

(147) Gill, S., Proc. Cambridge Phil. Soc., 47, 96 (1951).

(148) Morokuma, K. and M. Karplus, J. Chem. Phys., 55, 63 (1971).

(149) Wu, S. F. and R. A. Marcus, J. Chem. Phys., 53, 4026 (1970).

(150) Weston, R. E., J. Chem. Phys., 31, 892 (1959).

(151) Truhlar, D. G., J. Comp. Phys., 10, 123 (1972).

(152) Truhlar, D. G. and A. Kuppermann, J. Chem. Phys., 52, 3841 (1970).

(153) Diestler, D. J., D. G. Truhlar, and A. Kuppermann, Chem. Phys. Lett., 13, 1 (1972).

(154) Levine, R. D. and S. F. Wu, Chem. Phys. Lett., 11, 557 (1971).

(155) Johnson, B. R., Chem. Phys. Lett., 13, 172 (1972).

(156) Russell, J. D. and J. C. Light, J. Chem. Phys., 54, 4881 (1971).

(157) Saxon, R. P. and J. C. Light, J. Chem. Phys., 56, 3874 (1972); 56, 3885 (1972), and reference 110.

(158) Shavitt, I., R. M. Stevens, F. L. Minn, and M. Karplus, J. Chem. Phys., 48, 2700 (1968).

(159) Duff, J. W. and D. G. Truhlar, Chem. Phys. Lett., 23, 327 (1973).

(160) Truhlar, D. G., A. Kuppermann, and J. T. Adams, J. Chem. Phys., 59, 395 (1973).

(161) Koeppl, G. W. J., Chem. Phys., 60, 1684 (1974).

(162) Persky, A. and M. Baer, J. Chem. Phys., 60, 133 (1974) and M. Baer, J. Chem. Phys., 60, 1057 (1974).

(163) Porter, R. N., "Molecular Trajectory Calculations," Prepared for Annual Review of Physical Chemistry, Vol. 25 (1974).

(164) Raff, L. M., L. Stivers, R. N. Porter, D. L. Thompson, and L. B. Sims, J. Chem. Phys., 52, 3449 (1970).

(165) Westhaus, P. A., personal communication.

(166) Löwdin, Per-Olov, Preprint QB 7, "Some Aspects on the Biological Problems of Heredity, Mutations, Aging, and Tumors in View of the Quantum Theory of the DNA Molecule", November 11, 1963. Quantum Chemistry Group for Research in Atomic, Molecular, and Solid-State Theory, Uppsala University, Uppsala, Sweden.

(167) Reference 166, p. 62L.

(168) Ladik, I., Acta. Phys. Acad. Sci. Hung., 15, 287 (1963).

(169) Rein, R. and F. Harris, J. Chem. Phys., 41, 3393 (1964).

(170) Clementi, E., J. Mehl, and W. Niessen, J. Chem. Phys., 54, 508 (1971).

VITA

Glen Edward Kellerhals

Candidate for the Degree of

Doctor of Philosophy

Thesis: A COMPARISON OF QUANTUM MECHANICAL AND QUASICLASSICAL REACTION DYNAMICS FOR AN ASYMMETRIC A + BC EXCHANGE REACTION

Major Field: Chemistry

Biographical:

Personal Data: Born in Vinton, Iowa, September 29, 1945, the son of Mr. and Mrs. Ralph A. Kellerhals.

Education: Graduated from Geneseo Consolidated High School, Buckingham, Iowa, in May, 1963; received the Bachelor of Science degree from Upper Iowa College, Fayette, Iowa, with majors in Chemistry and Mathematics in May, 1967, graduating magna cum laude; completed requirements for the Doctor of Philosophy degree at Oklahoma State University in July, 1974.

Professional Experience: Student Assistant, Department of Chemistry, Upper Iowa College, September, 1964 through May, 1967; National Aeronautics and Space Administration Trainee, September, 1967 through January, 1969; Graduate Teaching Assistant, Oklahoma State University, January, 1971 through May, 1972; Continental Oil Company Fellow, Summer 1971; National Science Foundation Research Assistant, May, 1972 through May, 1974.

Membership in Honorary and Professional Societies: Member of American Chemical Society; member of Phi Lambda Upsilon, Honorary Chemical Society.